الج مهورية الج زائرية الديم قراطية الشعبية

REPUBLIQUE ALGERIENNE DEMOCRATIQUE ET POPULAIRE

وزارة التعليم العالي والبحث العلمي

Ministère de l'Enseignement Supérieur et de la Recherche Scientifique

جامعة سعيدة الدكتور الطاهر مولاي

Université de Saida Dr Tahar Moulay



Faculté des Sciences et de Technologie Département d'électrotechnique et d'automatique

MEMOIRE

pour l'obtention du Diplôme de MASTER

En : Électrotechnique

Spécialité : Électrotechnique Industrielle

Par: GHENNAM Bouziane et MECHEHED Mohamed

Intitulé

Sliding Modes Direct Torque Control of three-phase induction motor

Soutenu publiquement le 19/06/2025 devant le jury composé de :

M. ARZAG KaddourUniv. SaidaPrésidentM. AIMER Ameur FethiUniv. SaidaRapporteurMme. BELGACEM KheiraUniv. SaidaExaminateur

Année universitaire 2024/2025

Acknowledgment

First and foremost, I thank Allah, the Almighty and Merciful, for teaching me what I did not know, for granting me health, and for providing everything I needed to accomplish this work.

I extend my deepest gratitude to my beloved parents, whose unconditional love, encouragement, and sacrifices foundation have been the of my success. Their has guided unwavering throughout support me my academic journey.

A special thanks to supervisor *Dr. Aimer*, whose professionalism and guidance were instrumental in the completion of this Thesis. His expertise and support made this journey both enriching and structured.

I sincerely thank *Dr. Belgacem*, a true example of humility and kindness, always supporting her students with patience and generosity. I am equally grateful to *Dr. Arzag*, whose dedication and perseverance have profoundly shaped our understanding.

Finally, I would like to thank my dear friends, who have stood by me, offering their encouragement and companionship during this journey. Their support made this experience even more meaningful.

Ghennam Bouziane

Dedication

All praise and gratitude to **Allah, the Most Merciful**, for allowing me to witness a dream I have long awaited, now turned into a reality that fills me with pride.

With love and appreciation, I dedicate this humble work to those who have had the greatest impact on my academic and personal life:

- To my **dear parents**, whose unwavering support, encouragement, and wisdom have been the foundation of my journey. Their sacrifices and love have given me strength at every step.
- To my **brothers and sisters**, my lifelong companions in both challenges and success, whose love, prayers, and genuine smiles have been a source of motivation.
- To my loyal friends, who have stood by me throughout this path, providing support and encouragement in moments of doubt and determination.
- To my **respected professors**, whose knowledge and guidance have illuminated my way and remain a source of inspiration.
- To my honorable mentor, who has been my guide and advisor, instilling in me the love of learning and virtue. May Allah reward him abundantly.
- And as we celebrate this achievement, we do not forget our oppressed brothers and sisters in Palestine. We ask Allah to grant them victory and bring them peace and security.

To all of you, I dedicate this success, hoping that what I have learned will serve to **benefit others and contribute** to my community.

Abstract

This study focuses on the Direct Torque Control (DTC) strategy for three-phase induction motors, integrating Sliding Mode Control (SMC) to enhance robustness and reduce control limitations. Conventional DTC allows direct control of torque and flux, eliminating the need for coordinate transformations. However, it suffers from high torque and flux ripples, variable switching frequency, and sensitivity to parameter variations.

To address these issues, this work develops an optimized DTC scheme incorporating SMC, leveraging its nonlinear control properties to improve system stability. The proposed method ensures fast dynamic response, better flux regulation, and reduced electromagnetic torque oscillations. Through MATLAB/Simulink simulations, the performance of the DTC-SMC strategy is evaluated, demonstrating its advantages in terms of torque precision, flux stability, and harmonic suppression. The results confirm that DTC with SMC significantly enhances motor control efficiency, making it a viable solution for high-performance industrial applications.

Keywords: Direct Torque Control (DTC), Sliding Mode Control (SMC), Induction Motor, MATLAB Simulation, Robust Control

Résumé

Cette étude porte sur la commande directe du couple (DTC) des moteurs asynchrones triphasés, avec l'intégration du mode glissant (SMC) afin d'améliorer la robustesse.La méthode DTC classique permet un contrôle direct du couple et du flux, sans transformation de coordonnées. Cependant, elle présente des ondulations importantes du couple et du flux, une fréquence de commutation variable et une sensibilité aux variations des paramètres.

Pour pallier ces défauts, cette étude propose une approche DTC-SMC optimisée, exploitant les propriétés du contrôle non linéaire afin d'améliorer la stabilité du système et la résistance aux perturbations. Cette approche garantit une réponse dynamique rapide, une meilleure régulation du flux et une réduction des oscillations du couple électromagnétique. Les performances du DTC-SMC ont été évaluées par des simulations sous MATLAB/Simulink, démontrant ses avantages en termes de précision du couple, stabilité du flux et suppression des harmoniques. Les résultats confirment que l'association DTC et SMC améliore considérablement le contrôle du moteur, en faisant une solution performante pour les applications industrielles exigeantes.

Mots-clés : Commande directe du couple (DTC), Mode glissant (SMC), Moteur asynchrone, Simulation MATLAB, Commande robuste

الملخص

تركز هذه الدراسة على استراتيجية التحكم المباشر في العزم لمحركات الحث ثلاثية الطور، مع دمج التحكم في الوضع الانز لاقي لتعزيز المتانة وتقليل قيود التحكم. يتيح التحكم المباشر في العزم التحكم المباشر في العزم والتدفق دون الحاجة إلى تحويل الإحداثيات، لكنه يعاني من تموجات كبيرة في العزم والتدفق، وتردد تبديل غير ثابت، وحساسية لتغيرات المعاملات.

لمعالجة هذه المشكلات، تم تطوير نهج تحكم مباشر في العزم محسن مع التحكم في الوضع الانز لاقي، حيث يستفيد من خصائص التحكم غير الخطي لتحسين استقرار النظام . تضمن الطريقة المقترحة استجابة ديناميكية سريعة، وتنظيم أفضل للتدفق، وتقليل التذبذبات الكهر ومغناطيسية للعزم.

تم تقييم أداء استراتيجية التحكم المباشر في العزم مع Simulinkو MATLAB. من خلال عمليات محاكاة باستخدام التحكم في الوضع الانز لاقي، مما يبرز مزاياها من حيث دقة العزم، واستقرار التدفق، وقمع التوافقيات. تؤكد النتائج أن التحكم المباشر في العزم مع التحكم في الوضع الانز لاقي يعزز بشكل كبير كفاءة التحكم في المحركات، مما يجعله حلاً فعالاً للتطبيقات الصناعية عالية الأداء.

الكلمات المفتاحية : التحكم MATLABالتحكم المباشر في العزم، التحكم في الوضع الانز لاقي، المحرك الحثي، محاكاة المتين

List of Symbols

Symbol	Meaning	Unit
R _S	Stator winding resistance	Ω
R_T	Rotor winding resistance	Ω
L_{s}	Per-phase stator cyclic inductance	H
L_r	Per-phase rotor cyclic inductance	Н
M_s	Mutual inductance between two stator phases	Н
M_r	Mutual inductance between two rotor phases	Н
M	Mutual inductance	Н
M_{sr}	Maximum mutual inductance between stator and rotor phases	Н
p	Number of pole pairs	
J	Moment of inertia of rotating parts	kg.m ²
f	Viscous friction coefficient	N.m.s/rad
T_s	Stator time constant (Ls/Rs)	S
T_r	Rotor time constant (Lr/Rr)	S
σ	Blondel's dispersion coefficient	
X_{as}, X_{bs}, X_{cs}	Stator quantities in the three-phase (abc) reference frame	
X_{ar}, X_{br}, X_{cr}	Rotor quantities in the three-phase (abc) reference frame	
X_{ds}, X_{qs}	Stator quantities in the rotating two-phase (dq) reference frame	
X_{dr}, X_{qr}	Rotor quantities in the rotating two-phase (dq) reference frame	
$X_{\alpha s}, X_{\beta s}$	Stator quantities in the fixed two-phase $(\alpha\beta)$ reference frame linked to the stator	
$X_{\alpha r}, X_{\beta r}$	Rotor quantities in the fixed two-phase $(\alpha\beta)$ reference frame linked to the stator.	
θ	Angle between the stator and the rotor	rad
$ heta_{s}$	Angle between the stator and the d-axis	rad
$ heta_{ m r}$	Angle between the rotor and the d-axis	rad
$arOmega_{ extsf{s}}$	Synchronous speed	rad/s
$arOmega_{ m r,}$	Mechanical speed	rad/s
ω_{s}	Stator pulsation	rad/s
$\omega_{ m r}$	Rotor pulsation	rad/s
T_r	Load torque	N.m
T_{em}	Electromagnetic torque	N.m
$arphi_{ extsf{S}}^{*}$	Reference stator flux.	Wb
K_i, K_p	PI controller gains	
$\iota \wedge \rho$	<i>5</i>	

List of abreviations

Abreviation	Meaning
DTC	Direct Torque Control
SMC	Sliding mode Control
SVM	Space Vector Modulation
PWM	Pulse Width Modulation
CSVM	Controlled Space Vector Modulation
ASM	Asynchronous Machine
IM	Induction Machine

List of Figures and Tables

Figure	Title	Page
Fig. I.1	Structure of the Induction Machine	2
Fig. I.2	Typical Stator of Three-phase Induction Motor	3
Fig. I.3	Squirrel-Cage Rotor	4
Fig. I.4	Wound Rotor	4
Fig I.5	Representation of the windings of the three-phase Induction machine	e 9
Fig.I.6	Angular Positioning of the Machine's Fictitious Axis Systems	12
Fig. I.7	Representation of the fictitious windings along the 'd' and 'q' axes	15
Fig. I.8	Representation of the various reference frames	18
Figure I.9	Block diagram of the voltage-fed Induction machine	21
Figure I.10	Direct start of the Induction motor without an inverter	22
Figure II.1	Power Supply	24
Figure II.2	Representation of a Three-Phase Inverter	25
Figure II.3	Representation of a Three-Phase Two-Level Inverter	25
Figure II.4	Schematic Diagram of Hysteresis Control of an Inverter Arm	28
Figure II.5	Hysteresis Control	29
Figure II.6	Simplified Structure of a Three-Phase Inverter	30
Figure II.7	Representation of the Switching Polygon	33
Figure II.8	Calculation of Switching Times for Sector 1	36
Figure II.9	Description of the Conduction Sequences of the Switches	38
Figure II.10	Algorithm of Vector PWM	39
Figure II.11	Basic block of PI Controller	40
Figure II.12	Overview of the classical two-level DTC control	42
Fig. II.13	Development of the Voltage Vector Vs (Sa Sb Sc)	43
Fig. II.14	Development of the stator flux and operating sequences	44
Fig.II.15	The Rotation Angles in the Fixed α , β Reference Frame	46
Figure II.16	Flux corrector with hysteresis and selection of the correspondition voltage vectors	ng 49
Fig.II.17	Two-level Flux corrector	50
Fig.II.18	Three-level Flux corrector	51

Fig. II.19	Block diagram of the conventional DTC control	53
Fig. II.20	Simulation results of the conventional DTC control	55
Fig. II.21	Trajectory of the tip of the stator flux vector	56
Figure III.1	The different modes for the trajectory in the phase plane	58
Figure III.2	Trajectory of the state with respect to the sliding surface	60
Figure III.3	Control applied to the system	61
Figure III.4	Equivalent Control	61
Figure III.5	Representation of the "Sign" function	63
Figure III.6	Phenomenon of Reluctance or (Chattering)	64
Figure III.7	Sat Function	65
Figure III.8	Smoothing Function "cont(S)"	65
Figure III.9	Principle Diagram of Direct Torque Control Using Sliding Modes for an Asynchronous Machine.	70
Figure III.10	Principle Diagram of Direct Torque Control Using Sliding Modes for an Asynchronous Machine	71
Fig. III.11	Simulation results of DTC with SMC	73
Fig. III.12	Simulation results of DTC with SMC – Stator flux trajectory	74

Table	Title	Page
Table II.1	Calculation of Voltage Vectors	32
Table II.2	Command table considering both cases of the torque controller	51

Table of Contents

Genral Introduction	01
Chapitre 1: Overview of Three-Phase Induction Motors	
I.1 Introduction	02
I.2 Structure of the Induction Machine	02
I.2.1 Stator	03
I.2.2 Rotor	03
I.3 Operating Principles	04
I.3.1 Motor Mode Operation	05
I.3.2 Generator Mode Operation	06
I.4 Starting the Induction Machine	07
I.4.1 Direct Start in One Direction of Rotation	07
I.4.2 Direct Start in One Direction of Rotation	07
I.4.3 Star-Delta Motor Start	07
I.4.4 Auto-Transformer Start	07
I.4.5 Resistive Start	07
I.4.6 Rotor Resistance Start	08
I.5 Induction Motors braking methods	08
I.5.2 Braking by DC Injection	08
I.5.3 Braking by Hyper-Synchronous Operation	08
I.5.4 Braking by Induction Generator Operation	08
I.6 Simplifying Assumptions	09
I.7 Vector Representation of the Machine	09
I.8 Electrical Equations of the Machine	09
I.9 Coupling with the mechanical equation	11
I.10 Park's Model	12
I.10.1 Electrical Equations	14
I.10.2 Magnetic Equations	14
I.11 Choice of Reference Frame	16
I.12 State Representation of Park	18
I.12.1 Description	18
I.12.2 State Equations	18
I.13 Numerical Simulation	20
I.14 Results and Discussion	20
I.15 Conclusion	23
Chapitre 2: Study of Direct Torque Control (DTC)	
II Introduction	24
II.1 Definition of Inverter	24
II.2 Power Supply	24
II.3 Construction of a Three-Phase Inverter	25
II.4 Modeling of the Two-Level Voltage Inverter	25
II.5 Hysteresis Control	28
II.6 Pulse Width Modulation (PWM)	29
II.7 Space Vector Modulation	30
II.7.1 Advantages of Vectorial Modulation	31

II.7.2 Clark Transformation	31
II.7.3 Desired Voltage Vector	34
II.7.4 Approximation of the Desired Voltage Vector	35
II.7.5 Calculation of Switching Times	36
II.8 Overview of the Conventional PI controller	40
II.8.1 PI CONTROLLER	40
II.9 DTC (Direct Torque Control)	41
II.10 Generation of Space Voltage Vector	42
II.11 Qualitative Rules for the Electromagnetic State of the Machine	43
II.12 ESTIMATORS	46
II.12.1 Estimation of stator flux	46
II.12.2 Estimation of electromagnetic torque	48
II.13 Elaboration of the control vector	48
II13.1 Flux corrector	48
II.13.2 Torque corrector	49
II.13.3 Two-level corrector	50
II.13.4 Three-level corrector	50
II.13.5 Elaboration of the commutation table	51
II.14 Disadvantages of DTC	52
II.15 Numerical Simulation	52
II.15.1 Concordia Transformation	52
II.15.2 Estimation of Control Quantities	52
II 16 Decules And Discussion	53
II.16 Results And Discussion	
	54
II.17 Conclusion	
II.17 Conclusion Chapitre 3 : Sliding Mode-Based DTC	54
II.17 Conclusion Chapitre 3 : Sliding Mode-Based DTC III Introduction	54 57
II.17 Conclusion Chapitre 3 : Sliding Mode-Based DTC III Introduction III.1 Principle of sliding mode control	54
II.17 Conclusion Chapitre 3 : Sliding Mode-Based DTC III Introduction III.1 Principle of sliding mode control III.2 Design of the Sliding Mode Control Algorithm	54 57 57
II.17 Conclusion Chapitre 3 : Sliding Mode-Based DTC III Introduction III.1 Principle of sliding mode control	54 57 57 58
Chapitre 3 : Sliding Mode-Based DTC III Introduction III.1 Principle of sliding mode control III.2 Design of the Sliding Mode Control Algorithm III.2.1 Choice of sliding surface	54 57 57 58 58
Chapitre 3 : Sliding Mode-Based DTC III Introduction III.1 Principle of sliding mode control III.2 Design of the Sliding Mode Control Algorithm III.2.1 Choice of sliding surface III.2.2 Conditions for Existence and Convergence of Sliding Mode III.2.3 Determination of the Control Law	54 57 57 58 58 59 60
Chapitre 3 : Sliding Mode-Based DTC III Introduction III.1 Principle of sliding mode control III.2 Design of the Sliding Mode Control Algorithm III.2.1 Choice of sliding surface III.2.2 Conditions for Existence and Convergence of Sliding Mode III.2.3 Determination of the Control Law III.2.3.1 Definition of Control Quantities	54 57 57 58 58 59 60 61
Chapitre 3 : Sliding Mode-Based DTC III Introduction III.1 Principle of sliding mode control III.2 Design of the Sliding Mode Control Algorithm III.2.1 Choice of sliding surface III.2.2 Conditions for Existence and Convergence of Sliding Mode III.2.3 Determination of the Control Law III.2.3.1 Definition of Control Quantities III.2.3.2 Analytical Expression of the Control	54 57 57 58 58 59 60 61 62
Chapitre 3 : Sliding Mode-Based DTC III Introduction III.1 Principle of sliding mode control III.2 Design of the Sliding Mode Control Algorithm III.2.1 Choice of sliding surface III.2.2 Conditions for Existence and Convergence of Sliding Mode III.2.3 Determination of the Control Law III.2.3.1 Definition of Control Quantities III.2.3.2 Analytical Expression of the Control III.3 Phenomenon of Reluctance (chattering)	54 57 57 58 58 59 60 61 62 63
Chapitre 3 : Sliding Mode-Based DTC III Introduction III.1 Principle of sliding mode control III.2 Design of the Sliding Mode Control Algorithm III.2.1 Choice of sliding surface III.2.2 Conditions for Existence and Convergence of Sliding Mode III.2.3 Determination of the Control Law III.2.3.1 Definition of Control Quantities III.2.3.2 Analytical Expression of the Control III.3 Phenomenon of Reluctance (chattering) III.4 Continuous Approximation of Sliding Mode Control	54 57 57 58 58 59 60 61 62 63 64
Chapitre 3 : Sliding Mode-Based DTC III Introduction III.1 Principle of sliding mode control III.2 Design of the Sliding Mode Control Algorithm III.2.1 Choice of sliding surface III.2.2 Conditions for Existence and Convergence of Sliding Mode III.2.3 Determination of the Control Law III.2.3.1 Definition of Control Quantities III.2.3.2 Analytical Expression of the Control III.3 Phenomenon of Reluctance (chattering) III.4 Continuous Approximation of Sliding Mode Control III.5 Design of a Direct Torque Control Using Sliding Mode	54 57 57 58 58 59 60 61 62 63
Chapitre 3 : Sliding Mode-Based DTC III Introduction III.1 Principle of sliding mode control III.2 Design of the Sliding Mode Control Algorithm III.2.1 Choice of sliding surface III.2.2 Conditions for Existence and Convergence of Sliding Mode III.2.3 Determination of the Control Law III.2.3.1 Definition of Control Quantities III.2.3.2 Analytical Expression of the Control III.3 Phenomenon of Reluctance (chattering) III.4 Continuous Approximation of Sliding Mode Control	54 57 57 58 58 59 60 61 62 63 64 66
Chapitre 3 : Sliding Mode-Based DTC III Introduction III.1 Principle of sliding mode control III.2 Design of the Sliding Mode Control Algorithm III.2.1 Choice of sliding surface III.2.2 Conditions for Existence and Convergence of Sliding Mode III.2.3 Determination of the Control Law III.2.3.1 Definition of Control Quantities III.2.3.2 Analytical Expression of the Control III.3 Phenomenon of Reluctance (chattering) III.4 Continuous Approximation of Sliding Mode Control III.5 Design of a Direct Torque Control Using Sliding Mode III.5.1 Proposed Control Principle III.5.2 Induction Machine Model	54 57 57 58 58 59 60 61 62 63 64 66
Chapitre 3 : Sliding Mode-Based DTC III Introduction III.1 Principle of sliding mode control III.2 Design of the Sliding Mode Control Algorithm III.2.1 Choice of sliding surface III.2.2 Conditions for Existence and Convergence of Sliding Mode III.2.3 Determination of the Control Law III.2.3.1 Definition of Control Quantities III.2.3.2 Analytical Expression of the Control III.3 Phenomenon of Reluctance (chattering) III.4 Continuous Approximation of Sliding Mode Control III.5 Design of a Direct Torque Control Using Sliding Mode III.5.1 Proposed Control Principle	54 57 57 58 58 59 60 61 62 63 64 66 66
Chapitre 3 : Sliding Mode-Based DTC III Introduction III.1 Principle of sliding mode control III.2 Design of the Sliding Mode Control Algorithm III.2.1 Choice of sliding surface III.2.2 Conditions for Existence and Convergence of Sliding Mode III.2.3 Determination of the Control Law III.2.3.1 Definition of Control Quantities III.2.3.2 Analytical Expression of the Control III.3 Phenomenon of Reluctance (chattering) III.4 Continuous Approximation of Sliding Mode Control III.5 Design of a Direct Torque Control Using Sliding Mode III.5.1 Proposed Control Principle III.5.2 Induction Machine Model III.5.3 Torque and Stator Flux Regulation	54 57 57 58 58 59 60 61 62 63 64 66 66 66
Chapitre 3 : Sliding Mode-Based DTC III Introduction III.1 Principle of sliding mode control III.2 Design of the Sliding Mode Control Algorithm III.2.1 Choice of sliding surface III.2.2 Conditions for Existence and Convergence of Sliding Mode III.2.3 Determination of the Control Law III.2.3.1 Definition of Control Quantities III.2.3.2 Analytical Expression of the Control III.3 Phenomenon of Reluctance (chattering) III.4 Continuous Approximation of Sliding Mode Control III.5 Design of a Direct Torque Control Using Sliding Mode III.5.1 Proposed Control Principle III.5.2 Induction Machine Model III.5.3 Torque and Stator Flux Regulation III.6 Simulation Block	54 57 57 58 58 59 60 61 62 63 64 66 66 66 67 70
Chapitre 3 : Sliding Mode-Based DTC III Introduction III.1 Principle of sliding mode control III.2 Design of the Sliding Mode Control Algorithm III.2.1 Choice of sliding surface III.2.2 Conditions for Existence and Convergence of Sliding Mode III.2.3 Determination of the Control Law III.2.3.1 Definition of Control Quantities III.2.3.2 Analytical Expression of the Control III.3 Phenomenon of Reluctance (chattering) III.4 Continuous Approximation of Sliding Mode Control III.5 Design of a Direct Torque Control Using Sliding Mode III.5.1 Proposed Control Principle III.5.2 Induction Machine Model III.5.3 Torque and Stator Flux Regulation III.6 Simulation Block III.7 Results and Discussion	54 57 57 58 58 59 60 61 62 63 64 66 66 66 67 70 71
Chapitre 3 : Sliding Mode-Based DTC III Introduction III.1 Principle of sliding mode control III.2 Design of the Sliding Mode Control Algorithm III.2.1 Choice of sliding surface III.2.2 Conditions for Existence and Convergence of Sliding Mode III.2.3 Determination of the Control Law III.2.3.1 Definition of Control Quantities III.2.3.2 Analytical Expression of the Control III.3 Phenomenon of Reluctance (chattering) III.4 Continuous Approximation of Sliding Mode Control III.5 Design of a Direct Torque Control Using Sliding Mode III.5.1 Proposed Control Principle III.5.2 Induction Machine Model III.5.3 Torque and Stator Flux Regulation III.6 Simulation Block III.7 Results and Discussion III.8 Conclusion	54 57 57 58 58 59 60 61 62 63 64 66 66 66 67 70 71 72
Chapitre 3 : Sliding Mode-Based DTC III Introduction III.1 Principle of sliding mode control III.2 Design of the Sliding Mode Control Algorithm III.2.1 Choice of sliding surface III.2.2 Conditions for Existence and Convergence of Sliding Mode III.2.3 Determination of the Control Law III.2.3.1 Definition of Control Quantities III.2.3.2 Analytical Expression of the Control III.3 Phenomenon of Reluctance (chattering) III.4 Continuous Approximation of Sliding Mode Control III.5 Design of a Direct Torque Control Using Sliding Mode III.5.1 Proposed Control Principle III.5.2 Induction Machine Model III.5.3 Torque and Stator Flux Regulation III.6 Simulation Block III.7 Results and Discussion III.8 Conclusion General Conclusion	54 57 57 58 58 59 60 61 62 63 64 66 66 66 67 70 71 72 74

General Introduction

Induction motors have become an essential component in modern industrial applications due to their robustness, cost-effectiveness, and reliability. Their ability to function efficiently in various operating conditions makes them the preferred choice for numerous sectors. However, despite these advantages, the control of induction motors presents challenges due to their nonlinear nature, strong coupling, and sensitivity to parameter variations.

To address these challenges, advanced control techniques have been developed to improve the precision and efficiency of induction motor operation. Direct Torque Control (DTC) is one of the most widely used strategies, providing fast torque response and eliminating the need for rotor position sensors. However, conventional DTC techniques suffer from torque ripples and flux oscillations, leading to performance limitations that require further refinement.

To overcome these drawbacks, Sliding Mode Control (SMC) has been integrated with DTC to provide enhanced robustness and improved system stability. The nonlinear nature of SMC ensures better disturbance rejection, reduced torque oscillations, and optimized flux regulation. The combination of DTC with SMC offers a high-performance solution for induction motor control, minimizing harmonic distortions and improving dynamic response.

This Work focuses on the theoretical and practical aspects of DTC and SMC, providing a comprehensive analysis through mathematical modeling, control strategy design, and MATLAB/Simulink simulations. The study is structured into several chapters, each addressing critical aspects of induction motor control:

- Chapter I: Introduces the mathematical model of the induction motor, including fundamental principles, vector representations, and simulation-based validation.
- Chapter II: Examines Direct Torque Control (DTC), detailing its implementation, advantages, and challenges.
- Chapter III: Explores Sliding Mode Control (SMC), discussing its theoretical foundation and integration with DTC.

Through this study, we aim to provide a deeper understanding of induction motor control strategies, validating their effectiveness and exploring avenues for further optimization in high-performance industrial applications.

Chapter I Overview of Three-Phase Induction Motors

I Introduction:

Induction motor (Also called Induction motor) is an A.C. motor. The motor line current flows into the stator windings to set up a flux called the main flux or the stator flux, which passes through the air gap to be cut by the conductors of the rotor windings.

Consequently, an electromotive force to be induced in the rotor windings and produces currents flow in the rotor windings and producing flux called the rotor flux.

The interact between the two fluxes (stator and rotor fluxes) producing rotation of the rotating part of the motor (rotor). The rotor receives electrical power in the same way as the secondary winding of the electrical transformer receiving its power from the primary winding by means of the electrical induction. That is why an induction motor can be called as a rotating transformer i.e., in which primary winding is stationary but the secondary is free to rotate.

I.2 Structure of the Induction Machine:

The structure of an Asyncronous machine, commonly known as an induction motor consists of two main parts: the stator and the rotor. These components work together to convert electrical energy into mechanical energy.

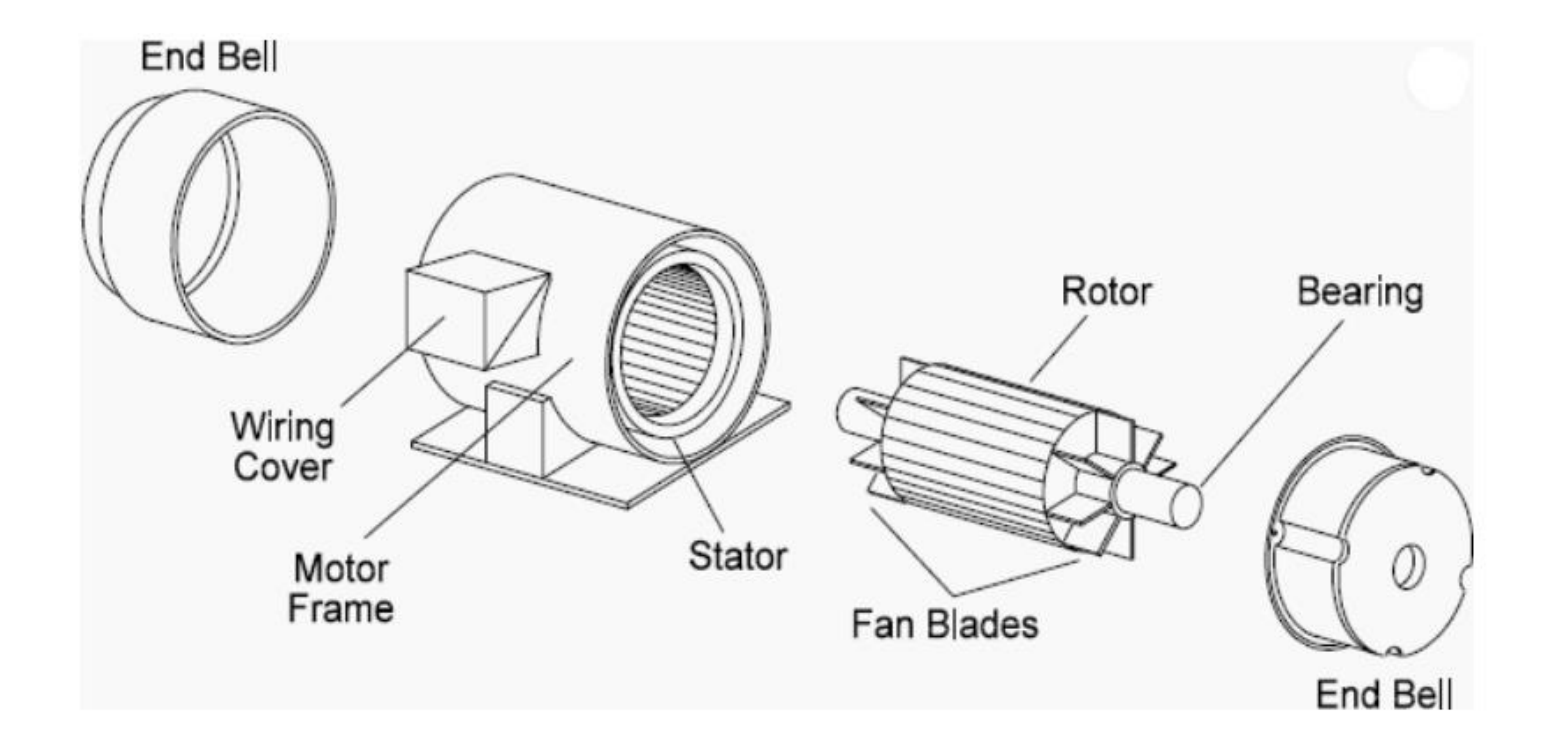
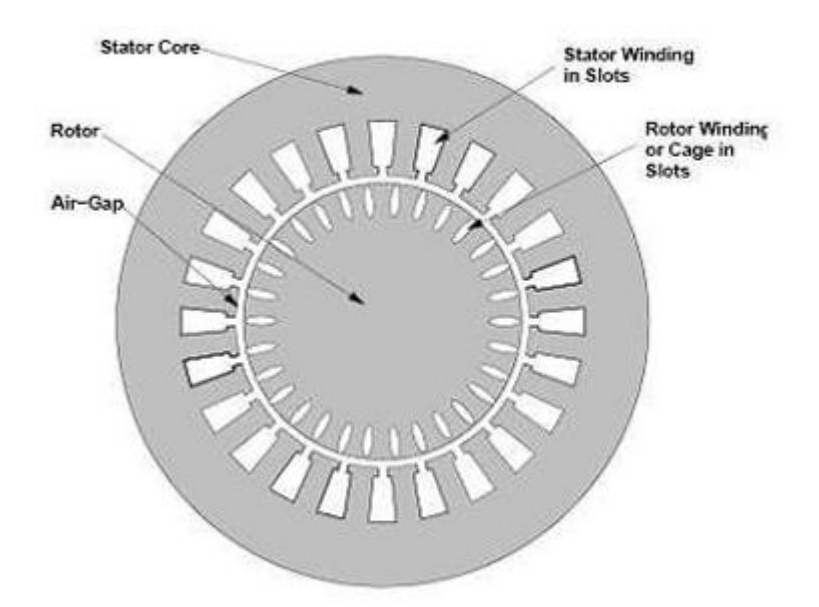


Fig. I.1: Structure of the Induction Machine

I.2.1 Stator:

The stator is the stationary part of the motor, and it has several key components:

- **Frame**: The outer casing that holds all the internal parts of the motor together. It provides mechanical protection and heat dissipation.
- Core: Made of laminated silicon steel sheets, the core's primary function is to carry the magnetic flux. The laminations reduce energy losses due to eddy currents.
- **Windings**: Copper or aluminum wire coils wound in specific patterns. When three-phase AC power is applied to these windings, it creates a rotating magnetic field. The windings are embedded in slots on the inner surface of the stator core (TIRUPATI,2018).



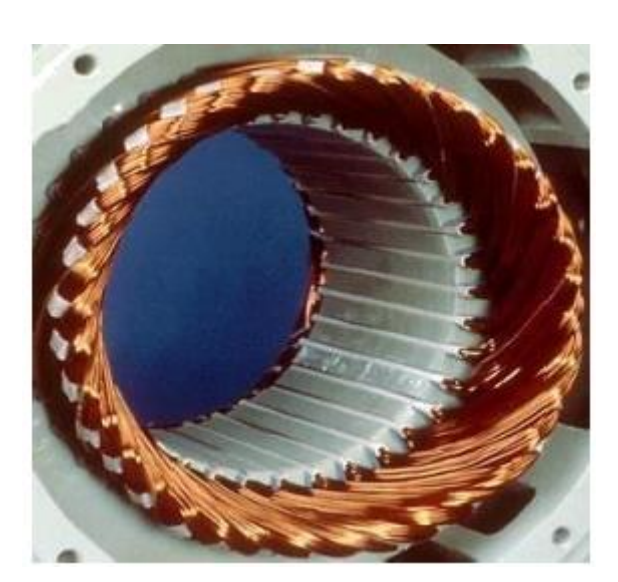


Fig. I.2: Typical Stator of Three-phase Induction Motor

I.2.2 Rotor:

The rotor is the rotating part of the motor, and it can be of two types:

- squirrel-cage rotor
- wound rotor.

Squirrel-Cage Rotor: This is the most common type. It consists of a cylindrical laminated core with conductive bars (usually aluminum or copper) embedded along its length, connected at both ends by conductive rings. The entire assembly looks like a squirrel cage.

Wound Rotor: This type has windings similar to the stator windings, connected to external slip rings. These rings allow for external resistances to be connected, which can control the motor's characteristics during startup and operation.

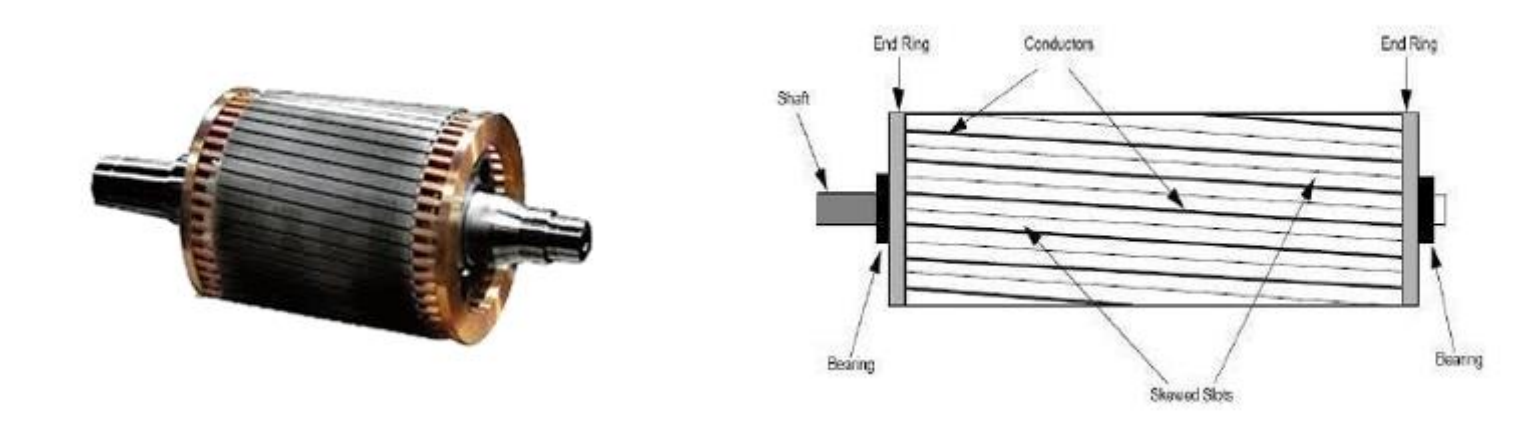


Fig. I.3: Squirrel-Cage Rotor

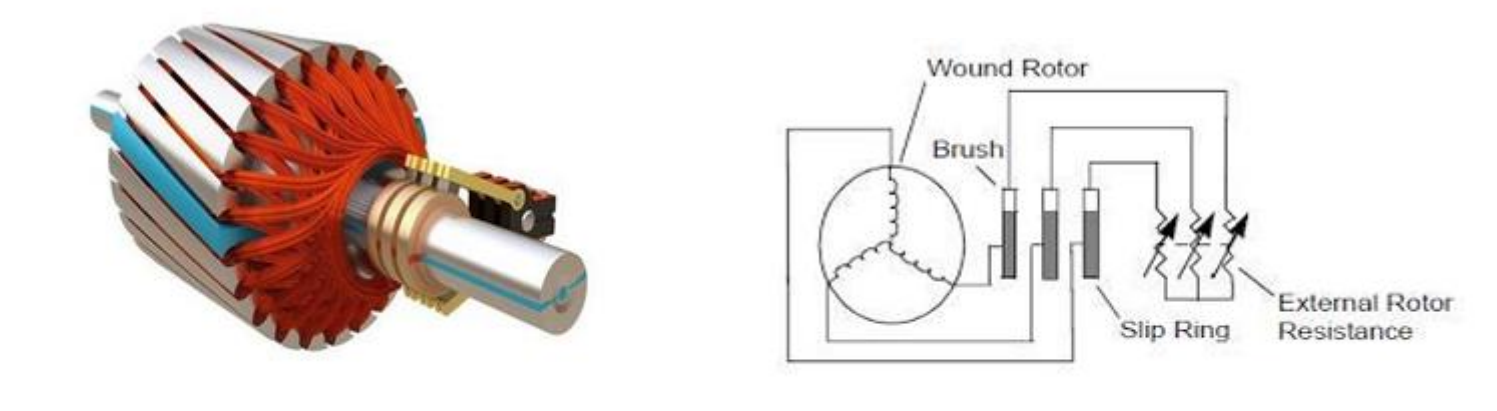


Fig. I.4: Wound Rotor

I.3 Operating Principles:

The operating principles of a three-phase induction motor involve understanding how the motor converts electrical energy into mechanical energy. This process can be explained in detail as follows:

I.3.1 Motor Mode Operation:

In motor mode, the Induction machine operates to convert electrical power into mechanical power.

Rotating Magnetic Field (RMF):

When a three-phase AC supply is applied to the stator windings, it creates a rotating magnetic field. This field rotates at the synchronous speed (ns), given by:

$$ns = \frac{60 \times f}{p}$$

where f is the frequency of the AC supply, and p is the number of poles in the motor.

• The rotating magnetic field is the result of the phase difference between the three currents, which creates a moving magnetic flux around the stator.

Induction of Electromotive Force (EMF):

- The rotating magnetic field cuts through the rotor conductors, inducing an EMF according to Faraday's Law. This induced EMF causes currents to flow in the rotor bars.
- The direction of the induced current in the rotor is such that it opposes the change in magnetic flux (Lenz's Law).

Torque Production:

- The interaction between the rotating magnetic field and the induced currents in the rotor produces a force known as Lorentz force. This force generates torque, causing the rotor to turn
- The torque (T) produced is proportional to the rotor current and the magnetic field strength, given by:

$$T=k \times \phi \times Ir \times \cos(\theta)$$

where k is a constant, ϕ is the magnetic flux, Ir is the rotor current, and θ is the phase angle between the rotor current and magnetic flux.

• The rotor speed (nr) is slightly less than the synchronous speed (ns) to allow continuous induction of EMF and current. This difference in speed is called slip (s), defined by:

$$S = \frac{ns - nr}{ns}$$

Slip and Rotor Speed:

Slip is crucial for the induction process to occur. A higher slip means more current is induced in the rotor, leading to more torque.

In steady state, the motor reaches an equilibrium where the electromagnetic torque produced matches the load torque, and the rotor rotates at a nearly constant speed.

I.3.2 Generator Mode Operation:

In generator mode, the Induction machine operates to convert mechanical power into electrical power under certain conditions.

Super-Synchronous Speed:

- When an external mechanical force (e.g., a turbine) drives the rotor to rotate faster than the synchronous speed (ns), the motor enters generator mode.
- The rotor speed (nr) is greater than the synchronous speed, resulting in a negative slip (s).

Induced EMF and Current Flow:

- As the rotor spins faster than the rotating magnetic field, it induces an EMF in the stator windings. This induced EMF causes currents to flow back into the power supply or electrical grid.
- The direction of the induced current in the stator is such that it produces a counteracting torque.

Power Generation:

- The excess mechanical energy supplied to the rotor is converted into electrical energy, which can be fed back into the electrical grid or used to power other devices.
- The power generated is proportional to the speed difference between the rotor and the synchronous speed.

Slip in Generator Mode:

- In generator mode, slip (s) is negative, indicating that the rotor speed (nr) is greater than the synchronous speed (ns).
- The negative slip causes the induced currents and generated power to flow in the opposite direction compared to motor mode.

I.4 Starting the Induction Machine:

When starting an Induction machine, the inrush current can reach several times the nominal current of the machine. If the application uses a variable speed drive or a starter, the latter will adapt the applied voltages to limit this current. In the absence of a variable speed drive, several methods exist to limit the starting current. These methods were developed before the advent of power electronics but are still used today in older installations or for cost-saving measures in applications that do not require a variable speed drive outside of startup.

I.4.1 Direct Start in One Direction of Rotation

A three-phase Induction motor is directly connected to the network. The motor is controlled by a start button and a stop button, with the stop being prioritized. This method primarily consists of a switch, a contactor, and a thermal relay.

I.4.2 Direct Start in One Direction of Rotation:

A three-phase Induction motor is directly connected to the network. The motor is controlled by a forward start button, a reverse start button, and a stop button, with the stop being prioritized. This method primarily consists of a switch, two contactors with interlocking mechanisms, and a thermal relay.

I.4.3 Star-Delta Motor Start:

In a star-delta start, the machine is initially connected to the network in a star configuration, then switched to a delta configuration once started. Starting in the star configuration allows the applied voltage to be divided by $\sqrt{3}$, thus reducing the starting current to one-third and the starting torque accordingly. The surge current during the transition from star to delta is lower than the inrush current of a direct delta start. This method is very economical and is implemented with contactors.

I.4.4 Auto-Transformer Start:

In this starting mode, the stator of the Induction machine is connected to an auto-transformer, which allows for a variable voltage start. The voltage is progressively increased, and the current intensity does not exceed the desired maximum value. This can be achieved by switching the auto-transformer's windings.

I.4.5 Resistive Start:

In a resistive start, resistances are inserted in series with the stator windings to limit the voltage at their terminals. Once the start is complete, these resistances are short-circuited. This operation can be performed progressively by an operator using starting rheostats.

I.4.6 Rotor Resistance Start

In a rotor resistance start, power resistances are inserted in series with the rotor windings. This type of start allows for a high starting torque with reduced starting currents, but it can only be implemented with wound rotor machines equipped with slip rings and brushes for electrical connections. These machines are more expensive than their squirrel-cage counterparts.

I.5 Induction Motors braking methods:

I.5.1 Counter-Current Braking

This braking method exploits the principle of rotor rotation to stop it. We know that our motor rotates because the stator generates a rotating magnetic field (CTS) and, in combination with the rotor current (CTR), the rotor is caught and put into rotation. We also know that the rotor will rotate in the same direction as the CTS. To achieve braking, we will invert two phases of the stator. This inversion should be brief, as the forces on the rotor will be significant. The rotor should not rotate in the opposite direction. This maneuver causes sudden variations in torque and stator current, which can be limited by inserting resistances in series with the stator windings during the phase inversion. It should be noted that the rotor voltage is almost double that at rest, requiring special insulation precautions. This system is mainly used for wound rotor motors.

I.5.2 Braking by DC Injection

This system is mainly used for squirrel-cage motors. It does not involve removing or reversing the rotating magnetic field but rather freezing it. This creates a magnetic brake. The rotor current (CTR) will rotate in a fixed field it must overcome, creating a braking effect proportional to the rotor speed. The braking torque is directly related to rotor rotation since it creates the flux variation for the conductors. The rotor current speed will match the rotor speed and decrease with it. However, this system becomes less effective at low speeds because the rotor current will be too weak.

I.5.3 Braking by Hyper-Synchronous Operation

In this case, the machine operates as a generator at a speed slightly above the synchronous speed. Here, the slip is negative, and it absorbs mechanical energy. This method is particularly effective for quickly braking an Induction machine without additional mechanical devices.

I.5.4 Braking by Induction Generator Operation

An Induction motor driven at a speed above synchronous speed can deliver active power to a network but will always absorb reactive power due to the high rotor frequency in this case. The phase shift of the rotor current is very high, forcing the machine to consume reactive power. This is due to the phase shift of the rotor current, which influences the phase shift of the stator current.

I.6 Simplifying Assumptions

We assume that:

- The rotor is of the squirrel-cage type, and the three-phase winding is considered equivalent for both the stator and the rotor.
- The axes of the stator and rotor phases are identically offset by an electrical angle of 120°.
- The Induction machine is perfectly symmetrical with p pairs of poles.
- The magnetomotive force created by each phase of the stator and rotor has a sinusoidal spatial distribution, resulting in a rotating magnetic field when the three-phase currents are balanced and sinusoidal.

I.7 Vector Representation of the Machine:

The Induction machine is represented in Figure I.5 by six windings in the electrical space. The angle θ marks the axis of the reference rotor phase relative to the fixed axis of the stator phase ($A\ddot{I}MER,2006$).

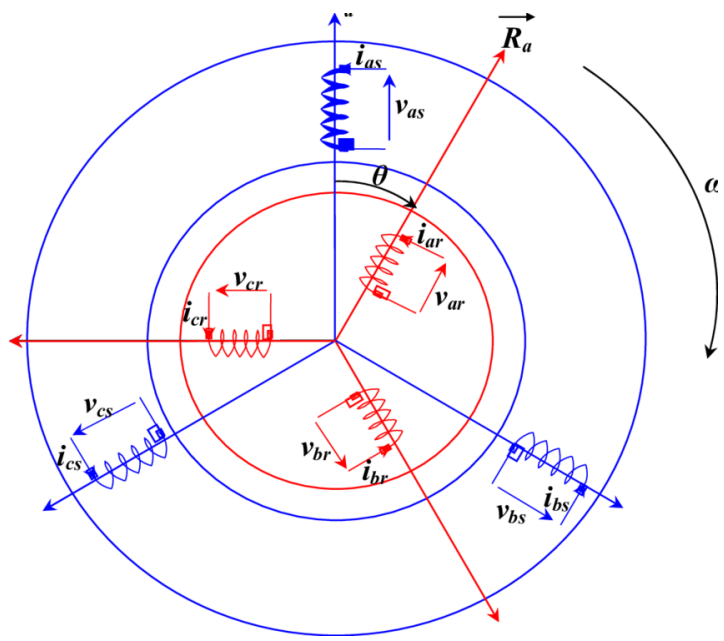


Fig I.5: Representation of the windings of the three-phase Induction machine.

I.8 Electrical Equations of the Machine:

By applying Faraday's law to the Induction machine, the mesh law is expressed by the relation (AÏMER,2006):

$$v = R i + \frac{d\phi}{dt}$$

(1.1)

The equations governing the electrical operation of the Induction machine for all stator phases can be written as follows:

$$\begin{bmatrix} v_{as} \\ v_{bs} \\ v_{cs} \end{bmatrix} = \begin{bmatrix} R_s & 0 & 0 \\ 0 & R_s & 0 \\ 0 & 0 & R_s \end{bmatrix} \cdot \begin{bmatrix} i_{as} \\ i_{bs} \\ i_{cs} \end{bmatrix} + \frac{d}{dt} \begin{bmatrix} \phi_{as} \\ \phi_{bs} \\ \phi_{cs} \end{bmatrix}$$

Or:

$$[V_s] = [R_s] \cdot [I_s] + \frac{d}{dt} [\phi_s]$$

(1.3)

(1.2)

We also deduce for all rotor phases that:

$$\begin{bmatrix} v_{ar} \\ v_{br} \\ v_{cr} \end{bmatrix} = \begin{bmatrix} R_r & 0 & 0 \\ 0 & R_r & 0 \\ 0 & 0 & R_r \end{bmatrix} \cdot \begin{bmatrix} i_{ar} \\ i_{br} \\ i_{cr} \end{bmatrix} + \frac{d}{dt} \begin{bmatrix} \phi_{ar} \\ \phi_{br} \\ \phi_{cr} \end{bmatrix}$$

$$(1.4)$$

Or:

$$[V_r] = [R_r] \cdot [I_r] + \frac{d}{dt} [\phi_r]$$
(1.5)

For a three-phase supply, and considering the previously mentioned assumptions, the relationships between flux and currents are written as follows:

$$\begin{bmatrix} [\phi_s] \\ [\phi_r] \end{bmatrix} = \begin{bmatrix} [L_s] & [M_{sr}] \\ [M_{rs}] & [L_r] \end{bmatrix} \cdot \begin{bmatrix} [I_s] \\ [I_r] \end{bmatrix}$$
(1.6)

With:

$$[L_s] = \begin{bmatrix} l_s & M_s & M_s \\ M_s & l_s & M_s \\ M_s & M_s & l_s \end{bmatrix} \text{ and } [L_r] = \begin{bmatrix} l_r & M_r & M_r \\ M_r & l_r & M_r \\ M_r & M_r & l_r \end{bmatrix}$$

And:

$$[M_{sr}] = [M_{rs}]^{-1} = M_{sr} \begin{bmatrix} \cos(\theta) & \cos\left(\theta + \frac{2\pi}{3}\right) & \cos\left(\theta - \frac{2\pi}{3}\right) \\ \cos\left(\theta - \frac{2\pi}{3}\right) & \cos(\theta) & \cos\left(\theta + \frac{2\pi}{3}\right) \\ \cos\left(\theta + \frac{2\pi}{3}\right) & \cos\left(\theta - \frac{2\pi}{3}\right) & \cos(\theta) \end{bmatrix}$$

(1.7)

Assuming that the machine has a constant air gap and its two armatures are three-phase and symmetrical, then the self and mutual inductances between windings of the same armature are constant and equal:

$$\begin{cases} 1_{As} = 1_{Bs} = 1_{Cs} = 1_{s} \\ l_{Ar} = l_{Br} = l_{Cr} = 1_{r} \end{cases}$$

$$\begin{cases} M_{AB(s)} = M_{AC(s)} = M_{BA(s)} = M_{BC(s)} = M_{CA(s)} = M_{CB(s)} = M_s \\ M_{AB(r)} = M_{AC(r)} = M_{BA(r)} = M_{BC(r)} = M_{CA(r)} = M_{CB(r)} = M_r \end{cases}$$

And:

$$\begin{cases} M_{s} = -1/2 * l_{s} \\ M_{r} = -1/2 * l_{r} \\ M_{sr} = N_{s}/N_{r} * l_{s} \end{cases}$$

Where:

 N_s : is the number of turns in each stator winding.

 N_r : is the number of turns in each rotor winding.

I.9 Coupling with the mechanical equation:

The simplest equation of a rotating body is given as (AÏMER,2006):

$$J\frac{d\Omega}{dt} + f\Omega = T_{em} - T_r$$

(1.8)

Where:

J : Moment of inertia of the rotating part;

f : Viscous friction coefficient;

 Ω : Angular velocity of rotation;

 T_{em} : Electromagnetic torque;

 T_r : Resistive torque.

I.10 Park's Model:

The system of equations for the Induction machine model is quite complex and nonlinear because the inductance matrices contain elements that vary with the rotation angle θ . To make the coefficients of this model's equation system independent of θ , the PARK transformation is used (BAGHLI.L, 2004).

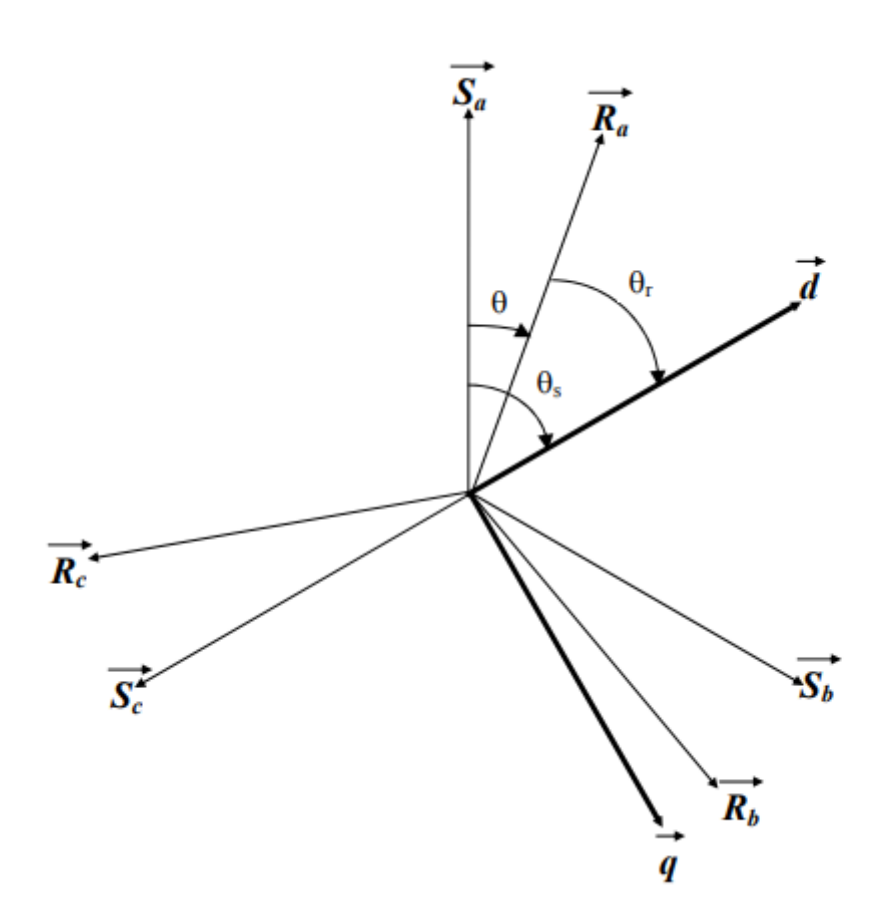


Fig. 1.6: Angular Positioning of the Machine's Fictitious Axis Systems

In the Park transformation, a single transformation matrix is defined as follows:

$$[P(\psi)] = \begin{pmatrix} \frac{2}{3} \end{pmatrix} \cdot k_1 \begin{bmatrix} \cos(\psi) & \cos\left(\psi - \frac{2\pi}{3}\right) & \cos\left(\psi + \frac{2\pi}{3}\right) \\ -\sin(\psi) & -\sin\left(\psi - \frac{2\pi}{3}\right) & -\sin\left(\psi + \frac{2\pi}{3}\right) \end{bmatrix}$$

$$\frac{1}{2k_0} \qquad \frac{1}{2k_0} \qquad \frac{1}{2k_0}$$

And its inverse is defined as:

$$[P(\psi)]^{-1} = k_1 \begin{bmatrix} \cos(\psi) & -\sin(\psi) & k_0 \\ \cos\left(\psi - \frac{2\pi}{3}\right) & -\sin\left(\psi - \frac{2\pi}{3}\right) & k_0 \\ \cos\left(\psi + \frac{2\pi}{3}\right) & -\sin\left(\psi + \frac{2\pi}{3}\right) & k_0 \end{bmatrix}$$
(1.10)

This allows, in general, the return from the two-phase d, q system to the initial three-phase a, b, c system, regardless of the electrical or electromagnetic quantities (flux, current, and voltage). The «d» axis is referred to as the direct axis and the «q» axis as the quadrature axis.

Two transformations are defined from the Park matrix, in which the angle ψ is replaced by θ_s for the stator quantities and by θ_r for the rotor quantities. These are denoted as $[P(\theta_s)]$ and $[P(\theta_r)]$. respectively. Ψ is the electrical angle between the d-axis and the a-axis of the stator or rotor phase.

They are denoted as:

 θ_s : the electrical angle (\vec{S}_a, \vec{d})

 θ_r : the electrical angle $(\overrightarrow{R_a}, \overrightarrow{d})$

It is observed from the figure that θ_s and θ_r are naturally linked to θ by a rigid relationship:

$$\theta = \theta_s - \theta_r \tag{1.11}$$

and consequently:

$$\frac{d\theta}{dt} = \frac{d\theta_s}{dt} - \frac{d\theta_r}{dt}$$

(1.12)

(1.9)

The transformation of the stator quantities is defined as:

$$\begin{cases}
[v_{dq}] = [P(\theta_s)] \cdot [v_{abc}] \\
[i_{dq}] = [P(\theta_s)] \cdot [i_{abc}] \\
[\phi_{dq}] = [P(\theta_s)] \cdot [\phi_{abc}]
\end{cases}$$
(1.13)

Where:

$$[P(\theta_s)] = \left(\frac{2}{3}\right) \begin{bmatrix} \cos(\theta_s) & \cos\left(\theta_s - \frac{2\pi}{3}\right) & \cos\left(\theta_s + \frac{2\pi}{3}\right) \\ -\sin(\theta_s) & -\sin\left(\theta_s - \frac{2\pi}{3}\right) & -\sin\left(\theta_s + \frac{2\pi}{3}\right) \\ \frac{1}{2} & \frac{1}{2} & \frac{1}{2} \end{bmatrix}$$

(1.14)

The transformation of the rotor quantities is obtained by replacing the index (s) with the index (r).

I.10.1 Electrical Equations:

The substitution of the fictitious windings S_d , S_q , R_d And R_q for the three-phase windings allows for the writing of the following equations (AÏMER, 2006):

$$\begin{aligned} \nu_{ds} &= R_s i_{ds} + \frac{d}{dt} \phi_{ds} - \frac{d\theta_s}{dt} \phi_{qs} \\ \nu_{qs} &= R_s i_{qs} + \frac{d}{dt} \phi_{qs} + \frac{d\theta_s}{dt} \phi_{ds} \\ \nu_{dr} &= R_r i_{dr} + \frac{d}{dt} \phi_{dr} - \frac{d\theta_r}{dt} \phi_{qr} \\ \nu_{qr} &= R_r i_{qr} + \frac{d}{dt} \phi_{qr} + \frac{d\theta_r}{dt} \phi_{dr} \end{aligned}$$

(1.15)

I.10.2 Magnetic Equations:

By applying the Park transformation to the flux and current equations, we obtain the electromagnetic relationships of the generalized KRON machine, as follows:

$$\begin{bmatrix} \phi_{ds} \\ \phi_{qs} \\ \phi_{dr} \\ \phi_{qr} \end{bmatrix} = \begin{bmatrix} L_s & 0 & M & 0 \\ 0 & L_s & 0 & M \\ M & 0 & L_r & 0 \\ 0 & M & 0 & L_r \end{bmatrix} \begin{bmatrix} i_{ds} \\ i_{qs} \\ i_{dr} \\ i_{qr} \end{bmatrix}$$

(1.16)

Given that: $\sigma = 1 - \frac{M^2}{L_S L_T}$; We can write:

$$\begin{bmatrix} i_{ds} \\ i_{qs} \\ i_{dr} \\ i_{qr} \end{bmatrix} = \begin{bmatrix} \frac{1}{\sigma L_s} & 0 & \frac{-M}{\sigma L_s L_r} & 0 \\ 0 & \frac{1}{\sigma L_s} & 0 & \frac{-M}{\sigma L_s L_r} \\ \frac{-M}{\sigma L_s L_r} & 0 & \frac{1}{\sigma L_r} & 0 \\ 0 & \frac{-M}{\sigma L_s L_r} & 0 & \frac{1}{\sigma L_r} \end{bmatrix} \begin{bmatrix} \phi_{ds} \\ \phi_{qs} \\ \phi_{dr} \\ \phi_{qr} \end{bmatrix}$$

(1.17)

The two-phase machine will be represented in the electrical space by figure 1.7.

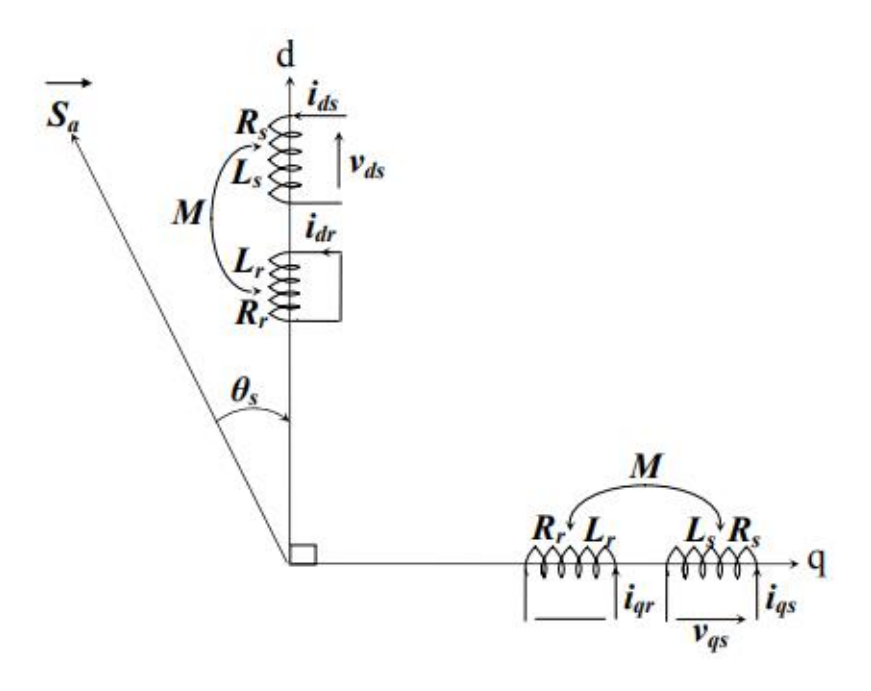


Fig. 1.7: Representation of the fictitious windings along the 'd' and 'q' axes

I.11 Choice of Reference Frame:

There are different possibilities regarding the choice of the d, q axis reference frame, depending on the application objectives (GRELLET.G, 2000):

- Axis rotating at the rotor speed $(\theta_r = 0)$: study of stator quantities.
- Axis aligned with the rotating field: study of the control.
- Axis linked to the stator ($\theta_s = 0$):: study of rotor quantities.

They are denoted as: $\omega_s = \frac{d\theta_s}{dt}$ the angular velocity of the d and q axes in the stator reference frame.

 $\omega_r = \frac{d\theta_r}{dt}$: the angular velocity of the d and q axes in the rotor reference frame, so that from the expression $(\theta = \theta_s - \theta_r)$, it follows by differentiation:

$$\omega_{s} - \omega_{r} = \frac{dq\theta}{dt} \tag{1.18}$$

The electrical equations of the machine are written as:

$$\begin{bmatrix} v_{ds} \\ v_{qs} \\ v_{dr} \\ v_{qr} \end{bmatrix} = \begin{bmatrix} R_s & 0 & 0 & 0 \\ 0 & R_s & 0 & 0 \\ 0 & 0 & R_r & 0 \\ 0 & 0 & 0 & R_r \end{bmatrix} \begin{bmatrix} i_{ds} \\ i_{qs} \\ i_{dr} \\ i_{qr} \end{bmatrix} + \frac{d}{dt} \begin{bmatrix} \phi_{ds} \\ \phi_{qs} \\ \phi_{dr} \\ \phi_{qr} \end{bmatrix} + \begin{bmatrix} -\omega_s & \phi_{qs} \\ +\omega_s & \phi_{ds} \\ -\omega_r & \phi_{qr} \\ +\omega_r & \phi_{dr} \end{bmatrix}$$

$$(1.19)$$

Rotor-Linked Reference Frame

This reference frame is denoted as (X,Y), represented by the conditions $\frac{d\theta_s}{dt} = \omega_m$ et $\frac{d\theta_r}{dt} = 0$. And the following equations:

$$v_{xs} = R_s i_{x_s} + \left(\frac{d \phi_{x_s}}{d t}\right) - \omega_r \phi_{y_s}$$

$$v_{Ys} = R_s i_{y_s} + \left(\frac{d \phi_{y_s}}{d t}\right) + \omega_r \phi_{x_s}$$

$$0 = R_r i_{x_r} + \left(\frac{d \phi_{x_s}}{d t}\right)$$

$$0 = R_r i_{y_r} + \left(\frac{d \phi_{y_r}}{d t}\right)$$

$$(1.20)$$

This choice is interesting in the study of transient states where the rotation speed is constant.

Rotating Field-Linked Reference Frame

This reference frame is denoted as (d, q). It is represented by the conditions $\frac{d\theta_s}{dt} = \omega_s$

And $\frac{d\theta_r}{dt} = \omega_s - \omega_m = \omega_{gl}$. Hence, the following equations:

$$v_{ds} = R_s i_{d_s} + \left(\frac{d \phi_{x_s}}{d t}\right) - \omega_s \phi_{q_s}$$

$$v_{qs} = R_s i_{q_s} + \left(\frac{d \phi_{q_s}}{d t}\right) + \omega_s \phi_{d_s}$$

$$0 = R_r i_{d_r} + \left(\frac{d \phi_{dr}}{d t}\right) - \omega_{gl} \phi_{qr}$$

$$0 = R_r i_{y_r} + \left(\frac{d \phi_{y_r}}{d t}\right) + \omega_{gl} \phi_{qr}$$

(1.21)

The rotating field requires the presence of an additional variable to define its position. This reference frame is chosen to perform classical control methods (scalar and vector control).

Stator-Linked Reference Frame

This reference frame is denoted as (α, β) and is represented by the conditions: $\frac{d\theta_s}{dt} = 0$; $\frac{d\theta_r}{dt} = -\omega_m$.

$$v_{as} = R_s i_{cs} + \left(\frac{d\phi_{cs}}{dt}\right)$$

$$v_{bs} = R_s i_{\beta s} + \left(\frac{d\phi_{\beta s}}{dt}\right)$$

$$0 = R_r i_{cx} + \left(\frac{d\phi_{cx}}{dt}\right) + \omega_m \phi_{\beta s}$$

$$0 = R_r i_{\beta r} + \left(\frac{d\phi_{\beta r}}{dt}\right) - \omega_m \phi_{cx}$$

(1.22)

This reference frame is chosen in cases of significant derivations in rotation speed, whether or not associated with variations in supply frequency. The representation of the various previously defined reference frames is illustrated in Figure 1.8.

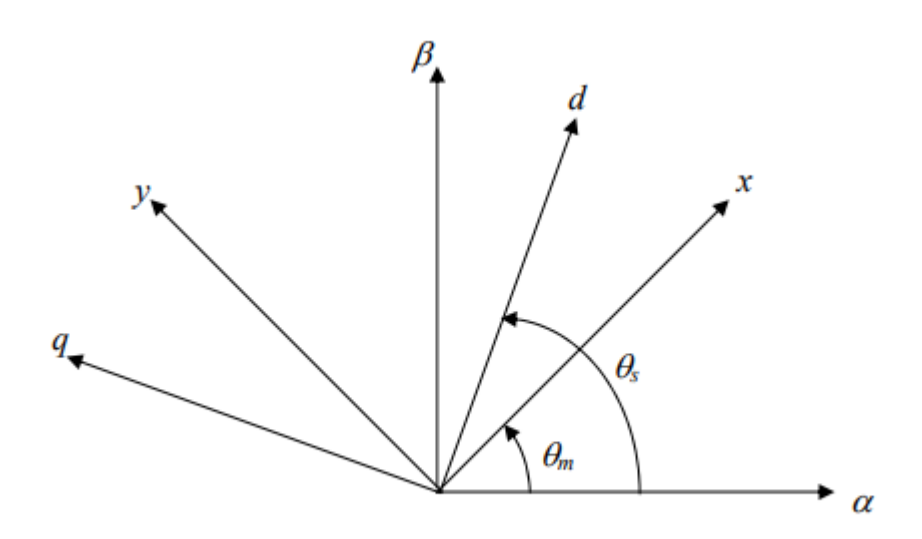


Fig. 1.8: Representation of the various reference frames

I.12 State Representation of Park:

I.12.1 Description:

For a three-phase Induction machine fed by voltage, the stator voltages $(v_{as}, v_{\beta s})$ are considered as input variables, and the load torque (T_r) as a disturbance. We choose the stator-linked reference frame, assuming that $(v_{\alpha r} = 0)$ and $(v_{\beta r} = 0)$ (AÏMER,2006).

I.12.2 State Equations:

The state representation involves expressing the mathematical model of the Induction machine in the following form:

$$\frac{dX}{dt} = AX + Bu$$

where: *X*: state vector

u:input vector

There are various possibilities for choosing the state vector. Among these possibilities, we can choose the stator currents, rotor currents, and electrical speed is $(i_{\alpha s}, i_{\beta s}, i_{\alpha r}, i_{\beta r}, \omega)$ or the stator fluxes, rotor fluxes, and electrical speed $(\phi_{\alpha s}, \phi_{\beta s}, \phi_{\alpha r}, \phi_{\beta r}, \omega)$ stator fluxes, stator currents, and electrical speed $(\phi_{\alpha r}, \phi_{\beta r}, i_{\alpha s}, i_{\beta s}, \omega)$, or the rotor fluxes, stator currents, and electrical speed $(\phi_{\alpha s}, \phi_{\beta r}, \phi_{\alpha r}, \phi_{\beta r}, \omega)$ as state variables.

First, let's consider the stator fluxes, rotor fluxes, and electrical speed $(\phi_{\alpha s}, \phi_{\beta s}, \phi_{\alpha r}, \phi_{\beta r}, \omega)$ as state variables.

From equation (1.22), we can write:

$$\frac{d}{dt} \begin{bmatrix} \phi_{\alpha s} \\ \phi_{\beta s} \\ \phi_{\alpha r} \\ \phi_{\beta r} \end{bmatrix} = -C \cdot \begin{bmatrix} i_{\alpha s} \\ i_{\beta s} \\ i_{\alpha r} \\ i_{\beta r} \end{bmatrix} - D \cdot \begin{bmatrix} \phi_{\alpha s} \\ \phi_{\beta s} \\ \phi_{\alpha r} \\ \phi_{\beta r} \end{bmatrix} + B \cdot u$$
(1.23)

Where:

By substituting the currents with their expression given by equation (1.17), we obtain the following state equation of the Induction machine model:

$$\frac{dX}{dt} = AX + Bu \tag{1.24}$$

Where:

$$\mathbf{A} = \begin{bmatrix} \frac{-1}{\sigma T_s} & 0 & \frac{M}{\sigma L_r T_s} & 0 \\ 0 & \frac{-1}{\sigma T_s} & 0 & \frac{M}{\sigma L_r T_s} \\ \frac{M}{\sigma L_s T_r} & 0 & \frac{-1}{\sigma T_r} & -\omega_m \\ 0 & \frac{M}{\sigma L_s T_r} & \omega_m & \frac{-1}{\sigma T_r} \end{bmatrix} \quad \text{et} \quad X = \begin{bmatrix} \phi_{\alpha s} \\ \phi_{\beta s} \\ \phi_{\alpha r} \\ \phi_{\beta r} \end{bmatrix}$$

 T_s : the stator time constant, its expression is written as $\frac{L_s}{R_s}$

 σ : the *leakage coefficient* or *dispersion factor*

Torque Equation

The torque expression is written as (AÏMER,2006):

$$T_{em} = p \frac{M}{\sigma L_s L_r} (\phi_{\alpha r} \phi_{\beta s} - \phi_{\alpha s} \phi_{\beta r})$$
(1.25)

The torque equation can be expressed in other forms:

$$T_{em} = pM(i_{\alpha r}i_{\beta s} - i_{\alpha s}i_{\beta r}) \tag{1.26}$$

$$T_{em} = p(\phi_{\alpha s}i_{\beta s} - \phi_{\beta s}i_{\alpha s}) \tag{1.27}$$

$$T_{em} = p \frac{M}{L_s} (\phi_{\beta s} i_{\alpha r} - \phi_{\alpha s} i_{\beta r})$$
(1.28)

$$T_m = p \frac{M}{L_r} (\phi_{\alpha r} i_{\beta s} - \phi_{\beta r} i_{\alpha s})$$
 (1.29)

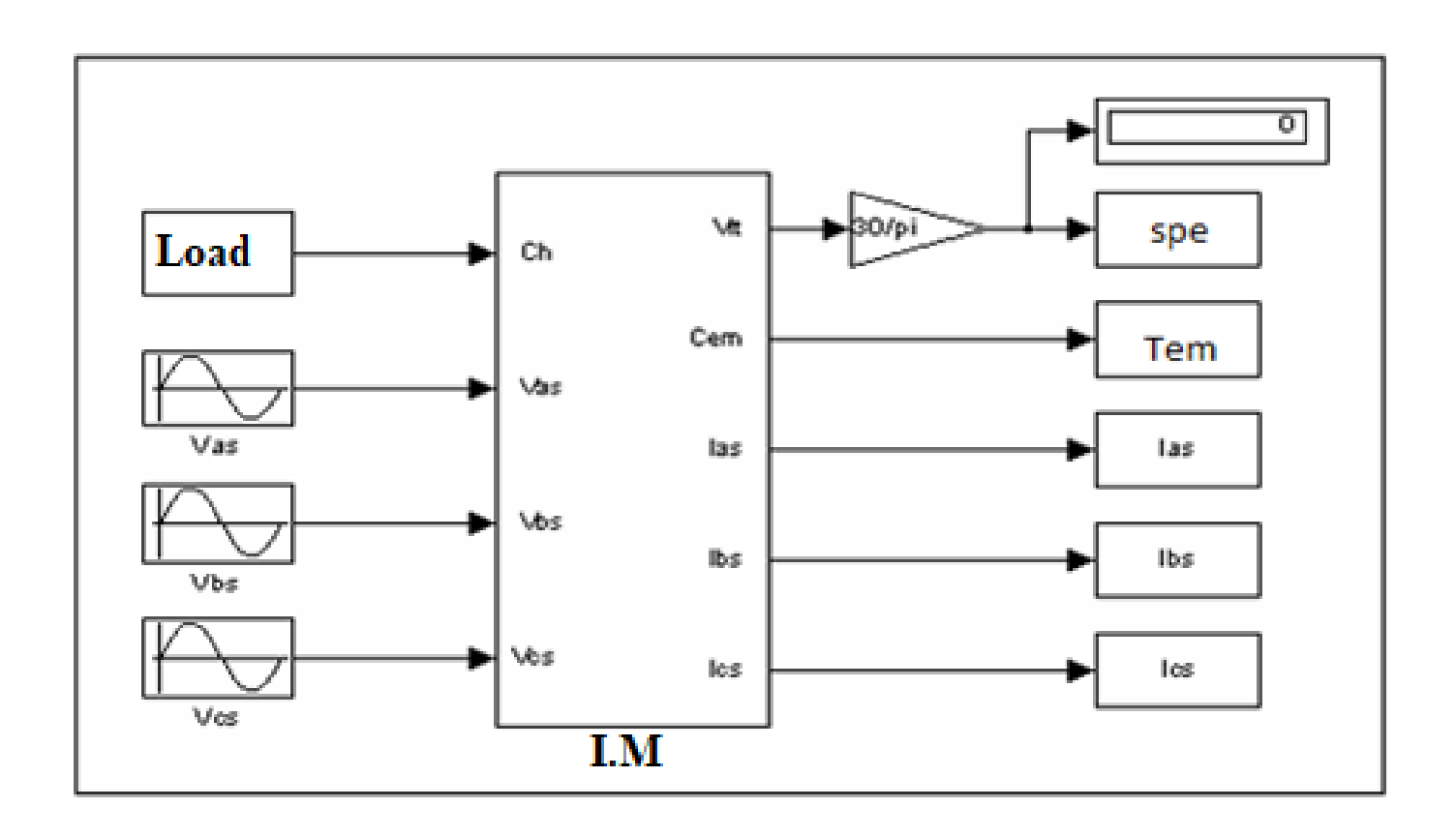
I.13 Numerical Simulation:

Numerical simulation is an efficient and economical means, commonly used in the field of electrical machines. Several simulation software packages are currently in use; we will use MATLAB/SIMULINK software to simulate the three-phase voltage-fed Induction machine and various associated controls to validate our models (KHERRAZ,2023).

- The block diagram representing the voltage-fed Induction machine is illustrated in Figure I.9
- Direct start of the unloaded Induction motor without an inverter is represented in Figure I.10.a.
- Direct start of the loaded Induction motor without an inverter is represented in Figure I.10.b.

I.14 Results and Discussion:

- Unloaded Start without Inverter (Figure I.10.a): During the unloaded start of the voltage-fed Induction motor, the electromagnetic torque is highly oscillatory and becomes almost zero in steady state. The starting torque reaches the value of 47.5 N.m, allowing for a quick dynamic response. As can be seen, the starting current reaches values equal to 5 times its steady-state value before returning to its nominal value. The motor runs near to the synchronous speed of 1500 rpm (157 rad/sec) since the load is zero (negligible slip). This speed is reached in approximately 0.22 sec.
- Loaded Start without Inverter (Figure I.10.b): During the start of the Induction motor with a 10 N.m load, the electromagnetic torque tends towards the value of the load torque in steady state, and the current amplitude reaches a value corresponding to the nominal current. The significant starting torque allows reaching steady state quickly. Regarding speed, a drop of 80 rpm is observed, primarily due to the application of the load. This speed is reached in approximately 0.36 sec.



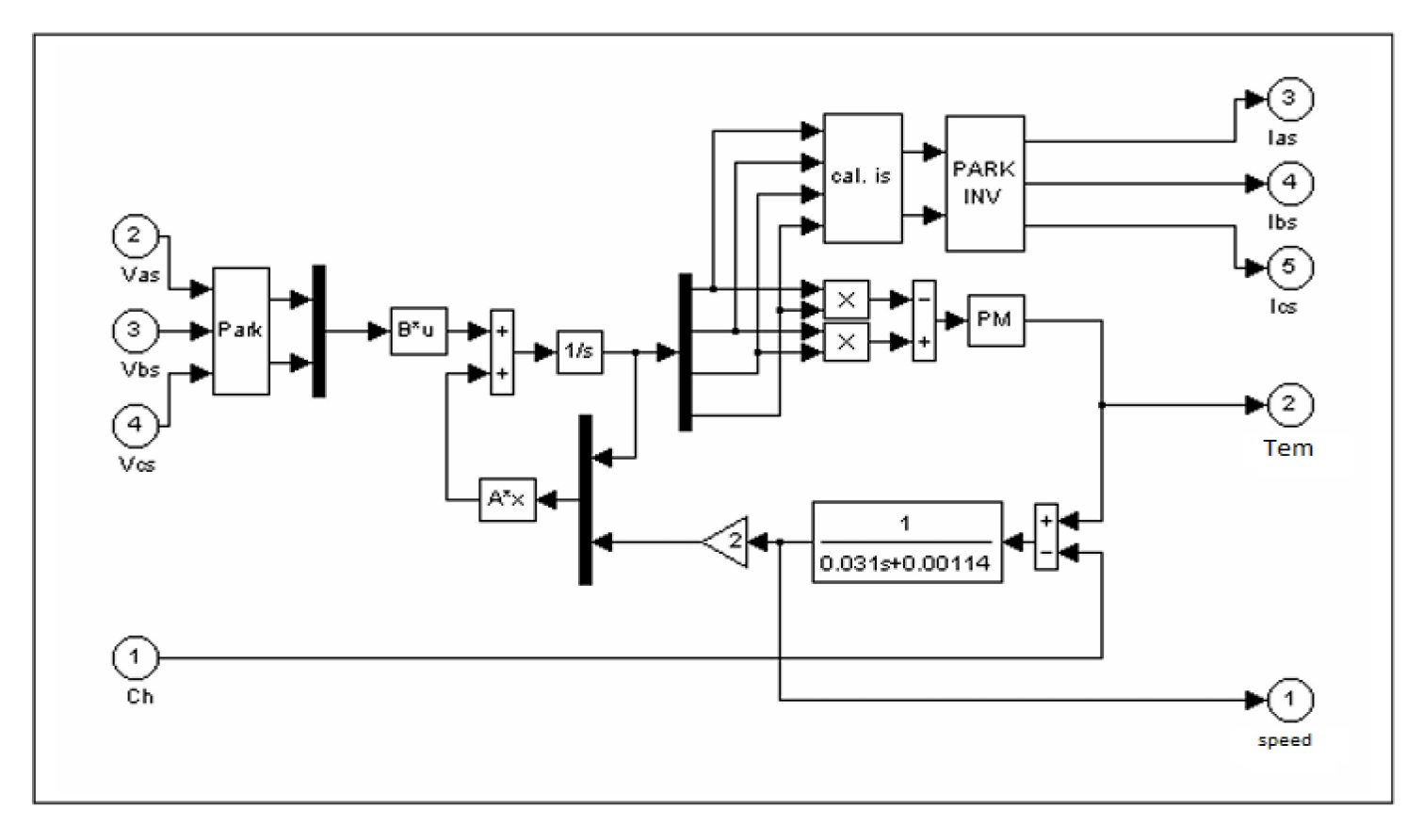


Figure 1.9: Block diagram of the voltage-fed Induction machine.

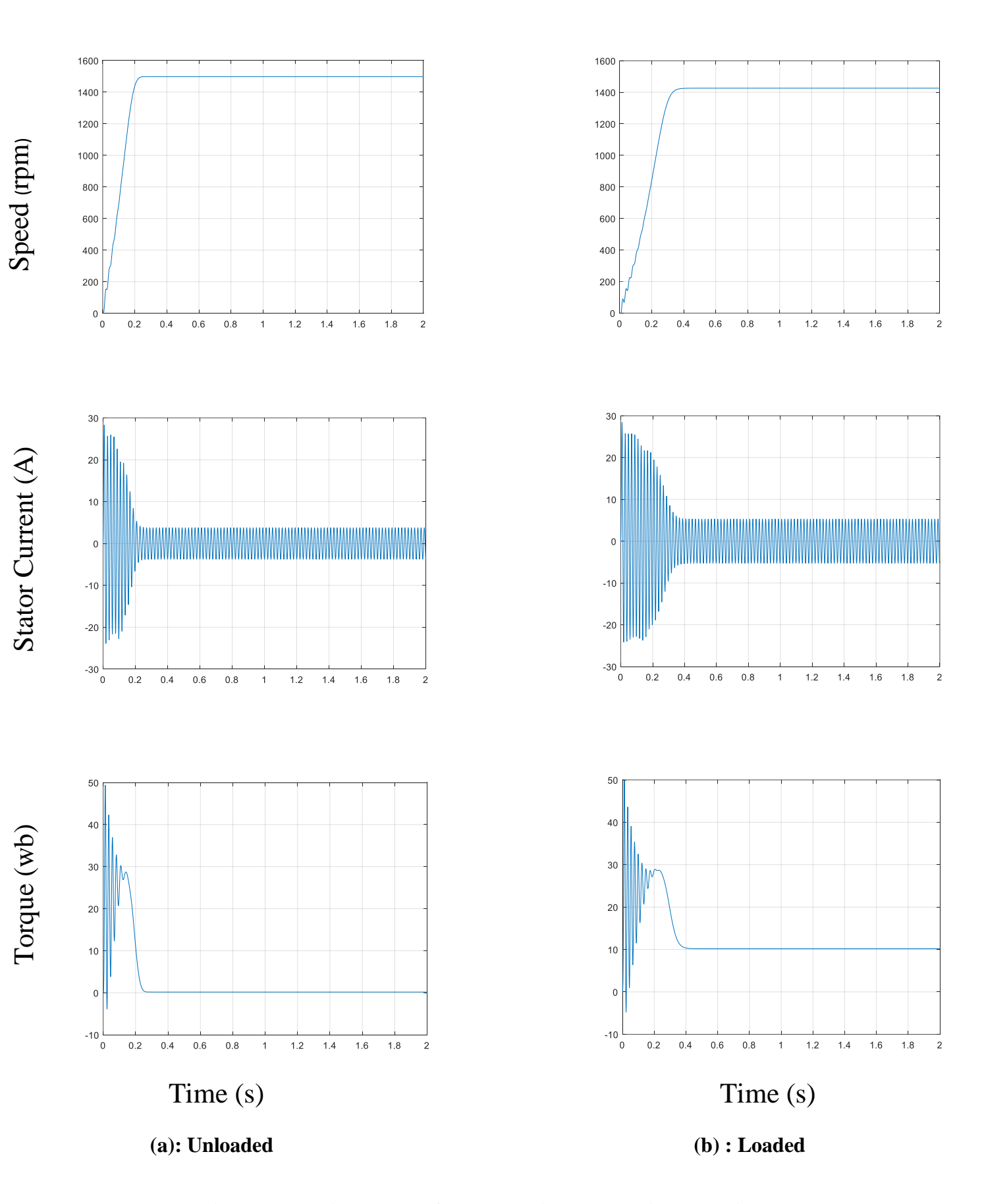


Figure 1.10: Direct start of the Induction motor without an inverter.

I.15 Conclusion:

This chapter has provided an in-depth exploration of three-phase induction motors, covering their structure, operating principles, starting methods, braking techniques, and mathematical models. Starting with an introduction, we detailed the components of the Induction machine, namely the stator and rotor, and their functions in motor operation.

In addition, simplifying assumptions allowed us to focus on core concepts, while vector representation and electrical equations provided a mathematical framework for analysis.

Furthermore, we explored different models like the Park models, which are crucial for understanding the motor's dynamic behavior. The chapter also included a numerical simulation, illustrating practical applications and validating theoretical models.

The discussion and interpretation section helped synthesize the information, highlighting key insights and practical implications. This comprehensive overview lays the groundwork for more advanced topics and simulations in the subsequent chapters, deepening our understanding of three-phase induction motors and their significance in modern engineering.

Building upon the fundamental principles explored in this chapter, the next section will focus on Direct Torque Control (DTC), an advanced control strategy designed to optimize torque and flux response in three-phase induction motors. This approach is particularly significant for highperformance applications, as it offers superior dynamic behavior and eliminates the need for traditional modulation techniques. The following chapter will delve into the theoretical foundations of DTC, its implementation with two-level voltage and the stability inverters, considerations essential for ensuring precise and efficient motor control.

Chapter II Study of Direct Torque Control (DTC)

II Introduction:

To overcome the sensitivity issues to parametric variations, control methods have been developed in which the flux and electromagnetic torque are estimated solely from the electrical quantities accessible at the stator, without the use of mechanical sensors. Among these methods, direct torque control, based on the orientation of the stator flux, was introduced in 1985 by TAKAHASHI and DEPENBROCK (TAKAHASHI,1986). The search for the most suitable switching state at any given moment relies on a heuristic approach to the behavior of flux and torque variations based on the considered switching states.

The aim of this chapter is to define an initial direct control strategy compatible with multilevel voltage inverters with any number of levels. At this stage of the study, the objective is to ensure the stability of the control of the machine's main variables (torque and stator flux).

II.1 Definition of Inverter:

Inverters are static converters that provide DC to AC conversion. For example, if we have a direct current (DC) input voltage, thanks to the presence of semiconductors, we can connect each terminal of the receiver sometimes to one input terminal and sometimes to another input terminal. This way, we can obtain a voltage that is sometimes positive and sometimes negative between the terminals of the receiver. By sufficiently controlling the semiconductor sequence, it is possible to produce an alternating voltage with an average value of zero, which may alternatively contain one or more slots depending on whether it is controlled by alternative modulation or pulse-width modulation (PWM). If the establishment, maintenance, and opening of connections between inputs and outputs depend solely on the control of semiconductors, the inverter is said to be autonomous.

II.2 Power Supply:

An inverter's power supply typically comes from a DC source, like batteries or rectified AC power. It converts DC into AC using electronic switches (MOSFETs, IGBTs) to regulate voltage and frequency. The output powers various applications, from motor drives to renewable energy systems.

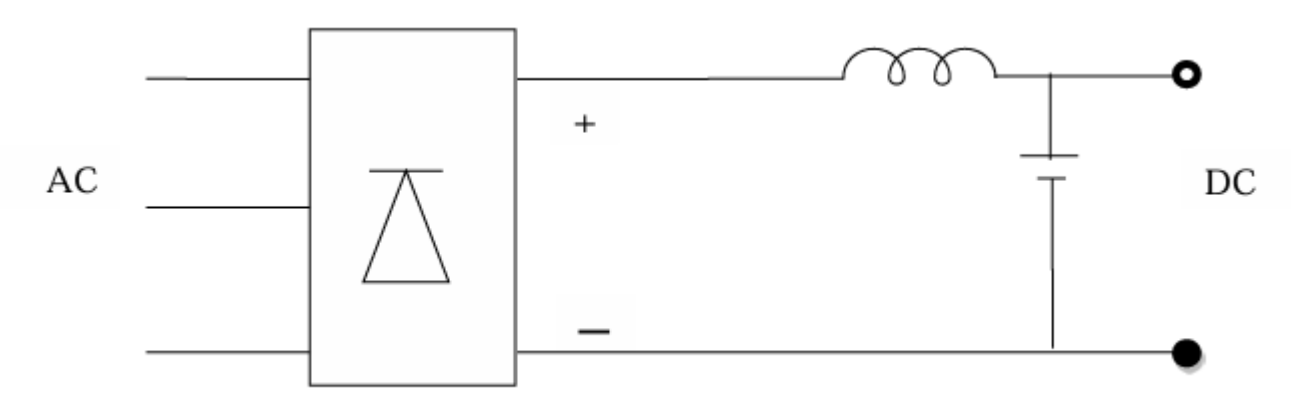


Figure II.1. Power Supply

II.3 Construction of a Three-Phase Inverter:

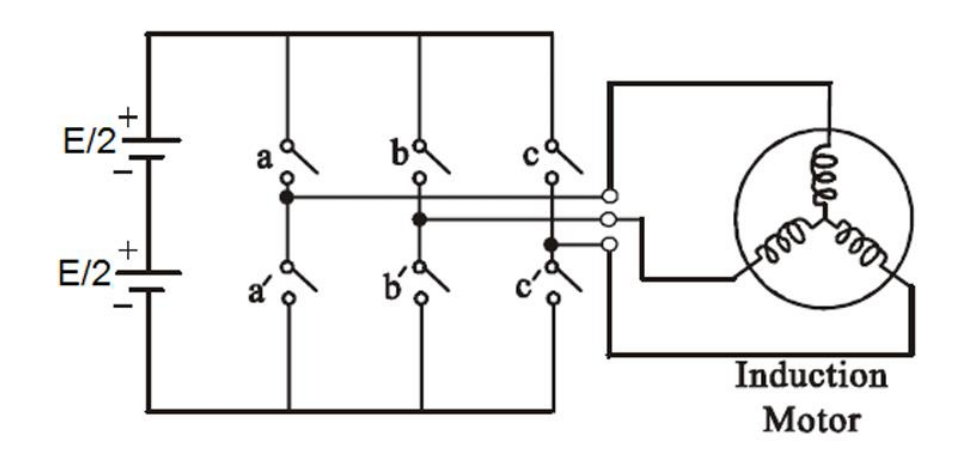


Figure II.2. Representation of a Three-Phase Inverter

II.4 Modeling of the Two-Level Voltage Inverter:

The schematic diagram of the principle of the three-phase inverter with two voltage levels, mounted in a bridge configuration and supplying a load, is given in figure II.3. The DC voltage is generally obtained by a three-phase diode rectifier followed by an LC filter.

It is a two-level voltage inverter, having six switching cells and six freewheeling diodes. Each arm of the inverter consists of two switching cells, each composed of a switch with its diode, with the output corresponding to the midpoint of the arm. The control signals of the switches in each arm must be complementary to avoid short-circuiting the DC supply of the inverter. To prevent accidental short circuits, it is necessary to introduce a waiting time for the switch to close, usually called dead time.

The most commonly used semiconductors for switches are power transistors (MOSFET, IGBT, Bipolar) and fast thyristors (mainly GTO).

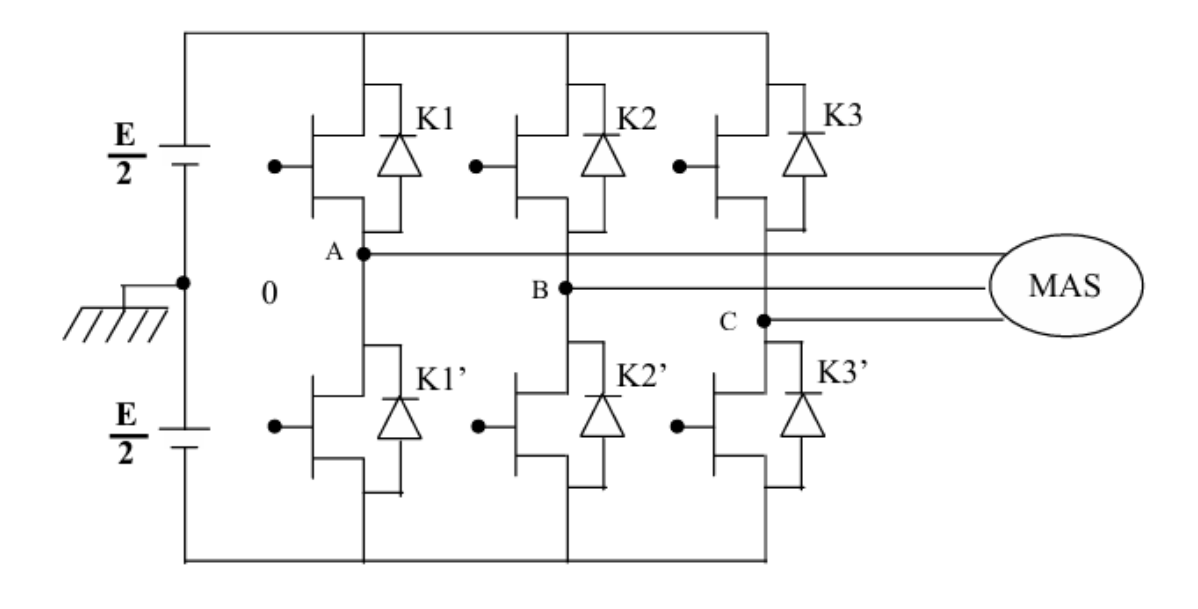


Figure II.3. Representation of a Three-Phase Two-Level Inverter

The three-phase inverter with six switches is formed by three single-phase half-bridges with two levels. The output voltages at the terminals of the inverter are referenced to the fictitious point 0 of the inverter source; they have the expression (KHERRAZ,2023):

$$v_{j} - v_{0} = \begin{cases} +\frac{E}{2} & \text{if Ki : closed} & j = A, B, C \\ -\frac{E}{2} & \text{if Ki' : closed} & i = 1, 2, 3 \end{cases}$$

$$(2.1)$$

Hence, We Can Write:

$$v_{AB} = (v_A - v_O) - (v_B - v_O)$$

$$v_{BC} = (v_B - v_O) - (v_C - v_O)$$

$$v_{CA} = (v_C - v_O) - (v_A - v_O)$$
(2.2)

The voltages at the terminals of the inverter can be written as:

$$v_{AB} = v_{AO} - v_{BO}$$
 $v_{BC} = v_{BO} - v_{CO}$
 $v_{CA} = v_{CO} - v_{AO}$
(2.3)

Knowing that:

$$\overrightarrow{\nu_{AN}} + \overrightarrow{\nu_{BN}} + \overrightarrow{\nu_{CN}} = 0 \tag{2.4}$$

We can write:

$$\begin{cases} v_{AN} = v_{AO} + v_{ON} \\ v_{BN} = v_{BO} + v_{ON} \\ v_{CN} = v_{CO} + v_{ON} \end{cases}$$
(2.5)

Single-phase voltages at the terminals of the star-connected load:

$$v_{AN} = \frac{1}{3}(2v_{AO} - v_{BO} - v_{CO})$$

$$v_{BN} = \frac{1}{3}(2v_{BO} - v_{AO} - v_{CO})$$

$$v_{CN} = \frac{1}{3}(2v_{CO} - v_{AO} - v_{BO})$$

(2.6)

 v_{AO} ; v_{BO} , and v_{CO} are respectively the voltages between phases A, B, and C and the fictitious neutral of the source.

We can rewrite equation (2.6) in matrix form (KHERRAZ,2023):

$$\begin{bmatrix} v_{AN} \\ v_{BN} \\ v_{CN} \end{bmatrix} = \frac{1}{3} \begin{bmatrix} 2 & -1 & -1 \\ -1 & 2 & -1 \\ -1 & -1 & 2 \end{bmatrix} \cdot \begin{bmatrix} v_{AO} \\ v_{BO} \\ v_{CO} \end{bmatrix}$$
(2.7)

The voltages between phases and the fictitious neutral can be given as a function of the signals by:

$$\nu_{AO} = E \cdot S_A$$

$$\nu_{BO} = E \cdot S_B$$

$$\nu_{CO} = E \cdot S_C$$
(2.8)

Where: Sj (j = A, B, C) are the logical functions representing the state of the electrical switches (K1, K2, K3), whose switching is assumed to be instantaneous.

- Sj=1: Upper switch (K) closed and lower switch (K') open.
- Sj=0: Upper switch (K) open and lower switch (K') closed.

The voltages at the terminals of the machine are given by:

$$\nu_{AN} = \frac{E}{3} (2S_A - S_B - S_C)$$

$$\nu_{BN} = \frac{E}{3} (2S_B - S_A - S_C)$$

$$\nu_{CN} = \frac{E}{3} (2S_C - S_A - S_B)$$

(2.9)

Equation (2.9) can be rewritten in matrix form:

$$\begin{bmatrix} v_{AN} \\ v_{BN} \\ v_{CN} \end{bmatrix} = \frac{E}{3} \begin{bmatrix} 2 & -1 & -1 \\ -1 & 2 & -1 \\ -1 & -1 & 2 \end{bmatrix} \cdot \begin{bmatrix} S_A \\ S_B \\ S_C \end{bmatrix}$$

(2.10)

II.5 Hysteresis Control

Hysteresis control, also known as on-off control, is a non-linear control method that uses the existing error between the reference current and the current produced by the inverter. This error is compared to a template called the hysteresis band.

The simplest approach used for this purpose is the control strategy that compares the measured phase current to the reference current (Fig. III-4) using a hysteresis comparator. This comparator produces triggering and blocking pulses for the inverter switches, thereby limiting the phase current within a hysteresis band around the reference current (**Figure (II.4)** (AKKOUCHI,2007).

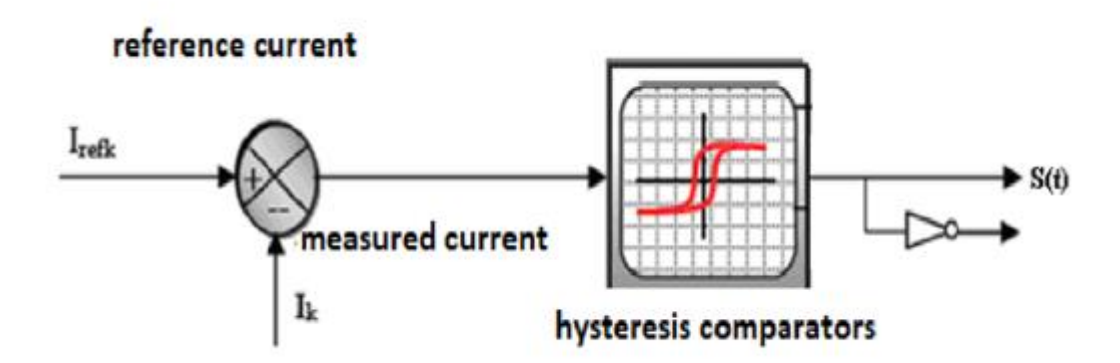


Figure (II.4): Schematic Diagram of Hysteresis Control of an Inverter Arm

As a result, the switching conditions of the three static switches Ki (i = a, b, c) of the inverter are defined in terms of the corresponding logical states as follows:

$$\begin{aligned} & \text{Ki} = +1 & \text{si} \quad I^*i - Ii > \Delta i. \\ & \text{Ki} = 0 & \text{si} \quad I^*i \cdot Ii < \Delta i. \\ & \text{K}_i = -\text{K}_{i-1} & \text{si} \quad I^*i = I_i. \end{aligned}$$

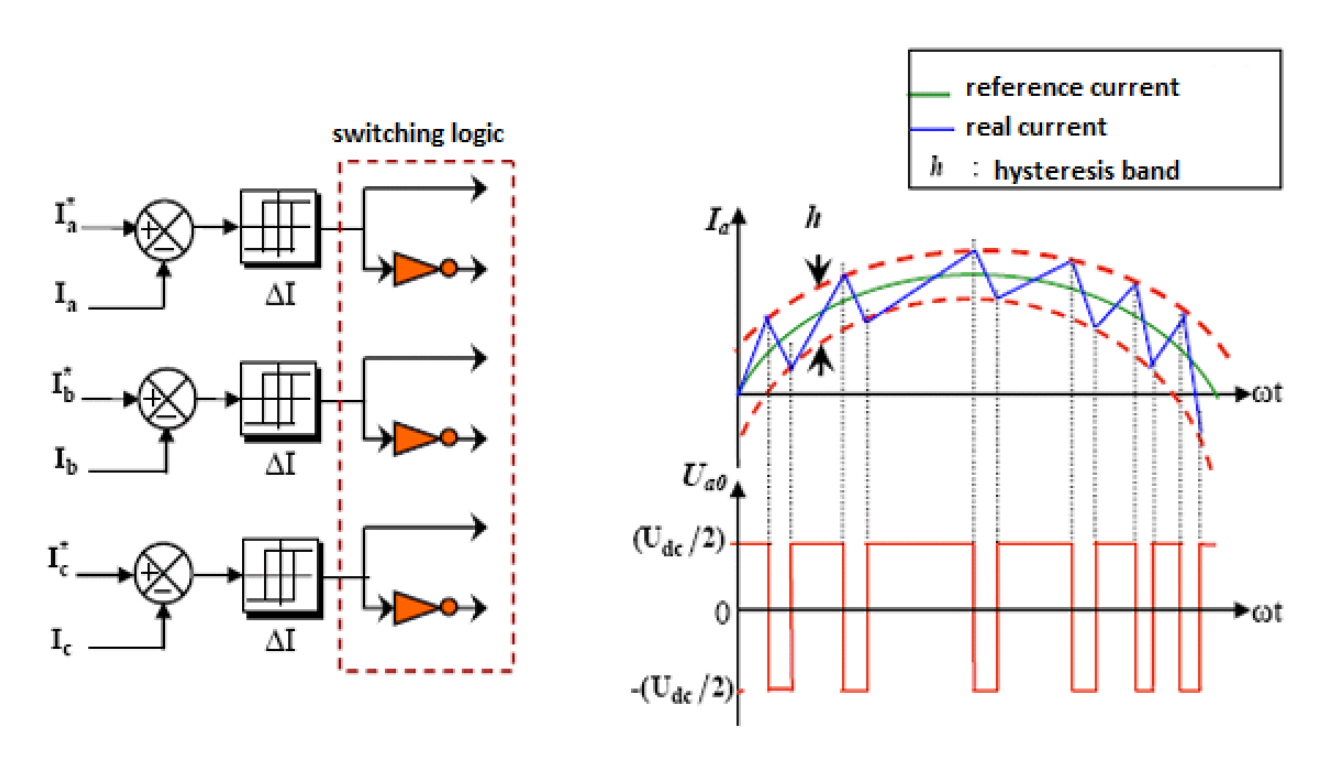


Figure (II-5): Hysteresis Control

Such as:

 I_i (i = a, b, c) are the stator phase currents (I_a, I_b, I_c)

 I^*i (i = a, b, c) are the reference currents from the control circuits of the three arms.

h: is the hysteresis band, it is chosen so as not to exceed the permissible switching frequency of the controlled semiconductors and to sufficiently minimize current harmonics.

II.6 Pulse Width Modulation (PWM):

The output quantities of the analog or digital inverter controls are used to obtain the desired voltages or currents at the terminals of the machine. The pulse width modulation technique (MLI in French and PWM for Pulse Width Modulation in English) allows these quantities to be reconstructed from a fixed-frequency and fixed-voltage source (generally a direct current voltage) through a direct converter. This method is commonly used in power electronics to efficiently control the power supplied to electrical devices.

This system establishes electrical connections between the source and the load. The control is carried out by adjusting the opening and closing times of switches and by modifying duty cycles.

There are multiple pulse width modulation techniques, but four main categories have been developed:

- **Sinusoidal-Triangle Modulation:** Compares a reference signal to a carrier, usually a triangular waveform.
- **Precomputed Modulations:** Switching angles are calculated offline to eliminate specific spectral components.
- **Postcomputed Modulations:** Also known as regular symmetric or vectorial PWM, where switching angles are calculated in real-time.
- Stochastic Modulations: Aim to whiten the spectrum (constant and minimal noise throughout). Pulse widths are distributed according to a probability density function representing the control law.

II.7 Space Vector Modulation:

Vectorial Pulse Width Modulation, also known as Space Vector Modulation (SVM), is widely used in modern control systems for induction machines. This method enables the generation of arbitrary waveforms that are not necessarily sinusoidal while maintaining a fixed switching frequency. In this study, it will be applied to a three-phase inverter, where the reference voltages correspond to the desired phase voltages.

This modulation technique follows these principles:

- The reference signal is sampled at regular intervals TT, ensuring a consistent modulation pattern (regular PWM).
- At each sampling interval, a pulse of width T is generated, centered within the interval (symmetric PWM), with its average value equal to the reference voltage at the midpoint of the sampling interval.
- All switches in the same half-bridge share the same state at the center and at both ends of the cycle. In the case of discontinuous PWM, one switch in each half-bridge remains constant, reducing switching losses but increasing harmonics.

This modulation is synchronized across all three phases and is known as Vectorial PWM. In this method, the three desired sinusoidal output voltages are represented by a single voltage vector.

The goal is to approximate the reference voltage vector as closely as possible during each modulation interval by controlling the three pairs of complementary switches: **K1 and K1', K2 and K2', K3 and K3'**, as shown in **Figure 2.2** (Benslimane, 2022).

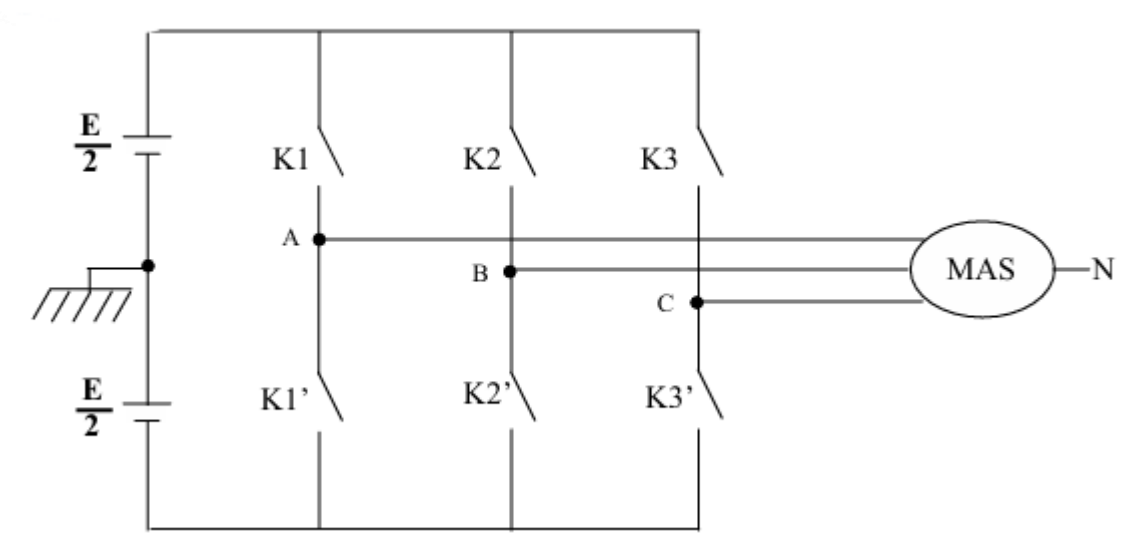


Figure II.6: Simplified Structure of a Three-Phase Inverter

A three-phase two-level inverter consists of six switching cells, providing eight possible configurations (2³) for all switches. These eight switching states can be represented in the (α, β) plane **as** eight voltage vectors.

Among these vectors, two are null, while the remaining six are evenly spaced every 60°.

II.7.1 Advantages of Vectorial Modulation :

Vectorial modulation does not provide significant benefits over sub-optimal sinustriangle modulation in terms of voltage loss or harmonic residue. However, it is increasingly preferred in variable-speed drive **systems** using synchronous or induction motors powered by voltage inverters. The reason for this preference is that vectorial modulation integrates naturally into the regulation systems of these drives, making it well-suited for efficient motor control.

II.7.2 Clark Transformation:

Let us consider $\begin{pmatrix} v_{AN} \\ v_{BN} \\ v_{CN} \end{pmatrix}$ as the desired voltage vector at the output of the inverter. The phase voltages are given by equation 2.6. If the load is balanced, we will have (AÏMER,2006):

$$\nu_{AN} + \nu_{BN} + \nu_{CN} = 0 {(2.11)}$$

Hence, we obtain:

$$v_{AN} = \frac{1}{3}(2 \quad v_{AO} - v_{BO} - v_{CO})$$

$$v_{BN} = \frac{1}{3}(2 \quad v_{BO} - v_{AO} - v_{CO})$$

$$v_{CN} = \frac{1}{3}(2 \quad v_{CO} - v_{AO} - v_{BO})$$
(2.12)

To simplify the calculations and represent these voltages, we use the three-phase/two-phase transformation known as CLARK transformation while respecting power transfer. The CLARK transformation consists of substituting the three real variables ν_A , ν_B and ν_C with their components ν_α , ν_β , and ν_O . These components are given by:

$$\nu_{s\alpha} = \sqrt{\frac{2}{3}} \left(\nu_{AN} - \frac{1}{2} \nu_{BN} - \frac{1}{2} \nu_{CN} \right)$$

$$\nu_{s\beta} = \sqrt{\frac{2}{3}} \left(\frac{\sqrt{3}}{2} \nu_{BN} - \frac{\sqrt{3}}{2} \nu_{CN} \right)$$

(2.13)

The equation in matrix form is expressed by the following relation:

$$\begin{bmatrix} v_{s\alpha} \\ v_{s\beta} \end{bmatrix} = \sqrt{\frac{2}{3}} \cdot \begin{bmatrix} 1 & -\frac{1}{2} & -\frac{1}{2} \\ 0 & \frac{\sqrt{3}}{2} & -\frac{\sqrt{3}}{2} \end{bmatrix} \cdot \begin{bmatrix} v_{AN} \\ v_{BN} \\ v_{CN} \end{bmatrix}$$

(2.14)

The component ν_o is identically zero, since the voltages ν_A , ν_B , and ν_C do not contain a zero-sequence component. The principle of vector PWM (Pulse Width Modulation) consists of projecting the desired stator voltage vector ν_S onto the two adjacent voltage vectors corresponding to two switching states of the inverter.

Table II.1: Calculation of Voltage Vectors

K ₁	\mathbf{K}_2	K ₃	\mathbf{v}_{AO}	\mathbf{v}_{Bo}	$\mathbf{v}_{\mathbf{co}}$	V _{AN}	\mathbf{V}_{BN}	\mathbf{v}_{cn}	\mathbf{v}_{α}	\mathbf{v}_{β}	$\mathbf{v}_{\mathbf{s}}$
0	0	0	-E/2	-E/2	-E/2	0	0	0	0	0	$\overset{ ightarrow}{V_0}$
1	0	0	E/2	-E/2	-E/2	2E/3	-E/3	-E/3	$\frac{\sqrt{2}}{\sqrt{3}}E$	0	\overrightarrow{V}_1
1	1	0	E/2	E/2	-E/2	E/3	E/3	-2E/3	$\frac{1}{\sqrt{6}}E$	$\frac{1}{\sqrt{2}}E$	\overrightarrow{V}_2
0	1	0	-E/2	E/2	-E/2	-E/3	2E/3	-E/3	$\frac{-1}{\sqrt{6}}E$	$\frac{1}{\sqrt{2}}E$	$\vec{V_3}$
0	1	1	-E/2	E/2	E/2	-2E/3	E/3	E/3	$\frac{-\sqrt{2}}{\sqrt{3}}E$	0	$\overrightarrow{V_4}$
0	0	1	-E/2	-E/2	E/2	-E/3	-E/3	2E/3	$\frac{-1}{\sqrt{6}}E$	$\frac{-1}{\sqrt{2}}E$	$\vec{V}_{\scriptscriptstyle{5}}$
1	0	1	E/2	-E/2	E/2	E/3	-2E/3	E/3	$\frac{1}{\sqrt{6}}E$	$\frac{-1}{\sqrt{2}}E$	$\overrightarrow{V_6}$
1	1	1	E/2	E/2	E/2	0	0	0	0	0	$\vec{V_7}$

We have indicated in Table II.1 the eight states that the switches of the three-phase bridge with six switches can take. This table shows, for each of these eight states, the voltage vectors (v_{AN}, v_{BN}, v_{CN}) the value of their CLARK components v_{α}, v_{β} and the reference vector v_{S} representative of these states.

Two of these vectors are identically zero. The other six have the same magnitude equal to: $\int_{3}^{2} E$

The ends of these six vectors define the vertices of a regular hexagon represented in Figure II.7, since two successive vectors form an angle of 60° .

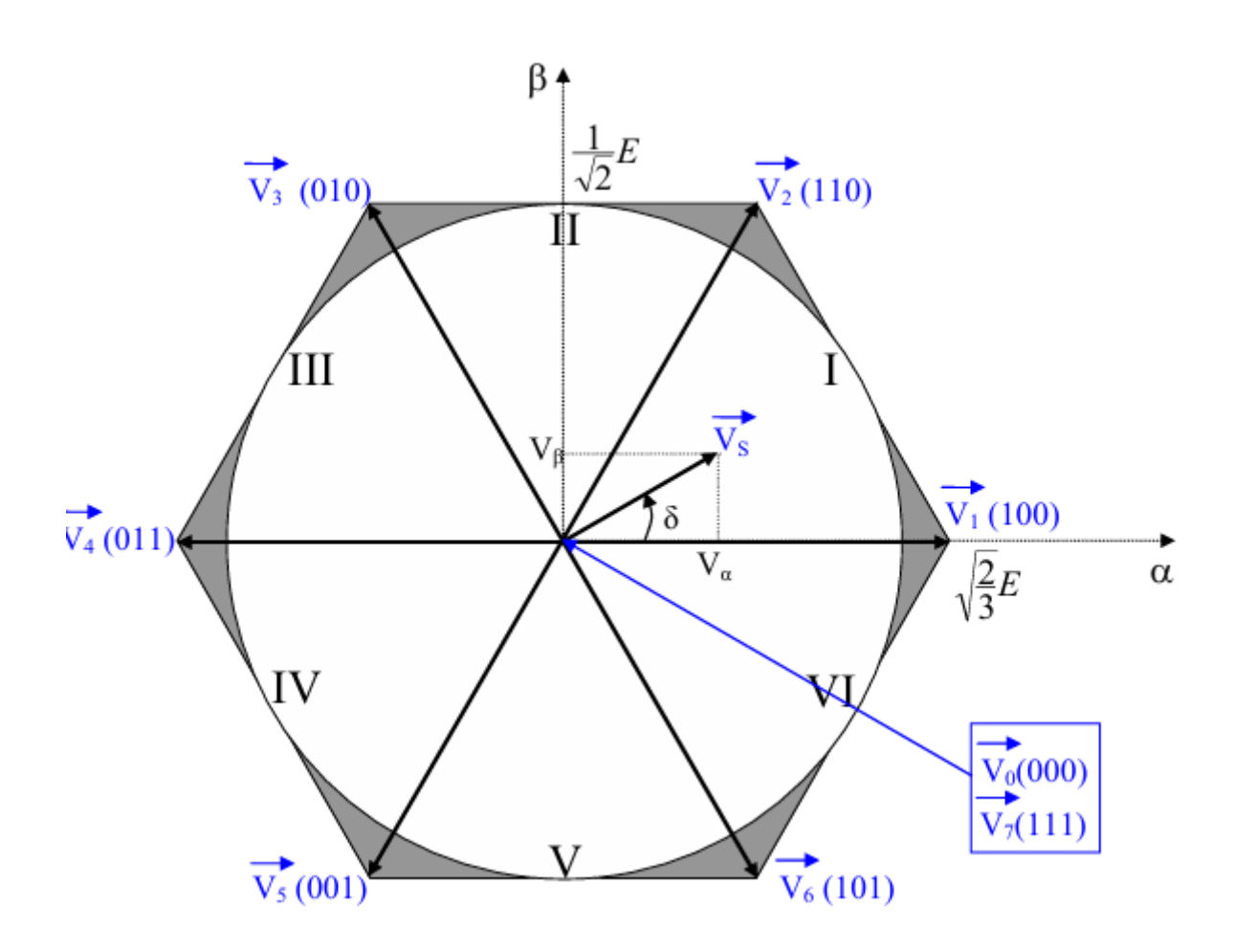


Figure II.7: Representation of the Switching Polygon

The notation VS (SA SB SC) used in Figure 2.3 represents the states of the switches K1, K2, and K3, where:

- 1 indicates the switch is closed
- 0 indicates the switch is open

II.7.3 Desired Voltage Vector:

A voltage vector v_S can be defined, where its coordinates are the Clark components $v_{S\alpha}$, $v_{S\beta}$ of the three-phase system v_{SA} , v_{SB} , v_{SC} that we aim to obtain at the output.

For three-phase voltages (AÏMER,2006):

$$v_{SA} = r \cdot \frac{E}{2} \cdot \cos(\delta)$$

$$v_{SB} = r \cdot \frac{E}{2} \cdot \cos\left(\delta - \frac{2\pi}{3}\right)$$

$$v_{SC} = r \cdot \frac{E}{2} \cdot \cos\left(\delta - \frac{4\pi}{3}\right)$$
(2.15)

The Clark Transformation Gives:

$$v_{s\alpha} = r \cdot \sqrt{\frac{3}{2} \cdot \frac{E}{2}} \cdot \cos(\delta)$$

$$v_{s\beta} = r \cdot \sqrt{\frac{3}{2} \cdot \frac{E}{2}} \cdot \sin(\delta)$$
(2.16)

The vector v_S is a vector of constant amplitude $\left(r \cdot \sqrt{\frac{3}{2}} \cdot \frac{E}{2}\right)$. The v_S vector rotates counterclockwise with an angular velocity equal to the frequency of the desired voltages.

At any given moment, the v_S vector can be expressed as a linear combination of the two adjacent vectors $v_{S(k)}$ and $v_{S(k+1)}$:

When the angle δ between ν_S and the α is between 0 and $\pi/3$:

$$\vec{V}_{s} = \frac{\sqrt{3}}{2} \cdot r \cdot \sin\left(\frac{\pi}{3} - \delta\right) \cdot \vec{V}_{1} + \frac{\sqrt{3}}{2} \cdot r \cdot \sin(\delta) \cdot \vec{V}_{2}$$
(2.17)

When the angle δ between ν_S and the α is between $\pi/3$ and $2\pi/3$:

$$\vec{V}_{s} = \frac{\sqrt{3}}{2} \cdot r \cdot \sin\left(\frac{2\pi}{3} - \delta\right) \cdot \vec{V}_{2} + \frac{\sqrt{3}}{2} \cdot r \cdot \sin\left(\delta - \frac{\pi}{3}\right) \cdot \vec{V}_{3}$$
(2.18)

And so on.

It is important to note that as long as the tip of the VS vector remains inside the hexagon defined by the endpoints of vectors V1 to V6, the coefficients $\frac{\sqrt{3}}{2} \cdot r \cdot \sin\left(\frac{\pi}{3} - \delta\right)$ and $\frac{\sqrt{3}}{2} \cdot r \cdot \sin(\delta)$ have a sum less than or equal to one as long as:

$$r \le \frac{2}{\sqrt{3}} = 1.155$$
(2.19)

r is defined as the radius of the circle that is inscribed within the hexagon formed by the endpoints of the non-zero voltage vectors.

II.7.4 Approximation of the Desired Voltage Vector:

If the previous condition (Equation 2.19) is met over a sufficiently short time interval **T**, such that the variation of VS during its duration can be neglected, the **average value** of this vector can be reconstructed using $v_{S(k)}$, $v_{S(k+1)}$ and the zero vectors V0 or V7.

To achieve this, as shown in Equation 2.17, the switches are set as follows:

- In the configuration corresponding to $v_S(k)$ for a fraction $\frac{\sqrt{3}}{2} \cdot r \cdot \sin\left(\frac{\pi}{3} \delta\right)$ of the interval **T**:
- In the configuration corresponding to $v_S(k+1)$ for a fraction $\frac{\sqrt{3}}{2} \cdot r \cdot \sin(\delta)$ of the interval **T**:
- And in a configuration that provides a zero output vector (V0 or V7) for the remainder of the interval **T**.

It is verified that, over the interval **T** in the first sector, the **average value** indeed matches v_s .

$$V_{moy} = \frac{1}{T} (T_1 V_1 + T_2 V_2 + T_l V_0)$$
(2.20)

Where:

$$\vec{V}_{S} = \frac{\sqrt{3}}{2} \cdot r \cdot \sin\left(\frac{\pi}{3} - \delta\right) \cdot \vec{V}_{1} + \frac{\sqrt{3}}{2} \cdot r \cdot \sin(\delta) \cdot \vec{V}_{2}$$
(2.21)

Vectorial modulation consists of reproducing the described process in each modulation period to ensure that, on average, the evolution of the VS vector is maintained.

II.7.5 Calculation of Switching Times:

We can calculate the switching times of the switches in each of the six sectors of the hexagon using the following figure, where the calculation is performed in the first sector (KHERRAZ,2023).

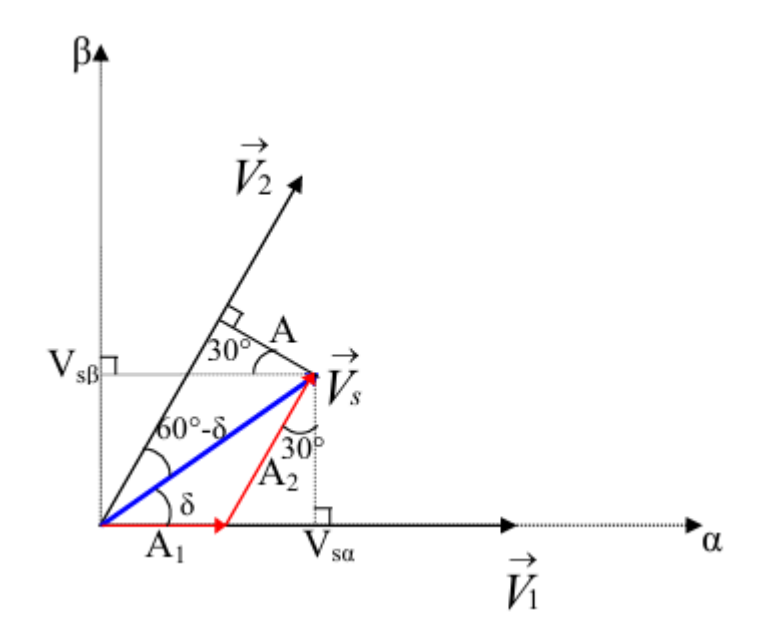


Figure II.8: Calculation of Switching Times for Sector 1

With: A1 and A2, respectively, the duty cycles of vectors V1 and V2, expressed by:

$$A_1 = \frac{T_1}{T} \overrightarrow{V_1}$$

$$A_2 = \frac{T_2}{T} \overrightarrow{V_2}$$
(2.22)

According to Figure 2.4, we have:

$$V_s = v_{s\alpha} + j \cdot v_{s\beta} \tag{2.23}$$

With:

$$v_{s\alpha} = V_s \cdot \cos(\delta)$$

 $v_{s\beta} = V_s \cdot \sin(\delta)$ (2.24)

It is observed that:

$$A = \frac{T_1 V_1}{T} \cdot \cos(30) = V_s \cdot \sin(60 - \delta)$$
(2.25)

Where:

$$V_1 = V_2 = \sqrt{\frac{2}{3}}E$$
 (2.26)

Thus:

$$T_{1} = \frac{V_{s} \cdot \sin(60 - \delta) \cdot T}{V_{1} \cos(30)} = V_{s} \cdot \sin(60 - \delta) \cdot \frac{2T}{\sqrt{2}E}$$
(2.27)

Which can be written in the form:

$$T_1 = V_S \cdot \left(\sin(60)\cos(\delta) - \cos(60)\sin(\delta)\right) \cdot \frac{2T}{\sqrt{2}E}$$
(2.28)

Thus, the switching time T_1 can be expressed as:

$$T_1 = \frac{\sqrt{6} \cdot V_{s\alpha} - \sqrt{2} \cdot V_{s\beta}}{2E} T$$
(2.29)

On the other hand, Figure 2.4 reveals that:

$$\cos(30) = \frac{V_{s\beta}}{\frac{T_2 V_2}{T}}$$
(2.30)

Thus, we can obtain:

$$T_2 = V_{s\beta} \cdot \frac{T}{V_2 \cdot \cos(30)} = V_{s\beta} \cdot \frac{T}{\sqrt{3}E \cdot \frac{\sqrt{3}}{2}}$$
(2.31)

Finally, the switching time T_2 can be expressed as:

$$T_2 = \frac{\sqrt{2} \cdot V_{s\beta}}{E} \cdot T \tag{2.32}$$

By performing the same calculation for each sector, the construction of Figure II.9 is obtained.

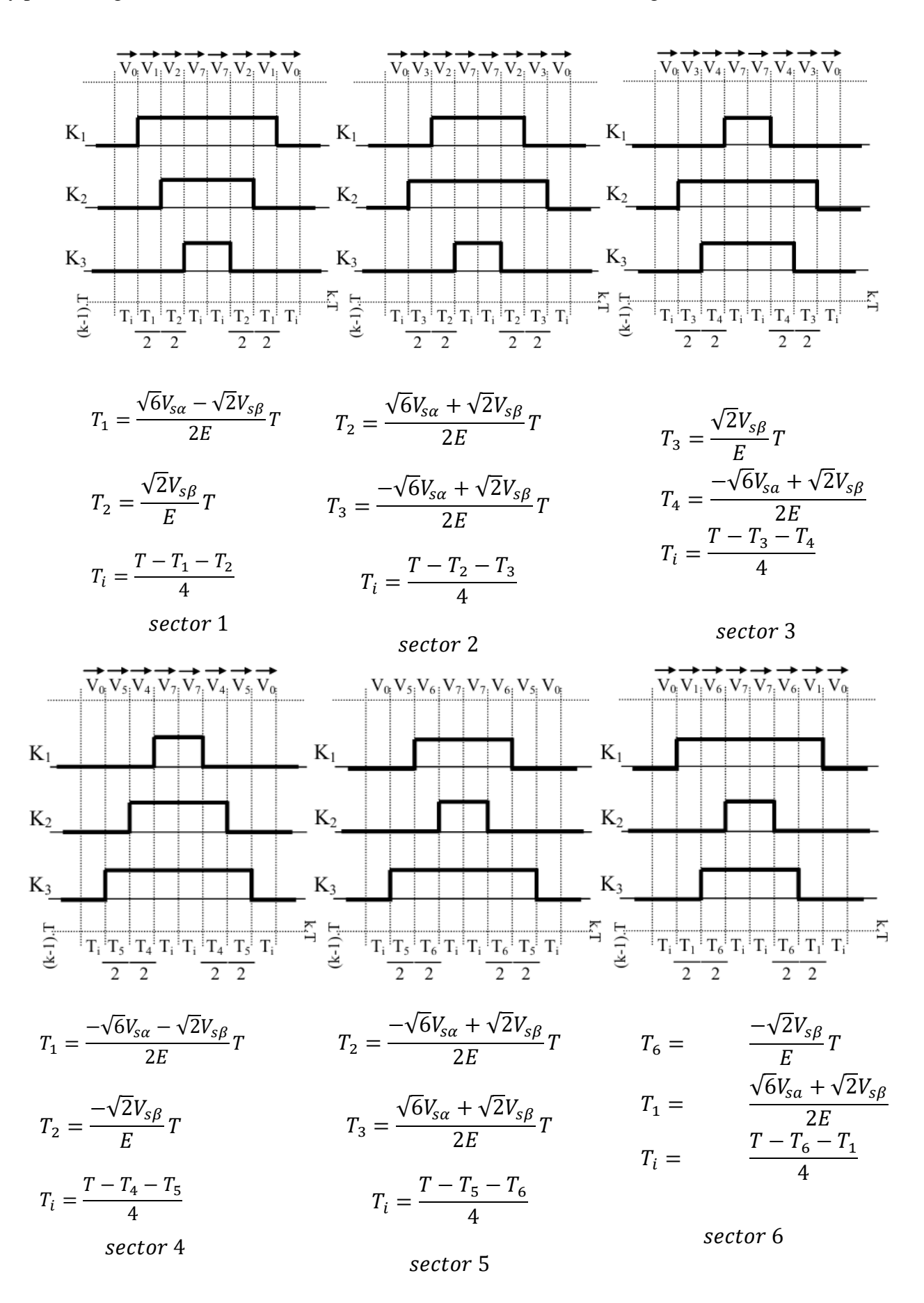


Figure II.9: Description of the Conduction Sequences of the Switches

The selection of the switching conduction sequences follows the algorithm below:

```
If V_{s\beta} > 0 then
       If V_{s\alpha} > 0 then
           If V_{s\beta} > \sqrt{3}V_{s\alpha} then
                  Compute switching times for sector 2
          Else
                  Compute switching times for sector 1
          End If
      Else If V_{s\beta} > -\sqrt{3}V_{s\alpha} then
                  Compute switching times for sector 2
           Else
                  Compute switching times for sector 1
          End If
      End If
 Else
          If V_{s\alpha} > 0 then
                 If V_{s\beta} > -\sqrt{3}V_{s\alpha} then
                  Compute switching times for sector 5
               Else
                     Compute switching times for sector 6
               End If
       Else
                    If -V_{s\beta} > -\sqrt{3}V_{s\alpha} then
                     Compute switching times for sector 5
                Else
                      Compute switching times for sector 4
                End If
       End If
End If
```

Figure II.10: Algorithm of Vector PWM

II.8 Overview of the Conventional PI controller:

Induction motors have much application in industry because of their low maintenance and robustness. The speed control of induction motor is more important to achieve maximum torque and efficiency. In recent years, the control of the induction motor drive is an active research area. And the technology has further advances in this field. Generally, the control and estimation of ac drives ware significantly more complex than that of dc drives, and this complexity increases to a large extent if the high performances are demanded. The need of variable frequency, machine parameter variations, and the difficulties of processing feedback signals in the presence of harmonics create this complexity.

Induction motor can be controlled with the help of conventional PI and PID controller with the use of vector control technique. Because of major advantages of vector control, this method of control will oust scalar control, and will be accepted as the industry-standard control for ac drives. PI and PID controllers are widely used in different industries for control of different plants and have a reasonable performance. The conventional PI controller increases the order of the system, improves damping, and reduces maximum overshoot, decreases bandwidth and increase the rise time. But the PI controller can never achieve perfect control, that is, keep the speed of induction motor continuously at a desired set point value in the presence of disturbance or set point change. Therefore, we need an advance control technique such as PID controller. In this Part, we will discuss the conventional PI controller. Finally, we will present the simulation result for speed control of induction motor using PI controller and a brief discussion.

II.8.1 PI CONTROLLER:

The PI controller (proportional integral controller) is a feedback controller. It drives the plant which is to be controlled with a weighted sum of error and the integral of that value (Madhavi, 2013).

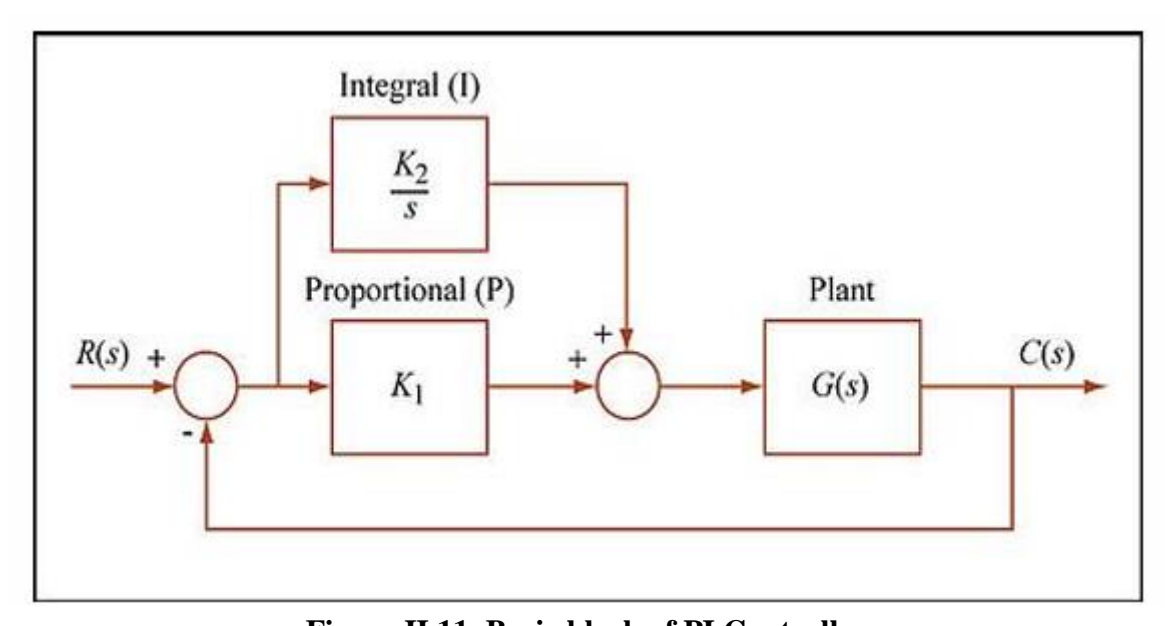


Figure II.11. Basic block of PI Controller

Advantages and disadvantages:

- 1)- PI controller increases the order and the type of the system by one. It also causes the steady state error to reduce to the zero, which is not the case for proportional only control in general.
- 2)- PI controller improves damping and reduces maximum overshoot. It also decreases the bandwidth and improves the rise time.
- 3)- The presence of derivative action may make the system steadier in the steady state in the case of noisy data. This is due to the derivative action which is more sensitive to the high frequency terms in the inputs.
- 4) -The PI controlled system is less responsive to real (non-noise) in the absence of derivative action.
- 5)- Also the relatively fast alterations in state and the system will be slower to reach to the set point due to the absence of derivative action. Therefore, so as to improve all the drawbacks of PI controlled system, we are using a derivative action i.e. PID controller which is used to minimize the settling time and to improve the steady state error.

II.9 DTC (Direct Torque Control):

This direct torque control (DTC) strategy for the induction machine was the first to appear in the literature under the name DTC, with its dissemination dating back to the mid-1980s. It was proposed by I. Takahashi and T. Noguchi and has been the subject of a widely cited publication (Takahashi,1985). It is now commonly accepted that when referring to classical DTC, one is referring to this strategy applied to a conventional 2-level voltage inverter. We will also adopt this designation throughout our study.

Its algorithm is based on hysteresis control of both the torque and the stator flux, and its control block diagram is detailed in Figure (II.12) (BOUTEBAK,2015).

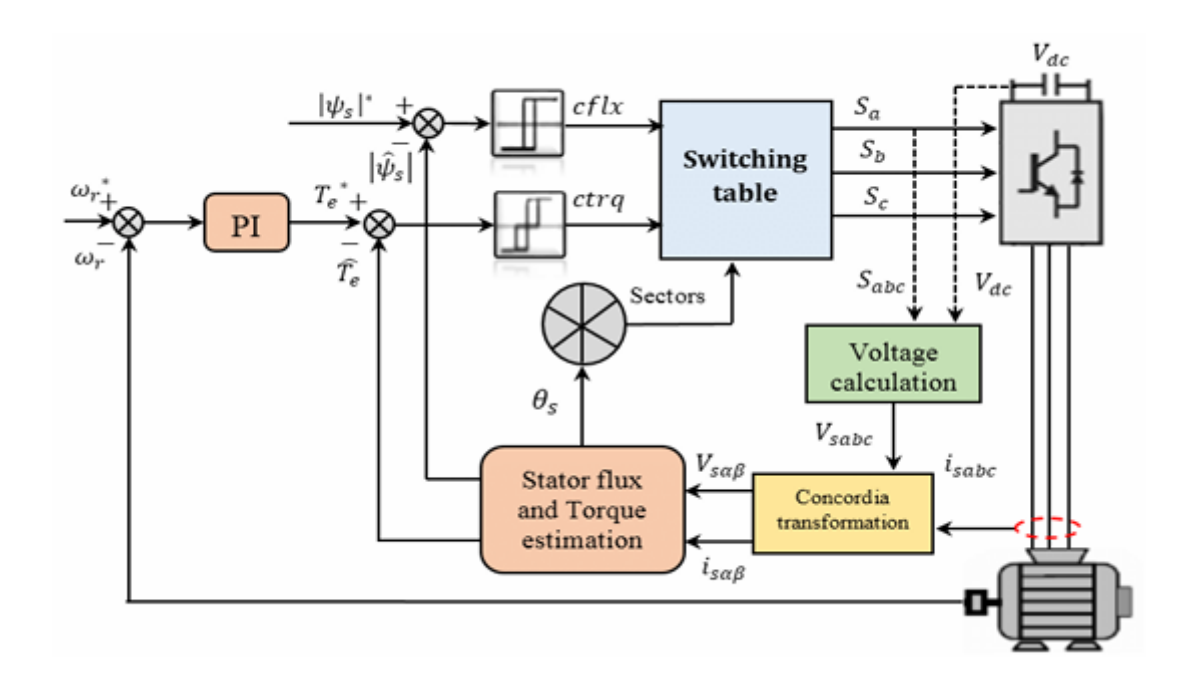


Figure II.12: Overview of the classical two-level DTC control.

The objective of classical Direct Torque Control (DTC) is the direct regulation of the machine's torque by applying various voltage vectors from the inverter, which determines its state. The two controlled variables are the stator flux and the electromagnetic torque, which are usually managed by hysteresis comparators. The aim is to keep the stator flux and the electromagnetic torque within these hysteresis bands. The output of these comparators determines the optimal voltage vector of the inverter to apply at each switching moment.

The general characteristics of direct torque control are as follows:

- Direct control of torque and flux through the selection of optimal switching vectors from the inverter.
- Indirect control of the stator currents and voltages of the machine.
- Achieving stator flux and currents that are close to sinusoidal shapes.
- A very fast dynamic response from the machine.
- The presence of torque ripples, which depend, among other factors, on the width of the hysteresis bands of the comparators.
- The switching frequency of the inverter depends on the amplitude of the hysteresis bands.

II.10 Generation of Space Voltage Vector:

Generation of Space Voltage Vector The estimation of the stator flux linkage components requires the stator terminal voltages. In a DTC scheme it is possible to reconstruct those voltages from the DC link voltage, V_s , and the switching states (Sa, Sb, Sc) of a six-step voltage-source inverter. When the stator windings are fed by an inverter, as shown in Fig. (II.2), the primary voltages Va, Vb, and Vc are determined by the status of the three switches, Sa, Sb, and Sc. If the switch is at state 0 that means the phase is connected to the negative and if it is at 1 it means that the phase is connected to the positive leg. For example, Va is connected to Vs if is one, otherwise Va is connected to zero. This is similar for Vb and Vc. The voltage vectors that are obtained this way are shown in Fig. II.13. There are six non-zero voltage vectors: V1(100), V2(110) ..., and V6(101) and two zero voltage vectors: V0(000) and V7(111). The six nonzero voltage vectors are 60° apart from each other as in Fig.II.13 (Touahar, 2021).

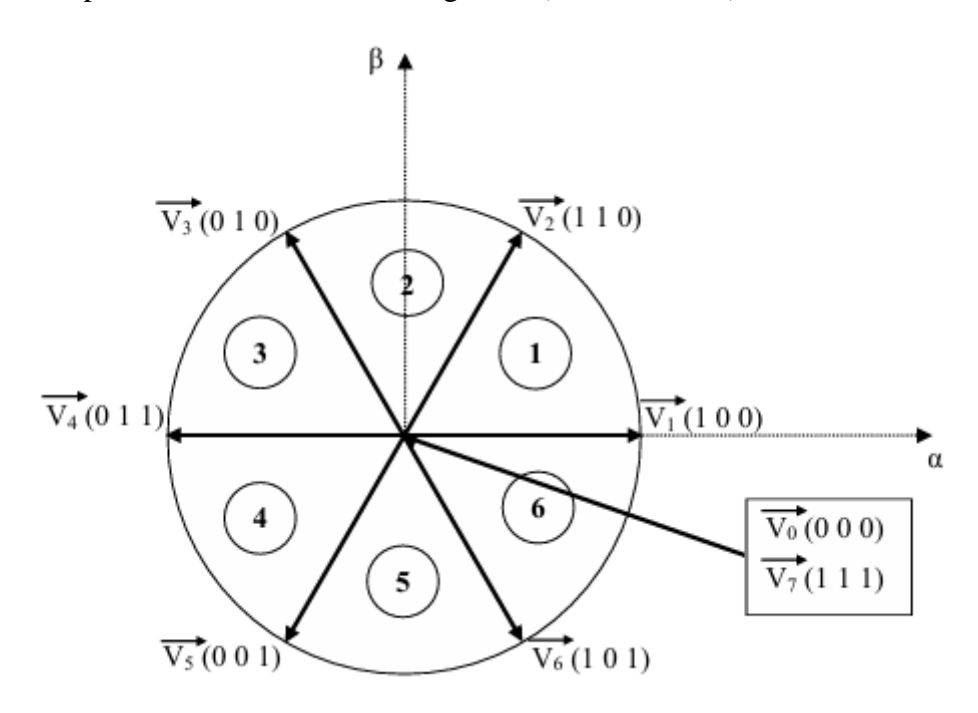


Fig. II.13: Development of the Voltage Vector Vs (Sa Sb Sc)

II.11 Qualitative Rules for the Electromagnetic State of the Machine:

To study the basic principles of the main direct control strategies for induction machines, it is essential to qualitatively characterize the behavior of the main variables governing the electromagnetic state of the machine, namely the electromagnetic torque and flux. For this

purpose, rules will be established below to describe the behavior of the stator flux and torque on the scale of the sampling period, thereby enabling the establishment of a relationship between the application of a voltage vector and the direction of variation of these variables.

Stator Flux Control:

The stator flux is estimated from the measure of the sizes of current and voltage and their transformation in the plane $\alpha\beta$. equations (2.33):

$$\Phi_{s\alpha} = \int_0^t (V_{s\alpha} - R_s I_{s\alpha}) dt$$

$$\Phi_{s\beta} = \int_0^t (V_{s\beta} - R_s I_{s\beta}) dt$$
(2.33)

the stator flux linkage phasor is given by equation:

$$\Phi s = \sqrt{\Phi_{s\alpha}^2 + \Phi_{s\beta}^2} \tag{2.34}$$

Over a period of sampling e Te, and by neglecting the term (Rs, Is) in equation of stator flux, valid hypothesis for high speeds, the evolution of this last one is given by the vector Vs during Te, equation:

$$\Delta \Phi_s = \Phi_s - \Phi_{s0} = V_s T_e \tag{2.35}$$

 Φ_{s0} is the initial stator flux linkage at the instant t_0

As shown in Figure (II.8), implies that the end of the stator flux vector $\Phi(t)$ s moves on a straight line whose direction is given by the applied voltage vector Vs, as shown in Figure II.14.

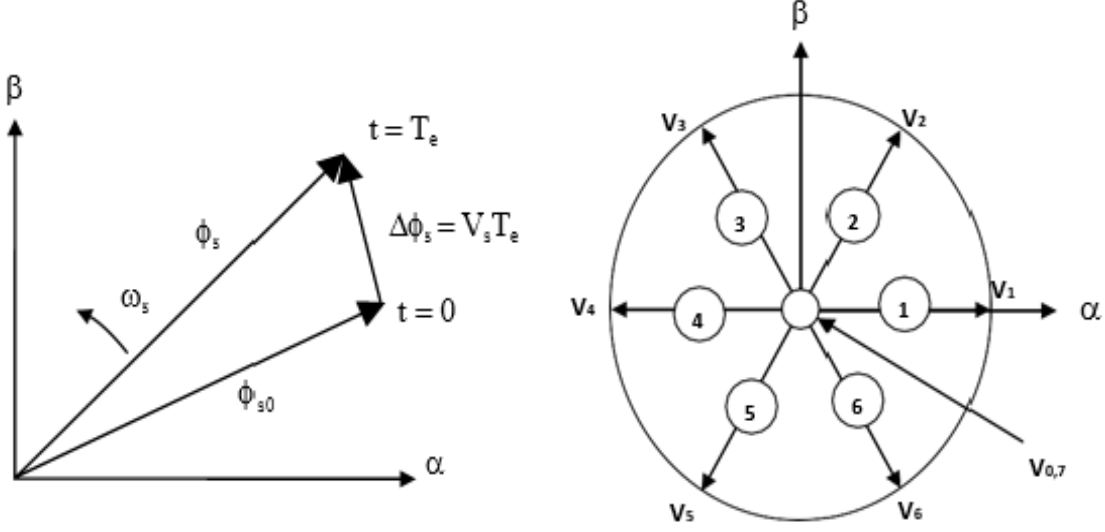


Fig. II.14: Development of the stator flux and operating sequences

The "flux component" of the voltage vector (radial component) varies the amplitude of Φ_s and its "torque component" (tangential component) varies the position of Φ_s .

By choosing an adequate sequence of vectors Vs over the control periods Te_n , it is, therefore, possible to operate with a practically constant flux modulus Φ_s , by causing the end of Φ s to follow an almost circular trajectory if the period Te_n , is very small compared to the rotation period of the stator flux.

When the selected voltage vector Vs is non-zero, the direction of displacement of the end of Φ_s is given by its derivative $\frac{d\Phi_s}{dt}$, thus the "speed" of displacement of the end of Φ_s .

The speed of rotation of Φ_s strongly depends on the choice of V_s ; it is maximum for a vector V_s perpendicular to the direction of Φ_s and zeroes if a zero vector is applied. It can also be negative.

Torque Control:

By putting θ_{sr} the angle between the rotor and stator flux vectors, the expression of electromagnetic torque as given by equation (2.36) (Touahar,2021):

$$T_{elm} = p \frac{L_m}{\sigma L_s L_r} \| \Phi_s \| \| \Phi_r \| \sin(\theta_{sr})$$
(2.36)

We deduct that the torque depends on the amplitude and on the position of stator and rotor vectors flux. On the other hand, the differential equation which binds the stator flux and the rotor flux of motor is given by equation (2.37):

$$\frac{d\Phi_r}{dt} + \left(\frac{1}{T_s} - j\omega\right)\Phi_r = \frac{L_m}{T_s L_s}\Phi_s \tag{2.37}$$

From this equation we deduct that the flux Φ_r follows the variations of the flux Φ_s with a constant of time T_s .

If we succeed in controlling perfectly the stator vector flux, from the vector V_s in module and in position, we can control the amplitude and the relative position of the rotor vector flux and consequently the electromagnetic torque. This is indeed on possible only if the period of command T_e of the voltage V_s is very lower in $\sigma \tau_r$.

The expression of the electromagnetic torque is only obtained from the statorique sizes flux $\Phi_{s\alpha}$, $\Phi_{s\beta}$ and currents $I_{s\alpha}$, $I_{s\beta}$ equation (2.38):

$$T_{elm} = p(\Phi_{s\alpha}I_{s\beta} - \Phi_{s\beta}I_{s\alpha})$$
(2.38)

Where: θ_{sr} : the angle between the stator flux and rotor flux, which is given by the following relation:

$$\theta_{sr} = \theta_s - \theta_r - \theta$$

With:

 θ_s : the angle between the stator flux and α_s .

 θ_r : the angle between the rotor flux and α_r .

 θ : the angle between the αs and αr axes.

With the representation of the stator flux and rotor flux vectors in the fixed α , β reference frame, we can introduce θ_{sr} , as shown in Figure II.15.

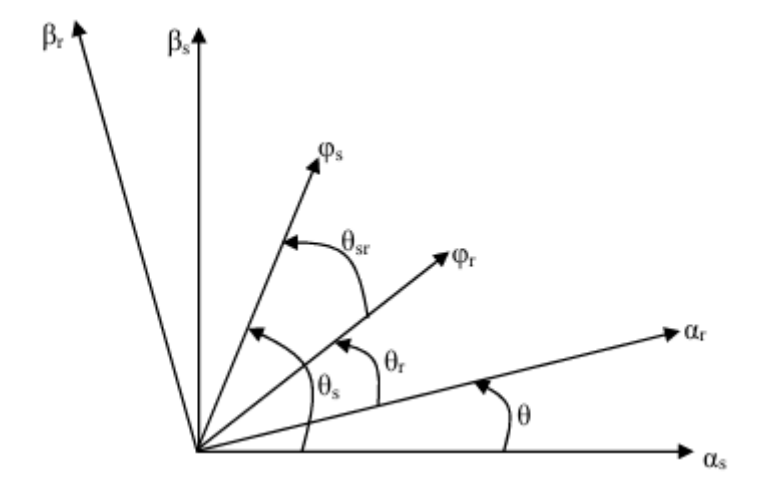


Fig.II.15: The Rotation Angles in the Fixed α , β Reference Frame

II.12 ESTIMATORS:

II.12.1 Estimation of stator flux :

The flux can be estimated from measurements of the stator current and voltage quantities of the machine.

From the equation:

$$\bar{\varphi}_S = \int_0^t (\bar{V}_S - \bar{R}_S \bar{I}_S)$$
(2.39)

We obtain the components α and β of the vector $\bar{\varphi}_s$:

$$\bar{\varphi}_{S\alpha} = \int_0^t (\bar{V}_{S\alpha} - \bar{R}_S \bar{I}_{S\alpha})$$
(2.40)

And

$$\bar{\varphi}_{S\beta} = \int_0^t (\bar{V}_{S\beta} - \bar{R}_S \bar{I}_{S\beta}) \tag{2.41}$$

The voltages $V_{s\alpha}$ and $V_{s\beta}$ are obtained from the $S_aS_bS_c$ commands of the measurement of the voltage U_0 and by applying the CONCORDIA transform:

$$\bar{V}_s = V_{s\alpha} + jV_{s\beta}$$

$$V_{s\alpha} = \sqrt{\frac{2}{3}} U_0 \left(S_a - \frac{1}{2} (S_b + S_c) \right)$$

$$V_{s\beta} = \frac{1}{\sqrt{2}} U_0 (S_b - S_c)$$

(2.42)

Similarly, the currents $I_{s\alpha}$ and $I_{s\beta}$ are obtained from the measurement of the real currents i_{sa} , i_{sb} and $i_{sc}(i_{sa}+i_{sb}+i_{sc})=0$ by applying the CONCORDIA transformation:

$$\bar{I}_{s} = I_{s\alpha} + jI_{s\beta}$$

$$I_{s\alpha} = \sqrt{\frac{2}{3}}i_{s\alpha}$$

$$I_{s\beta} = \frac{1}{\sqrt{2}}(i_{sb} - i_{sc})$$
(2.43)

The modulus of the stator flux is written:

$$\varphi_{s} = \sqrt{\varphi_{s\alpha}^{2} + \varphi_{s\beta}^{2}}$$
(2.44)

The zone N_i in which the vector $\bar{\varphi}_s$ is located is determined from the components $\varphi_{s\alpha}$, $\varphi_{s\beta}$.

The angle θ_s between the frame (S) is the vector $\bar{\varphi}_s$, is equal to:

$$\theta_s = \tan^{-1} \frac{\varphi_{s\beta}}{\varphi_{s\alpha}} \tag{2.45}$$

II.12.2 Estimation of electromagnetic torque :

The torque T_{em} can only be estimated from the flux and current stator quantities. Their components (α , β), the couple can be put in the form:

$$T_{em} = p(\varphi_{s\alpha}I_{s\beta} - \varphi_{s\beta}I_{s\alpha})$$
(2.46)

II.13 Elaboration of the control vector:

II.13.1 Flux corrector:

With this type of controller, one can easily control and trap the extremity of the flux vector in a circular crown, as shown in the figure II.16. The output of the controller, represented by a Boolean variable $(C_{nx} = 0)$ indicates directly if the amplitude of the flow must be increased $(C_{flx} = 0)$ or decreased $(C_{flx} = 0)$ in order to maintain (Touahar,2021):

$$|(\Phi_s)_{\text{ref}} - \Phi_s| \le \Delta \Phi_s \tag{2.47}$$

With:

 $(\Phi_s)_{ref}$: is the reference fow.

 $\Delta \Phi_{\rm s}$:is the hysteresis width of the corrector.

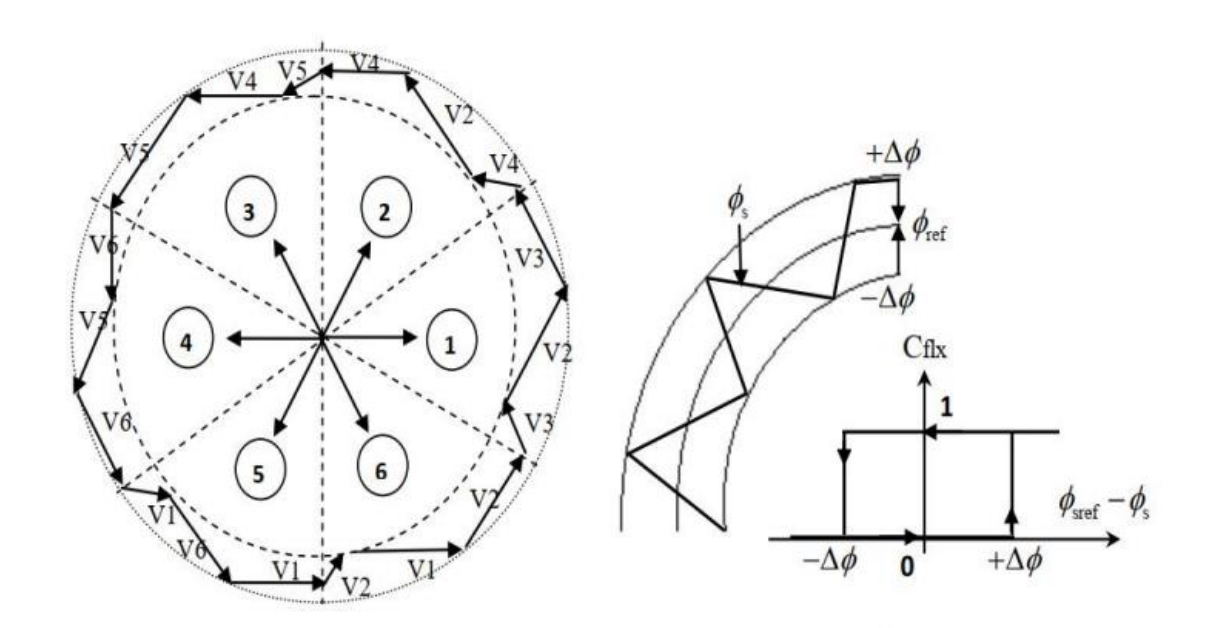


Figure II.16 Flux corrector with hysteresis and selection of the corresponding voltage vectors.

$$\begin{cases} \text{if} \quad \Delta\phi_s > \varepsilon_{\phi} & \text{so} & \text{Cflx} = 1 \\ \text{if} \quad 0 \leq \Delta\phi_s \leq \varepsilon_{\phi} & \text{and} \Delta\phi_s/\text{dt} > 0 & \text{so} & \text{Cflx} = 0 \\ \text{if} \quad 0 \leq \Delta\phi_s \leq \varepsilon_{\phi} & \text{and} \Delta\phi_s/\text{dt} < 0 & \text{so} & \text{Cflx} = 1 \\ \text{if} \quad 0 \leq \Delta\phi_s < -\varepsilon_{\phi} & \text{so} & \text{Cflx} = 0 \end{cases}$$

Indeed, if we introduce the difference $\Delta \phi_s$ between the reference flux ϕ_{ref} and the estimated flux $\hat{\phi}_s$ in a two-level hysteresis comparator ,this generates at its output the value $C_{fix} = +1$ to increase the flux($C_{fix} = 0$ to reduce it); this also makes it possible to obtain a very good dynamic performance of the flow.

Thus, only the vectors Vi+1 or Vi+2 can be selected to change the stator flux vector ϕ_s .

On the other hand, this corrector does not allow the inversion of the direction of rotation of the flux vector ϕ_s . Thus, to go in reverse, one has to cross one arm of the converter.

II.13.2 Torque corrector:

Torque corrector We define the error on the torque, note ε_{Tem} , as the difference between the reference torque and b its estimated value.

$$\varepsilon_{\text{Tem}} = |T_{\text{emref}} - T_{\text{em}}|$$
(2.48)

The purpose of the torque corrector is to maintain the torque within the admissible limits defined as follows:

$$|T_{em} - Te_s| \le \Delta Te$$

(2.49)

With:

T_{em}: is the reference torque

 Δ Te: is the corrector hysteresis band.

However, a difference with flux control is that the torque can be positive or negative depending on the direction of rotation of the machine. Two solutions can be envisaged:

- A three-level hysteresis corrector
- A two-level hysteresis corrector

II.13.3 Two-level corrector:

This controller is identical to the one used for flux vector control. The two-level controller is used in the case of torque control in only one direction of rotation. Only the voltage vectors \bar{V}_{i+1} and \bar{V}_{i+2} and zero vectors can be selected to evolve the flux vector. The torque reduction is ensured by the selection of zero voltage vectors (Touahar,2021)..

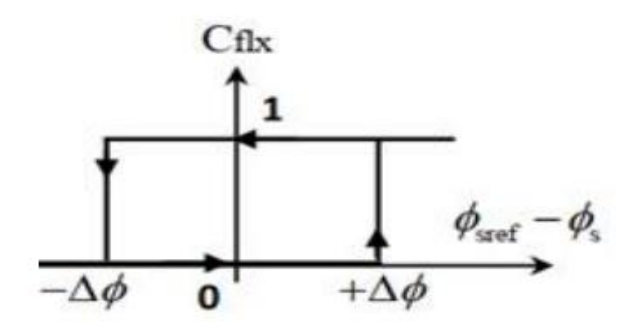


Fig.II.17: Two-level Flux corrector

II.13.4 Three-level corrector:

It allows the motor to be controlled in both directions of rotation, either for positive or negative torque.

The corrector output, represented by the Boolean variable Ctrq indicates directly whether the torque amplitude must be increased in absolute value (Ctrq =1 for a positive setpoint and C_{flx} =-1 for a negative setpoint) or reduced (C_{flx} =0).

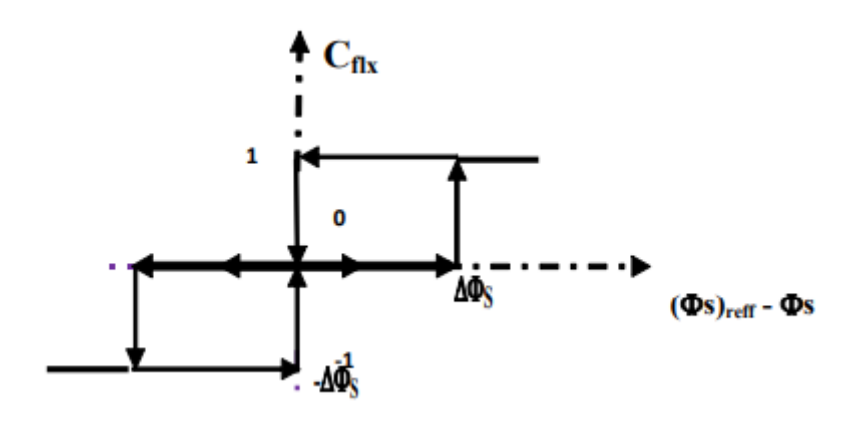


Fig.II.18: Three-level Flux corrector

II.13.5 Elaboration of the commutation table:

The command table is constructed according to the state of the variables C_{flx} and Ccpl, and the position zone of N_i It therefore takes the following form:

1	N	1	2	3	4	5	6	COMPARATOR
$C_{flx}=1$	C _{trq} =1	V2	V3	V_4	V_5	V ₆	V_1	2LEVELS
	C _{trq} =0	V_7	V_0	V_7	V_0	V_7	V_0	
	C _{trq} =-1	V_{ϵ}	V_1	V_2	V_3	V_4	V ₅	3LEVELS
$C_{flx}=0$	C _{trq} =1	V_3	V_4	V_5	V_6	V_1	V_2	2LEVELS
	$C_{trq}=0$	V_0	V_7	V_0	V_7	V_0	V ₇	
	C _{trq} =-1	V ₅	V_6	V_1	V_2	V_3	V_4	3LEVELS

Table II.2 Command table considering both cases of the torque controller

II.14 Disadvantages of DTC:

The disadvantages of the classic DTC (Direct Torque Control) strategy are significant, and most of them stem from the fact that the switching frequency is highly variable. This can naturally raise electromagnetic compatibility issues, as it becomes difficult to guarantee the absence of harmonics at certain frequencies.

Additionally, the variations in switching frequency depending on speed and torque—from a few tens of Hz at low speed to a few kHz at medium speed—necessarily generate high-intensity audible noise, which can be particularly bothersome at low speeds.

The heating of power semiconductors is consequently influenced by the operating point in the torque-speed plane, which may compromise the effectiveness of this control strategy in high-power applications.

Due to the variation in switching frequency, the distortion energy of the torque is concentrated in a range of harmonics whose frequency is difficult to control. As a result, in many applications, these harmonics may excite the mechanical resonance modes of the traction chain and significantly contribute to its premature aging.

As a consequence of the lack of control over the derivative of torque on the sampling period scale, band overshoots are substantial due to sampling, to the extent that torque ripple can be several times greater than the width of the hysteresis band, and typically greater than that obtained with a control law involving a PWM module.

II.15 Numerical Simulation:

II.15.1 Concordia Transformation:

The three currents (I_{SA}, I_{SB}, I_{SC}) , the states of the switches (S_A, S_B, S_C) at the inverter input, and the DC voltage are used as inputs for the CONCORDIA block, which serves to transform the aforementioned three-phase quantities into two-phase quantities: $I_{S\alpha}$, $I_{S\beta}$ and $V_{S\alpha}$, $V_{S\beta}$ in the stationary reference frame linked to the stator using equations (2.26).

II.15.2 Estimation of Control Quantities

The outputs of the CONCORDIA block ($I_{s\alpha}$, $I_{s\beta}$, $V_{s\alpha}$, $V_{s\beta}$) are used to estimate the stator flux and the electromagnetic torque based on equations (2.22) and (2.29). The two components of the flux, $\phi s\alpha$ and $\phi s\beta$, will be used to determine the sector (N) through a predefined function, and subsequently, to estimate the electromagnetic torque.

After the development of the sub-blocks, they can be interconnected to create the overall block diagram. Thus, the block diagram for simulating the conventional DTC control in

MATLAB/SIMULINK is illustrated in figure (II.19). The simulation results of the conventional DTC control are presented in figures (II.20) and (II.21).

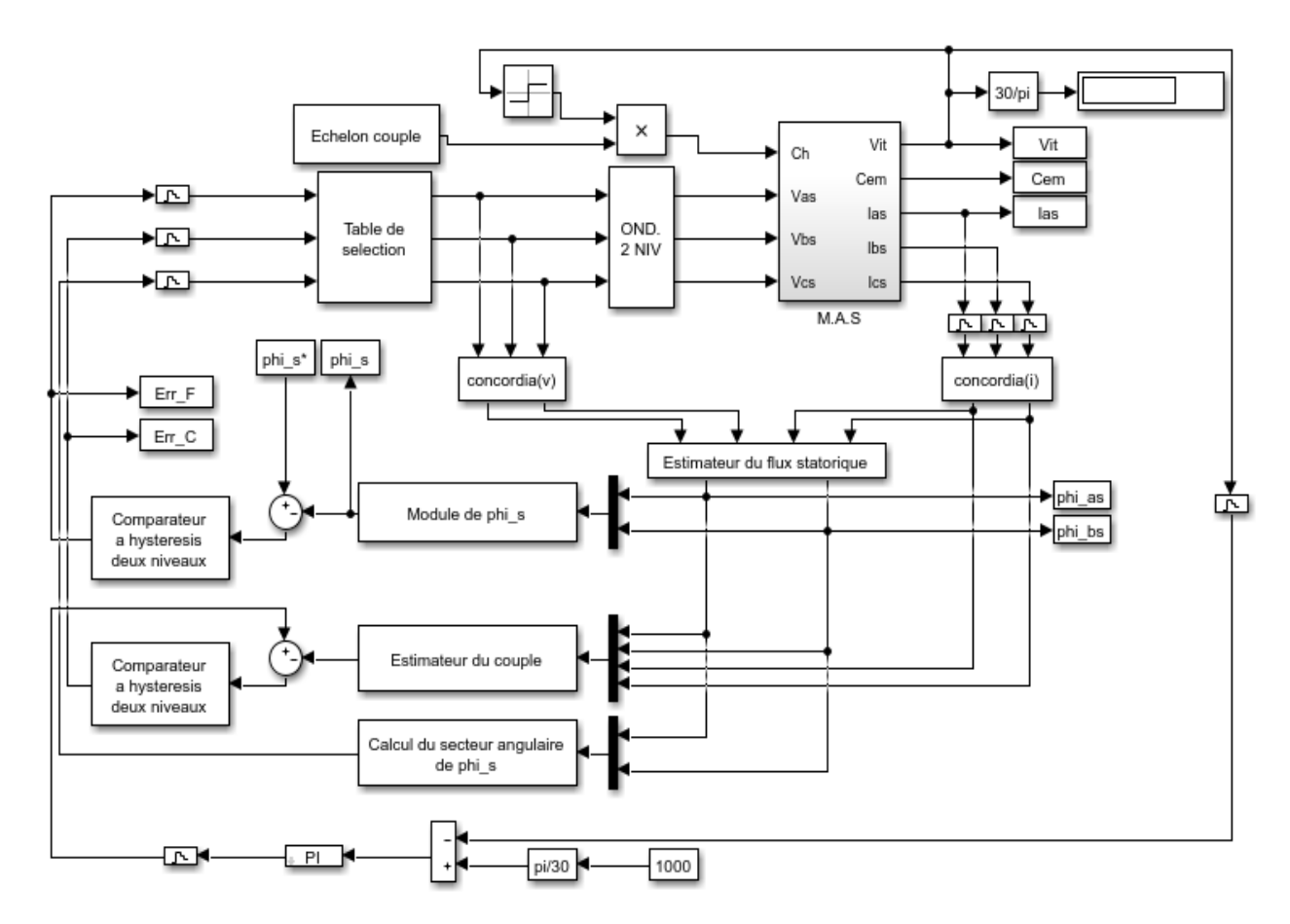


Fig. II.19: Block diagram of the conventional DTC control

II.16 Results And Discussion:

The rotational speed shows zero overshoot; it increases rapidly in an almost linear manner until t=0.134 seconds, where it stabilizes at a constant value equal to the setpoint (1000 rpm). This rapid dynamic response is due to the absence of a PI controller for the current.

The stator current is characterized by a high starting current reaching up to 26 A, then it stabilizes at its nominal value. A magnified view of the current during the steady-state regime reveals a relatively high distortion.

The electromagnetic torque, in the transient regime, experiences oscillatory growth up to a maximum value of 38 N.m, then almost instantly decreases to its reference value of 10 N.m, with an amplitude ripple of 4.2 N.m in the steady-state regime.

The stator flux immediately reaches its reference value of 1.2 Wb with a slight oscillatory overshoot of 0.08 Wb in amplitude around the reference value. The components of the stator flux exhibit an almost sinusoidal shape.

The trajectory of the tip of the stator flux, according to Figure (II.19) takes an almost circular shape with a radius of 1.2 Wb, with a slight deviation at the boundary during the zone change of the stator flux vector.

II.17 Conclusion:

In this chapter, we explored the classical Direct Torque Control (DTC) approach, analyzing its practical implementation and challenges, including torque and flux regulation using hysteresis controllers. Additionally, the role of PI controllers in motor control was examined, highlighting their influence on system stability and response dynamics. While these control strategies provide essential functionalities, their limitations such as variable switching frequency in hysteresis control and response constraints in PI-based regulation necessitate further optimization. In the next chapter, we will investigate advanced DTC strategy tailored for two-level voltage inverter, aiming to enhance control precision and efficiency while mitigating these constraints.

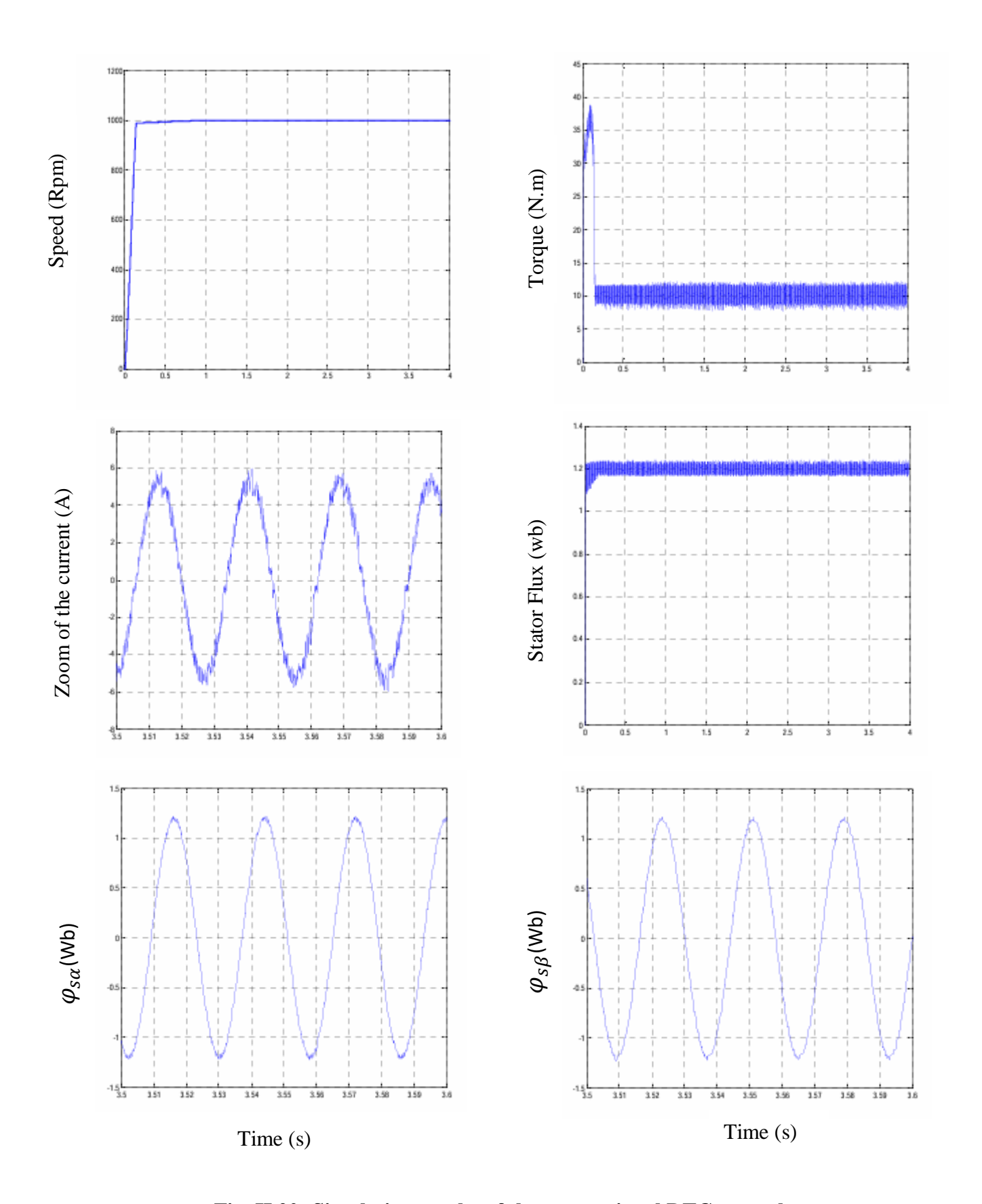


Fig. II.20: Simulation results of the conventional DTC control.

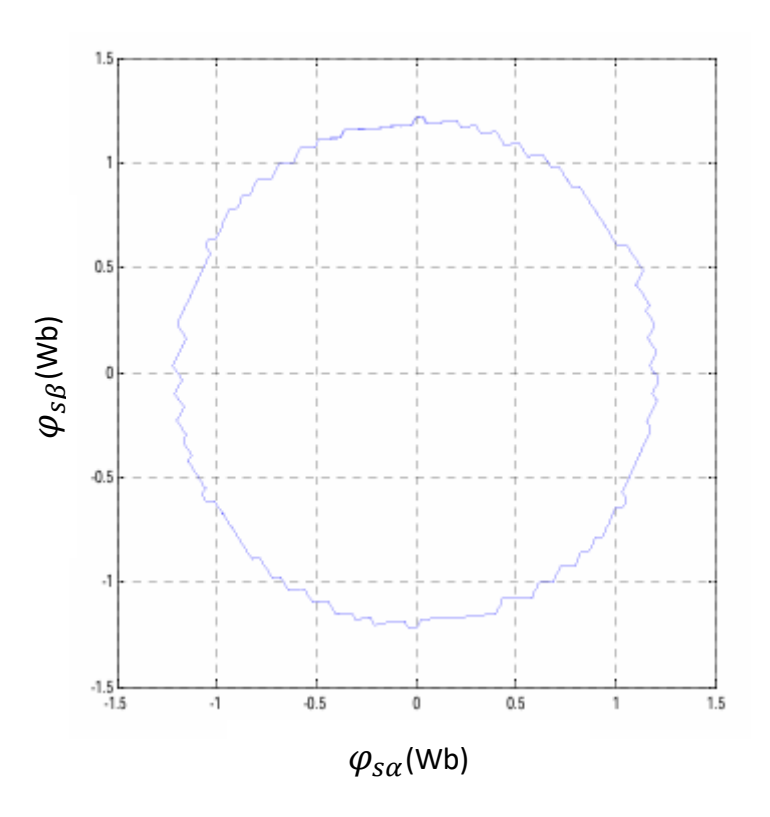


Fig. II.21: Trajectory of the tip of the stator flux vector

Chapter III Sliding Mode-Based DTC

III Introduction:

In modern electric drive systems, achieving precise control of torque and flux is essential for optimizing efficiency and dynamic performance. Direct Torque Control (DTC) has emerged as a popular approach for induction motor control due to its fast transient response and reduced dependence on motor parameters. However, conventional DTC methods often suffer from issues such as torque ripples and sensitivity to parameter variations.

To address these challenges, Sliding Mode Control (SMC) has been integrated with DTC, offering robust control performance and enhanced disturbance rejection. SMC introduces a nonlinear control strategy, ensuring improved stability, reduced torque oscillations, and superior flux regulation. By combining DTC with SMC, the system benefits from fast torque dynamics, high accuracy, and improved electromagnetic efficiency.

In this chapter, we introduce some fundamental concepts of variable-structure control, along with the basic principles of sliding mode theory. Additionally, we present an application of these techniques to induction machines, demonstrating their effectiveness in motor control. Through MATLAB simulations, the system's performance is analyzed, highlighting its ability to deliver smooth motor operation with minimal harmonic distortion.

III.1 Principle of sliding mode control:

Sliding mode control aims to bring the state trajectory of a system towards the sliding surface and make it switch around it using a switching logic until reaching the equilibrium point, which gives rise to the phenomenon of sliding. Some properties of sliding modes include:

- **Reduced order**: The sliding process is of lower order compared to the original system.
- **Determined dynamics**: The dynamics of the system in sliding mode depend solely on the choice of coefficients for the sliding surface.
- **Robustness**: High resilience to variations in certain types of parameters.

The trajectory in the phase plane comprises three distinct parts:

- Convergence mode (CM): During this mode, the variable to be regulated moves from any initial point in the phase plane and tends toward the switching surface S(x1, x2) = 0. This mode is characterized by the control law and convergence criteria.
- Sliding mode (SM): In this mode, the state variable has reached the sliding surface and moves toward the origin of the phase plane. The dynamics of this mode are defined by the determination of the sliding surface S(x) = 0.
- **Steady-state mode (SSM)**: Added for studying the system response around its equilibrium point (the origin of the phase plane), this mode is characterized by the quality and performance of the control system (Benattous, 1998).

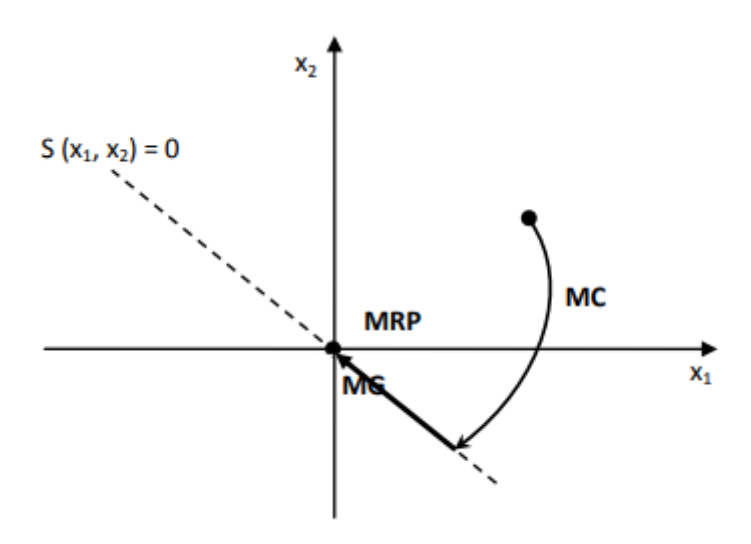


Figure (III.1): The different modes for the trajectory in the phase plane.

III.2 Design of the Sliding Mode Control Algorithm:

The design of the sliding mode control algorithm systematically addresses stability and performance issues in its approach, which is carried out in three complementary steps as defined by:

- Selection of sliding surfaces.
- Definition of the conditions for existence and convergence of the sliding regime.
- Determination of the control law.

III.2.1 Choice of sliding surface:

The design of the control system will be demonstrated for the following nonlinear system.

$$\dot{x} = f(x,t) + g(x,t). u \tag{3.1}$$

Where : $x \in \mathbb{R}^n$ is the state vector $u \in \mathbb{R}^m$ is the control vector $f(x,t) \in \mathbb{R}^n$, $g(x,t) \in \mathbb{R}^{n^*m}$.

The general equation form for the sliding surface, proposed by (J.J. Slotine) and ensuring the convergence of a variable to its desired value, is given by:

$$S(x) = \left(\frac{d}{dt} + \lambda\right)^{n-1} e$$
(3.2)

With:

 λ : Positive coefficient,

 $e = x - x_d$:É Difference (or error) between the variable to be controlled and its desired value,

 x_d : Desired value

n: Order of the system, it is the smallest positive integer representing the number of times it must be derived in order for the command to appear.

S(x) is an autonomous linear differential equation whose response 'e' tends toward zero for a correct choice of the gain λ , and that is the objective of the control.

The objective of this command is to keep the surface tending toward zero. This is a linear differential equation whose unique solution is e(x)=0 for a suitable choice of the parameter λ . This corresponds to a trajectory tracking problem, which is equivalent to an exact linearization of the deviation while respecting the convergence condition.

III.2.2 Conditions for Existence and Convergence of Sliding Mode:

The conditions for existence and convergence are the criteria that allow the dynamics of the system to converge toward the sliding surface and remain on it, regardless of disturbances. There are two aspects related to the mode of convergence of the system state. Two types of conditions are presented:

• **Direct Switching Function**: This is the first and oldest convergence condition, proposed and studied by EMILYANOV and UTKIN. It involves giving the surface a convergent dynamic toward zero. It is expressed in the form:

(3.3)

In this condition, it is necessary to introduce, for S(x) and its derivative S(x) the correct values on the left and right sides of the switching.

• Lyapunov Function: The Lyapunov function is a positive scalar function V(x) > 0 for the state variables of the system. The control law must decrease this function, i.e., V(x) < 0.

The idea is to choose a scalar function S(x) to ensure the attraction of the variable to be controlled toward its reference value and to construct a control UU such that the square of the surface corresponds to a Lyapunov function. By defining the Lyapunov function as:

$$V(X) = \frac{1}{2}S^2(X)$$

(3.4)

By differentiating the latter, we obtain (Soukkou, 2020):

$$\dot{V}(x) = S(x).\dot{S}(x)$$

(3.5)

For the function V(x)V(x) to decrease, it is sufficient to ensure that its derivative is negative, S(x). $\dot{S}(x) < 0$. This is only verified if condition (3.5) is satisfied.

Equation (3.4) explains that the square of the distance between a given point in the phase plane and the sliding surface, expressed as $S^2(X)$, decreases continuously, forcing the system's trajectory to move toward the surface from both sides.

This condition assumes an ideal sliding mode where the switching frequency is infinite.

This function is used to assess the performance of the control, such as the study of robustness and stability in nonlinear systems.

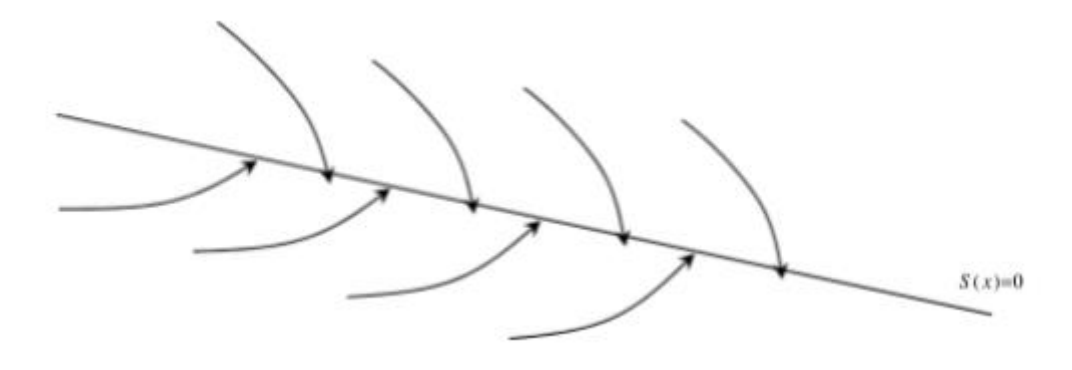


Figure (III.2): Trajectory of the state with respect to the sliding surface.

III.2.3 Determination of the Control Law:

Once the sliding surface is chosen, along with the convergence criterion, it remains to determine the control necessary to bring the variable to be adjusted toward the surface and then to its equilibrium point (the origin of the phase plane) while maintaining the condition for the existence of the sliding mode.

The system dynamics are independent of the control law. Therefore, a continuous component can be introduced to reduce the amplitude of discontinuity.

One of the essential assumptions in the design of variable structure systems for sliding mode control is that the control must switch between U^+ and U^- instantaneously (infinite frequency) depending on the sign of the sliding surface (Figure III.3).

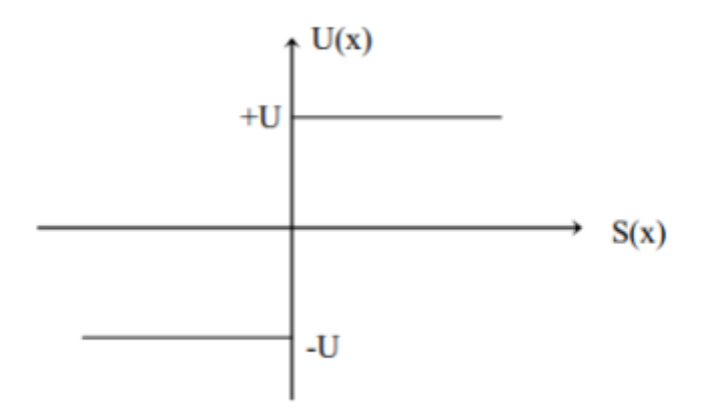


Figure (III.3): Control applied to the system.

III.2.3.1 Definition of Control Quantities:

The structure of a sliding mode controller consists of two parts: one concerning exact linearization u_{eq} , and the other concerning stability u_n .

The latter is very important in sliding mode control techniques, as it is used to eliminate the effects of model inaccuracies and reject external disturbances. Thus, the total control is given by:

$$u = u_{eq} + u_n$$

(3.6)

 u_{eq} : corresponds to the equivalent control proposed by Filipov and Utkin. It can be considered as the continuous average value. Its role is to keep the variable to be controlled on the sliding surface S(x). It is derived by assuming that the derivative of the surface is zero $\dot{S}(x) = 0$ and can be interpreted as a specific state feedback control during the rapid switching between the values U^+ and U^- (Figure III.4).

The equivalent control u_{eq} is calculated by recognizing the dynamic behavior during sliding.

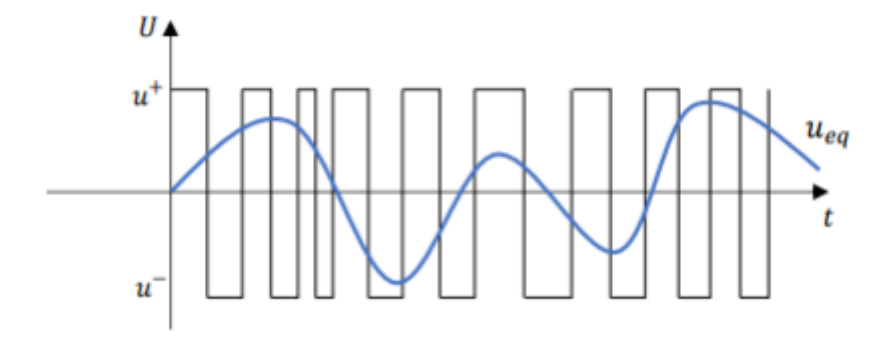


Figure (III.4): Equivalent Control.

 u_n : corresponds to the control that ensures the attraction of the variable to be controlled toward the surface and satisfies the condition S(x). $\dot{S}(x) < 0$. The discrete control u_n is determined to verify the convergence condition despite inaccuracies in the system model parameters.

III.2.3.2 Analytical Expression of the Control:

We are interested in calculating the equivalent control and subsequently the attractive control of the system defined in the state space by Equation (3.1) (Soukkou, 2020):

$$\dot{x} = f(x,t) + g(x,t).u$$

The vector U is composed of two components: U_{eq} and U_n , such that: We have:

$$\dot{S} = \frac{ds}{dt} = \frac{\partial s}{\partial x} \frac{\partial x}{\partial t} = \frac{\partial s}{\partial x} \left\{ f(x, t) + g(x, t) u_{eq} \right\} + \frac{\partial s}{\partial x} \left\{ g(x, t) u_n \right\}$$
(3.7)

In sliding mode and under steady-state conditions, the derivative of the surface is zero (since the surface itself equals zero). Thus, we obtain:

$$u_{eq} = -\left\{\frac{\partial s}{\partial x}g(x,t)\right\}^{-1}\left\{\frac{\partial s}{\partial t}f(x,t)\right\} \quad u_n = 0$$
(3.8)

During the convergence mode, by replacing the term with its value from (3.8) in equation (3.7), we obtain a new expression for the derivative of the surface, which is:

$$\dot{S} = \frac{\partial S}{\partial x} \{ g(x, t) u_n \}$$
(3.9)

The problem then comes down to finding u_n such that:

$$S(x).\dot{S}(x) = S(x)\frac{\partial s}{\partial x} \{g(x,t)u_n\} < 0$$
(3.10)

The simplest solution is to choose in the form of a relay, as shown in Figure (III.5). In this case, the control is written as follows:

$$u_n = -K.\,sign(S) \tag{3.11}$$

$$sign(S) = \begin{cases} 1 & \text{if } S > 0 \\ 0 & \text{if } = 0 \\ -1 & \text{if } S < 0 \end{cases}$$

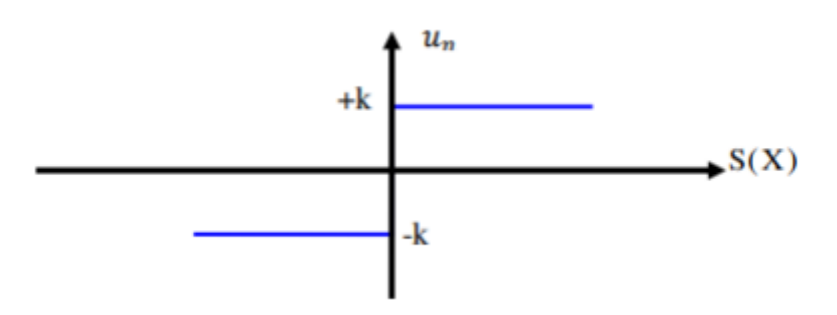


Figure (III.5): Representation of the "Sign" function.

By substituting the expression (3.10) into (3.11), we obtain:

$$S(x)\dot{S}(x) = \frac{\partial s}{\partial x}g(x,t)K|S(x)| < 0$$
(3.12)

Where the factor $\frac{\partial s}{\partial x}g(x,t)$ is always negative for the class of systems we are considering.

The gain K is chosen to be positive to satisfy condition (3.12). The choice of this gain is highly influential because, if it is too small, the response time will be very long; and if it is chosen too large, there will be strong oscillations in the control mechanism. These oscillations may excite neglected dynamics (the phenomenon known as Chattering) or even damage the control mechanism.

III.3 Phenomenon of Reluctance (chattering):

In practice, an ideal sliding regime does not exist because the switching frequency of control mechanisms has a finite limit. In other words, there is no switching mechanism capable of operating at an infinite frequency (as such a mechanism would need to deliver infinite energy).

The discontinuous nature of the control generates a particular dynamic behavior around a boundary layer of the sliding surface, commonly referred to as chattering or the phenomenon of reluctance (Figure III.6). This oscillation near the surface is caused by imperfections in the switching elements or technological and physical limitations, such as delays in switching or hysteresis behaviors, which can excite neglected (unmodeled) dynamics at high frequencies (SAOUDI,2014).

It has several undesirable effects on the quality of control and the system, including:

- Reduced precision.
- Significant heat loss in electrical machines.
- Fatigue of moving mechanical parts.

This phenomenon is considered a real obstacle to the application of variable structure control.

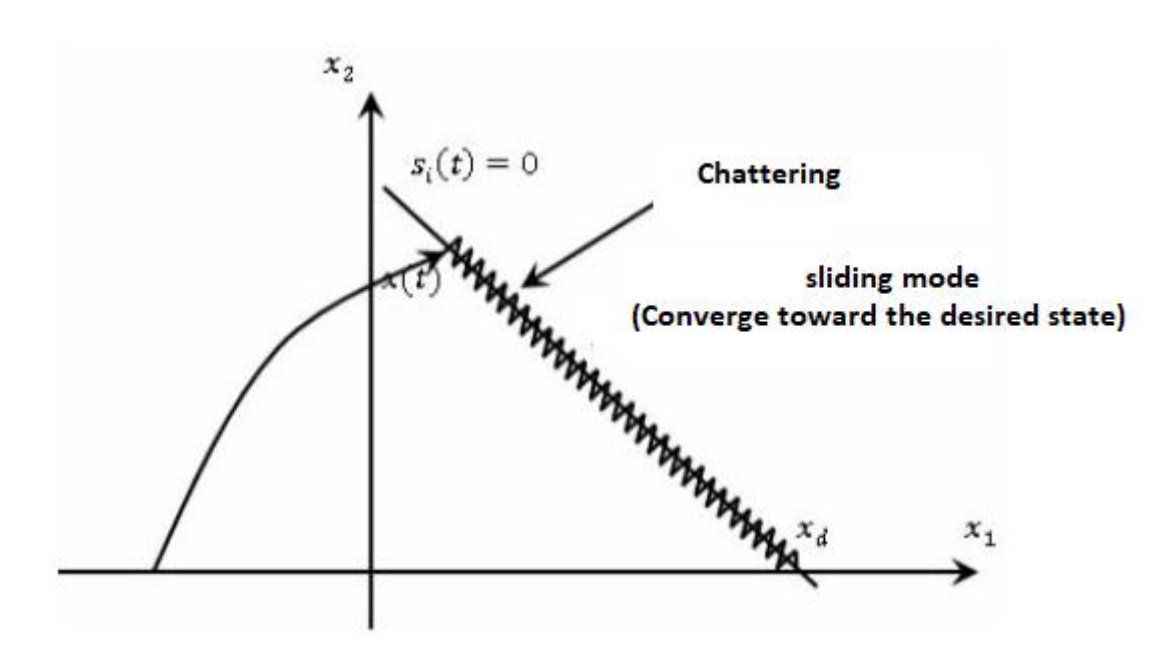


Figure (III.6): Phenomenon of Reluctance or (Chattering).

Chattering can degrade system performance and even lead to instability. Reluctance also involves significant mechanical stress on the actuators, increasing energy consumption, which can damage power electronic circuits.

III.4 Continuous Approximation of Sliding Mode Control:

The phenomenon of chattering is the main drawback of first-order sliding mode control. To address this problem, numerous variable structure algorithms have been developed. These include continuous control within a band around the surface, control with integral correction in steady-state, the use of an observer to estimate the equivalent control, and solutions that limit the sliding condition. Among the many methods proposed to solve the problem of chattering, we will focus particularly on a synthesis method where The "sign" function is replaced by a "sat" function for the calculation of the control. In this section the discontinuous component becomes (Soukkou,2020):

$$Sat(S/\Phi) = \begin{cases} 1 & \text{if } S > \Phi & 1\\ -1 & \text{if } S > -\Phi \\ \frac{S}{\Phi} & \text{if } S < |\Phi| \end{cases}$$

$$(3.13)$$

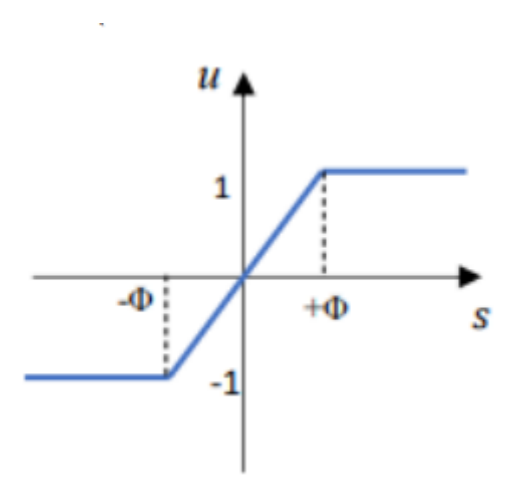


Figure (III.7): Sat Function

Another solution to smooth the control near the sliding surface S = 0 is to replace the discontinuous function sign(S) with a continuous function within the band |S| < 0.

$$cont(S) = \frac{S}{|S| + \delta}$$
 avec $\delta > 0$ (3.14)

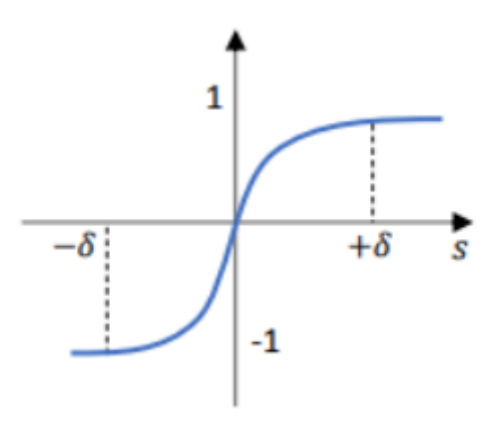


Figure (III.8): Smoothing Function "cont(S)".

III.5 Design of a Direct Torque Control Using Sliding Mode:

III.5.1 Proposed Control Principle:

We present here an alternative method for direct torque control of an induction machine based on sliding mode theory. Its objective is to control the magnitude of the stator flux to enable torque control. The basic idea of the proposed control method is to force the system state, through a discontinuous control, to evolve in finite time on a sliding surface according to the tracking error of the torque and the magnitude of the stator flux. The outputs of this regulation will be the reference voltages (BOUNADJA,2010).

III.5.2 Induction Machine Model:

We first recall the dynamic model of the asynchronous machine expressed in a (d,q) reference frame, which highlights only the stator quantities:

$$\begin{cases} \frac{di_{ds}}{dt} = -\beta i_{ds} + (\omega_s - p\Omega) \left(i_{qs} - \frac{\Phi_{qs}}{\sigma L_s} \right) + \frac{\eta_r}{\sigma L_s} \Phi_{ds} + \frac{\nu_{ds}}{\sigma L_s} \\ \frac{di_{qs}}{dt} = -\beta i_{qs} - (\omega_s - p\Omega) \left(i_{ds} - \frac{\Phi_{ds}}{\sigma L_s} \right) + \frac{\eta_r}{\sigma L_s} \Phi_{qs} + \frac{\nu_{qs}}{\sigma L_s} \end{cases}$$

$$(3.15)$$

The components of the stator flux are given by:

$$\begin{cases} \frac{d\Phi_{ds}}{dt} = -R_s i_{ds} + \omega_s \Phi_{qs} + v_{ds} \\ \frac{d\Phi_{qs}}{dt} = -R_s i_{qs} - \omega_s \Phi_{ds} + v_{qs} \end{cases}$$
(3.16)

The magnitude of the stator flux is given by:

$$\Phi_{S} = \sqrt{\Phi_{dS}^2 + \Phi_{qS}^2} \tag{3.17}$$

Given that the fluxes are known and the currents are measured, the torque is obtained by:

$$T_{em} = \rho \left(\Phi_{ds} i_{qs} - \Phi_{qs} i_{ds} \right) \tag{3.18}$$

The model (3.15)-(3.18) is used for the synthesis of the sliding mode control law. To overcome the drawback of rotor position measurement, the torque and stator flux are estimated using the voltage model in the (α,β) reference frame:

$$\begin{cases} \frac{d\Phi_{as}}{dt} = -R_s i_{as} + v_{as} \\ \frac{d\Phi_{\beta s}}{dt} = -R_s i_{\beta s} + v_{\beta s} \end{cases}$$
(3.19)

$$\Phi_{s} = \sqrt{\Phi_{as}^2 + \Phi_{\beta s}^2}$$

$$\tag{3.20}$$

$$T_{em} = \rho \left(\Phi_{as} i_{\beta s} - \Phi_{\beta s} i_{as} \right) \tag{3.21}$$

"The transformation of quantities from the rotating (d,q) reference frame to the fixed (α,β) reference frame is performed using the rotation matrix (BOUNADJA,2010):

$$\begin{bmatrix} x_{bs} \\ x_{as} \end{bmatrix} = \begin{bmatrix} \cos\theta_s & -\sin\theta_s \\ \sin\theta_s & \cos\theta_s \end{bmatrix} \cdot \begin{bmatrix} x_{ds} \\ x_{qs} \end{bmatrix}$$
(3.22)

$$\theta_{s} = \arctan\left(\frac{\Phi_{\beta s}}{\Phi_{\alpha s}}\right) \tag{3.23}$$

Where $(x_{\alpha s}, x_{\beta s})$ and (x_{ds}, x_{qs}) can represent components of flux, voltage, or current, and θ_s is the angle of reference frame transformation

III.5.3 Torque and Stator Flux Regulation:

To design a control law that ensures torque and stator flux tracking for the machine, the tracking errors are defined as:

$$\begin{cases}
e_{Tem} = T_{em}^* - T_{em} \\
e_{\phi_S} = \Phi_S^* - \Phi_S
\end{cases}$$
(3.24)

Where T_{em}^* and Φ_s^* are the reference values for torque and stator flux. The sliding surfaces are defined as follows:

$$\begin{cases} s_{Tem} = \frac{1}{p} e_{Tem} \\ s_{\phi s} = e_{\phi s} \end{cases}$$

$$(3.25)$$

The sliding regimes $s_{Tem} = 0$ and $s_{\Phi s} = 0$ achieved when the torque and the magnitude of the stator flux converge to their reference values.

By differentiating the equations of the two sliding surfaces, we obtain:

$$\begin{cases} \dot{s}_{Tem} = \frac{1}{p} \left(\dot{T}_{em}^* - \dot{T}_{Tem} \right) \\ \dot{s}_{\phi S} = \dot{\phi}_S^* - \dot{\phi}_S \end{cases}$$
(3.26)

Taking into account expressions (3.17) and (3.18), expression (3.26) is rewritten as follows:

$$\begin{cases} \dot{s}_{Tem} = \frac{1}{p} \dot{T}_{em}^* - (\dot{\phi}_{ds} i_{qs} + \dot{\phi}_{ds} i_{qs} - \dot{\phi}_{qs} i_{ds} - \dot{\phi}_{qs} i_{ds}) \\ \dot{s}_{\phi_S} = \dot{\phi}_S^* - \frac{\dot{\phi}_{ds} \dot{\phi}_{ds} + \dot{\phi}_{qs} \dot{\phi}_{qs}}{\phi_S} \\ \end{cases}$$
(3.27)

By substituting the machine model (3.15), we obtain:

$$\begin{cases} \dot{s}_{Tem} = f_{Tem} - \left(i_{qs} - \frac{\Phi_{qs}}{\sigma L_s}\right) v_{ds} - \left(-i_{ds} + \frac{\Phi_{ds}}{\sigma L_s}\right) v_{qs} \\ \dot{s}_{\Phi s} = \dot{\Phi}_s - \frac{\Phi_{ds}}{\Phi_s} v_{ds} - \frac{\Phi_{qs}}{\Phi_s} v_{qs} \end{cases}$$

$$(3.28)$$

Where f_{Tem} and $f_{\Phi s}$ are continuous functions given by:

$$\begin{cases} f_{Tem} = \frac{1}{p} \dot{T}_{em}^* - \beta \left(\Phi_{qs} i_{ds} - \Phi_{ds} i_{qs} \right) - p\Omega \left(\Phi_{ds} i_{ds} + \Phi_{qs} i_{qs} \right) - \frac{\Phi_s^2}{\sigma L_s} (\omega_s - p\Omega) \\ f_{\Phi s} = \dot{\Phi}_s^* + \frac{R_s}{\Phi_s} \left(\Phi_{ds} i_{ds} + \Phi_{qs} i_{qs} \right) \end{cases}$$
(3.29)

By rewriting (3.28) in matrix form, we obtain:

$$\dot{s} = F + Nu \tag{3.30}$$

Where
$$s = [s_{Tem} \quad s_{\Phi s}]^T$$
; $F = [f_{Tem} \quad f_{\Phi s}]^T$; $u = [v_{ds} \quad v_{qs}]^T$; $N = \begin{bmatrix} -i_{qs} + \frac{\phi_{qs}}{\sigma_{L_s}} & i_{ds} - \frac{\phi_{ds}}{\sigma_{L_s}} \\ -\frac{\phi_{ds}}{\phi_s} & -\frac{\phi_{qs}}{\phi_s} \end{bmatrix}$.

To determine the discontinuous control and thus ensure the convergence of the torque and stator flux regulators, the following candidate Lyapunov function is considered: $V = \frac{1}{2}s^Ts$. The derivative of V is defined by (BOUNADJA,2010):

$$\dot{V} = s^T \dot{s} = s^T (F + Nu) \tag{3.31}$$

Following the methodology introduced in (V. I. Utkin,1999), the discontinuous control is defined as follows:

$$u = E \operatorname{sign}(s^*) \tag{3.32}$$

Where $s^* = \begin{bmatrix} s_{\text{Tem}}^* \\ s_{\text{DS}}^* \end{bmatrix} = N^{-1}s$ And E is the continuous voltage at the inverter input

Thus, expression (3.31) can be rewritten in the following form:

$$\dot{V} = (s_{\text{Tem}}^* f_1^* - E | s_{\text{Tem}}^* |) + (s_{\phi_s}^* f_2^* - E | s_{\phi_s}^* |)$$
(3.33)

Where $\begin{bmatrix} f_1^* \\ f_2^* \end{bmatrix} = (N^{-1}F)$. Note that $\det(N) \neq 0$.

According to (3.32), if E satisfies the following condition:

$$E > \max_{i=1,2} |f_i^*|$$
 (3.34)

We can affirm that V > 0, and therefore all trajectories will reach the surface s^* in finite time and remain on this surface. Thus, since N is non-singular, we have s = 0, which ensures that the estimated variables converge to their reference values.

Therefore, the reference voltages can be determined from (3.32) using the inverse Park transformation.

$$\begin{bmatrix} v_{\rm ms}^* \\ v_{\rm bs}^* \\ v_{\rm cs}^* \end{bmatrix} = \sqrt{\frac{2}{3}} \begin{bmatrix} \cos\theta_{\rm s} & -\sin\theta_{\rm s} \\ \cos(\theta_{\rm s} - 2\pi/3) & -\sin(\theta_{\rm s} - 2\pi/3) \\ \cos(\theta_{\rm s} + 2\pi/3) & -\sin(\theta_{\rm s} + 2\pi/3) \end{bmatrix} \begin{bmatrix} v_{\rm ds}^* \\ v_{\rm qs}^* \end{bmatrix}$$

(3.35)

Figure (III.9) illustrates the proposed principle for direct torque control using sliding modes in an asynchronous machine.

However, the voltage of an inverter leg can take only two distinct values: $+U_d$ and $-U_d$. Therefore, expression (3.35) cannot be implemented directly but must be applied using pulse width modulation (PWM). To achieve this, the next section proposes a PWM strategy based on the sliding mode principle (BOUNADJA,2010).

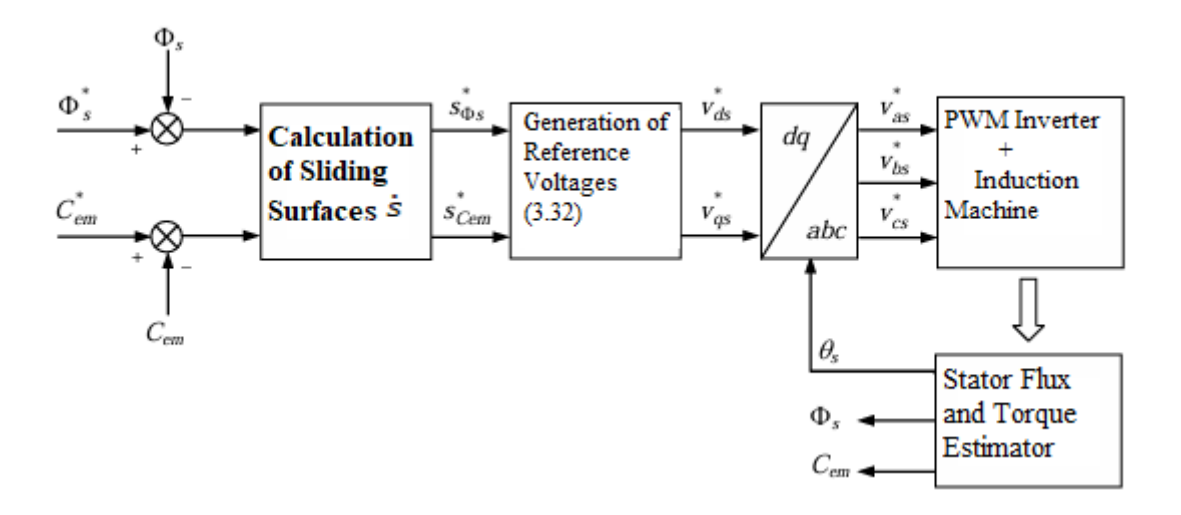


Figure III.9: Principle Diagram of Direct Torque Control Using Sliding Modes for an Asynchronous Machine.

III.6 Simulation Block:

The simulation block for the control of the asynchronous machine in the Simulink environment is represented by the blocks in Figure III.11:

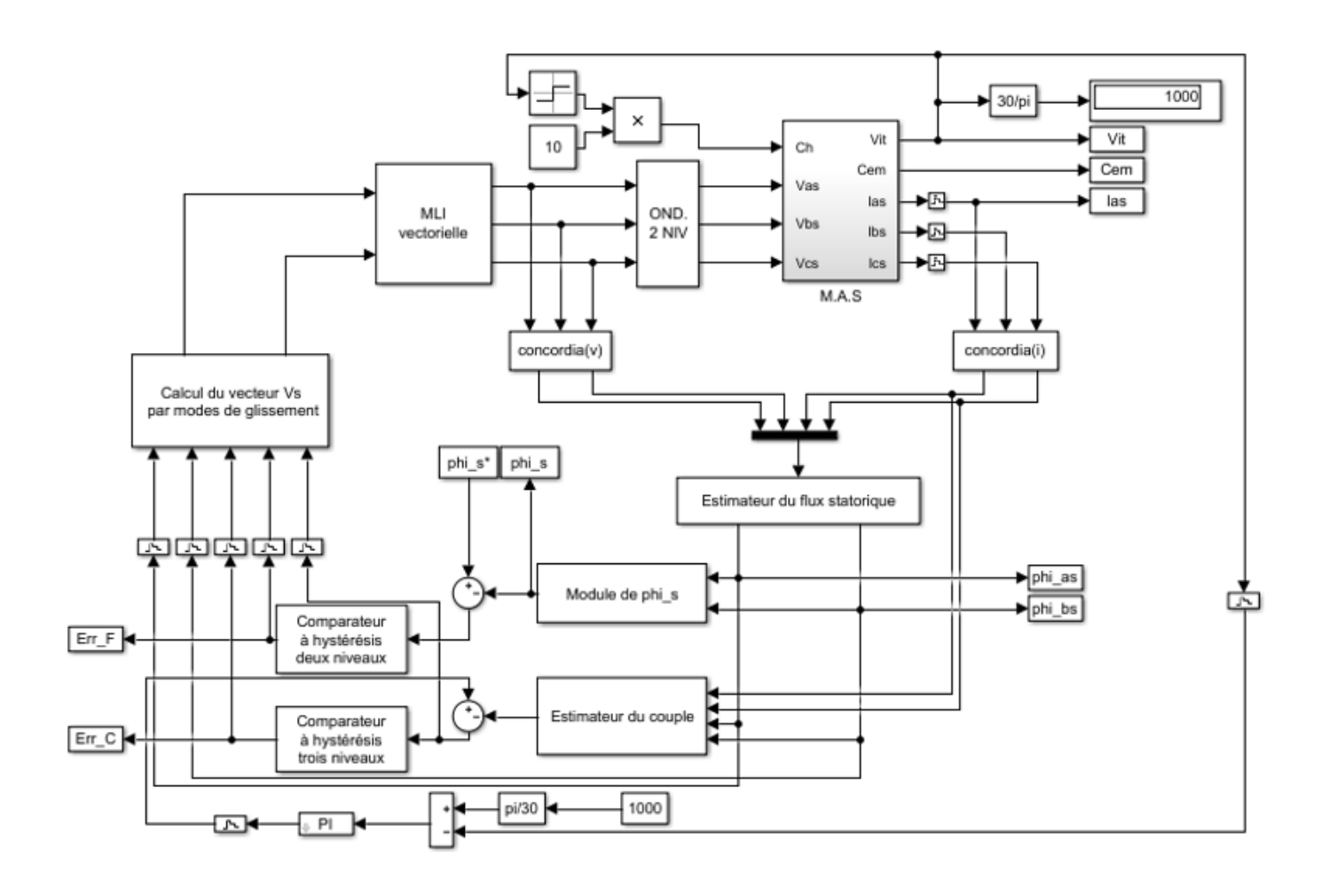


Figure III.10: Principle Diagram of Direct Torque Control Using Sliding Modes for an Asynchronous Machine.

III.7 Results and Discussion:

The motor's speed response demonstrates rapid convergence to its reference value of 1000 rpm, indicating an efficient control strategy. The absence of overshoot and oscillations confirms that Sliding Mode Control (SMC) effectively stabilizes the system. The smooth transition showcases good dynamic performance, ensuring that torque and flux variations do not disrupt speed regulation.

The torque curve shows an initial sharp drop, stabilizing at 10 units within 0.5 seconds. This rapid correction suggests that the control strategy swiftly adjusts torque to the desired operating level. The steady-state behavior indicates minimal torque ripple, confirming that SMC enhances robustness against disturbances while maintaining precision in torque tracking.

The stator flux magnitude remains stable at approximately 1.2, demonstrating consistent flux control. This stability directly contributes to reduced torque oscillations, improving motor performance and overall efficiency. The alpha and beta flux components exhibit clean sinusoidal oscillations, further validating effective flux tracking.

The nearly perfect circular trajectory of the flux confirms balanced electromagnetic performance and steady-state operation. The trajectory's symmetry indicates that DTC with SMC maintains consistent stator flux, preventing unwanted disturbances. This behavior ensures optimal motor control, minimizing flux ripple and enhancing efficiency.

III.8 Conclusion:

The results confirm that DTC with SMC successfully enhances motor control precision, ensuring fast speed tracking, stable torque regulation, and smooth current and flux behaviors. The control strategy effectively mitigates disturbances, demonstrating robust performance and improved efficiency. The system operates with minimal overshoot, reduced torque ripple, and harmonic suppression, reinforcing the effectiveness of the applied techniques.

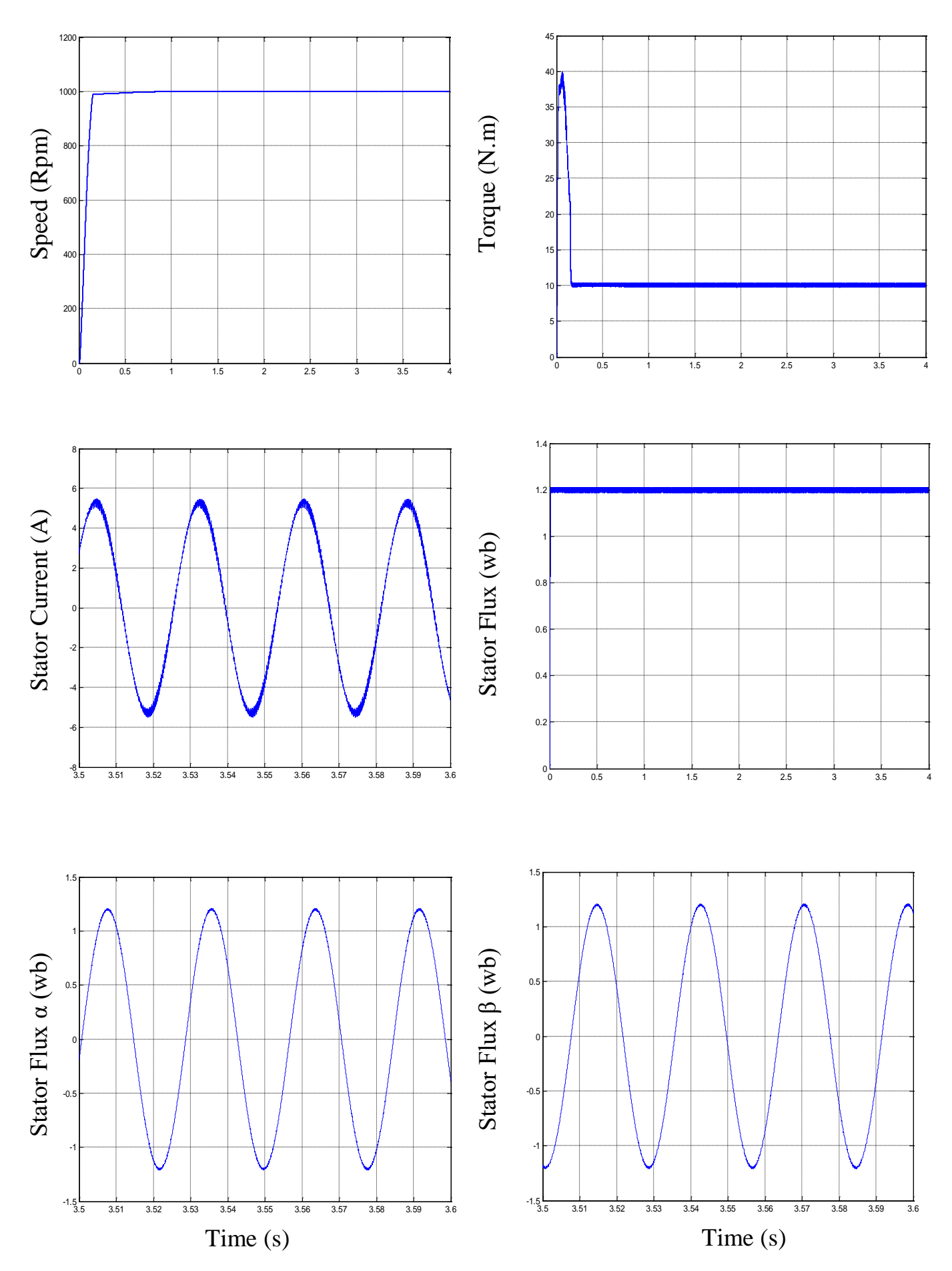


Fig. III.11: Simulation results of DTC with SMC

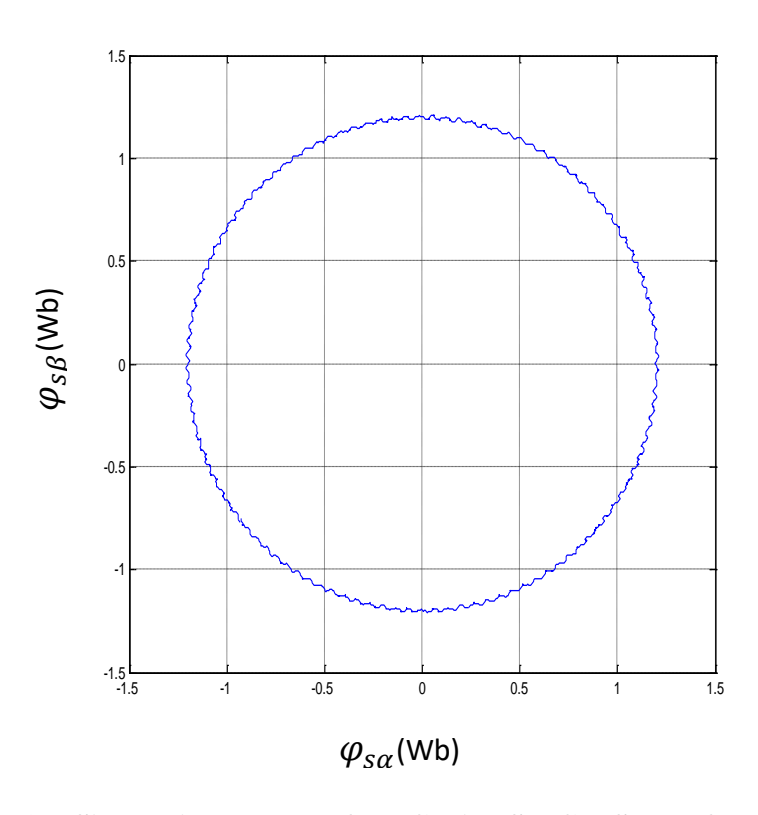


Fig. III.12: Simulation results of DTC with SMC - Stator flux trajectory

General Conclusion

This Work has provided a detailed exploration of induction motor control, emphasizing the role of Direct Torque Control (DTC) and Sliding Mode Control (SMC) in enhancing performance and efficiency. Beginning with the mathematical modeling of induction motors, the study progressed through classical DTC strategies, highlighting their advantages and limitations.

The integration of SMC with DTC was thoroughly examined, demonstrating its ability to reduce torque ripples, improve flux regulation, and enhance system robustness. Through MATLAB/Simulink simulations, the effectiveness of this approach was validated, confirming its potential for high-performance motor applications.

Key conclusions from this work include:

- DTC alone provides fast torque response but suffers from flux and torque oscillations.
- SMC significantly improves system stability, reducing disturbances and ensuring precise control.
- Combining DTC with SMC enhances electromagnetic performance, minimizing harmonic distortions.

Overall, this study confirms that DTC with SMC is an effective solution for improving induction motor control, offering better precision, faster dynamic response, and increased reliability. Future research could focus on refining these techniques through adaptive control strategies, AI-driven optimizations, and multilevel inverter applications to further enhance system efficiency and stability.

Reference:

AÏMER.F, OUALI.Y.-Contribution à l'amélioration de la commande directe du couple de la machine asynchrone : Utilisation de la MLI vectorielle. Centre Universitaire Dr Moulay Tahar,2006.

AKKOUCHI.K.-Commande Directe Du Couple (DTC) d'une Machine Asynchrone. UNIVERSITE BADJI MOKHTAR- ANNABA ,2007.

BENATTOOUS.Y GOLEA.D. A,ABDELSSEMED.A. -Commande à structure variable par mode glissant pour la commande vectorielle dun moteur asynchrone=, « ICEL98, 5-7 Octobre 1998, UST Oran, Algérie ».

BOUNADJA.M.- Contribution à la Commande Directe du Coupled'une Machine Asynchrone pour l'Alterno-démarreur Intégré, Université des Sciences et de la Technologie d'Oran Mohamed BOUDIAF.2010.

BOUTEBAK.A,RABAH.HAFS.-Commande Directe Du Couple d'une Machine Asynchrone Alimentée Par Un Onduleur Multi-Niveaux. UNIVERSITÉ IBN-KHALDOUN DE TIARET ,2015.

BENSLIMANE.A,LEMBARKI.A.-Comparaison Des Différentes Commandes d'un Onduleur à Deux Niveaux Associé à Un Moteur Asynchrone .UNIVERSITE KASDI MERBAH OUARGLA Faculté des Sciences Appliquées Département de Génie Electrique , 2022.

BAGHLI.L. -Modélisation et commande de la machine asynchrone. Note de cours, IUFM de Lorraine, UHP, France. 2004.

GRELLET.G et CLERC.G. -Actionneurs électriques : Principes, modèles et commandes. Eyrolles, Paris, France. 2000.

MADHAVI,M,shubhada.M. -Speed Control of Induction Motor Using PI and PID Controller .*College of Engineering Nagpur,440016, India.*, IOSR Journal of Engineering (IOSRJEN) , 2013.

KHERRAZ.M, Leila.R. -Contrôle Intelligent de La Machine Asynchrone à Cage Par l'utilisation de La Commande Directe Du Couple. Université Saida Dr Tahar Moulay, 2023.

SAOUDI,M.-Contrôle Par Mode Glissant d'ordre Deux de La Machine Asynchrone . Université Mohamed Khider , Biskra, 7 Oct. 2014.

SOUKKOU.H, DOUIEB.H.-Commande Par Mode Glissant de La Machine Asynchrone. Université Mohamed Seddik Benyahia Jijel, 2020.

TOUAHAR.A,ZEMIT.A.-DTC-SVM Control of Induction Motor Fed by PWM Inverter.2021.

TAKAHASHI and T.NOGUCHI.-A New Quick-Response and High-Efficiency Control Strategy of an Induction Motor,IEEE Transactions. on Industry Applications, Vol. IA 22, N° 5, pp. 820-827, 1985.

V. I. UTKIN, J. GULDNER, J. SHI, -Sliding mode control in electromechanical systems,

Taylor & Francis, New York, 1999.

Appendix A

1. Vector Pulse Width Modulation (PWM) Control Strategy.

```
function y=svm(x);
 V0 = [0;0;0]; V1 = [1;0;0]; V2 = [1;1;0]; V3 = [0,1,0]; V4 = [0;1;1]; V5 = [0;0;1]; V6 = [1;0;1]; V7 = [1;1;1]; V6 = [1;0;0]; V1 = [1;0;0]; V2 = [1;1;0]; V3 = [0,1,0]; V4 = [0;1;1]; V5 = [0;0;1]; V6 = [1;0;1]; V7 = [1;1;1]; 
 Va=x(1);
Vb=x(2);
t=x(3);
T=1.0e-4;
E=500;
if Va==0;
      if Vb==0;
                  teta=0;
       elseif Vb<0;
                  teta=3*pi/2;
       elseif Vb>0;
                  teta=pi/2;
       end;
else
        teta=atan(Vb/Va);
       if Va<0;
               teta=teta+pi;
      elseif Vb<0
               teta=teta+2*pi;
        end;
end;
secteur=floor(rem(teta+10*pi,2*pi)/pi*3)+1;
% Calculation of Voltage Vector Application Times
secteur=floor(rem(teta+10*pi,2*pi)/pi*3)+1;
if secteur==1;
        t1 = (sqrt(6)*Va-sqrt(2)*Vb)/(2*E);
        t2=sqrt(2)*Vb/E;
        s1=V1;
        s2=V2;
elseif secteur==2;
       t2 = (sqrt(6)*Va + sqrt(2)*Vb)/(2*E);
        t1 = (-sqrt(6)*Va + sqrt(2)*Vb)/(2*E);
        s1=V3;
        s2=V2;
```

```
elseif secteur==3;
 t1=sqrt(2)*Vb/E;
 t2 = (-sqrt(6)*Va-sqrt(2)*Vb)/(2*E);
 s1=V3;
 s2=V4;
elseif secteur==4;
  t2 = (-sqrt(6)*Va + sqrt(2)*Vb)/(2*E);
 t1 = -sqrt(2)*Vb/E;
 s1=V5;
 s2=V4;
elseif secteur==5;
 t1 = (-sqrt(6)*Va-sqrt(2)*Vb)/(2*E);
  t2 = (sqrt(6) * Va - sqrt(2) * Vb)/(2 * E);
 s1=V5;
  s2=V6;
elseif secteur==6;
 t2=-sqrt(2)*Vb/E;
 t1 = (sqrt(6)*Va + sqrt(2)*Vb)/(2*E);
 s1=V1;
  s2=V6;
end;
ti=(1-t1-t2)/4;
dteta=rem(t,T)/T;
if dteta<=ti;
 y=V0;
elseif dteta<=ti+t1/2;
 y=s1;
elseif dteta<=ti+t1/2+t2/2;
 y=s2;
elseif dteta<=3*ti+t1/2+t2/2;
 y=V7;
elseif dteta<=3*ti+t1/2+t2;
 y=s2;
elseif dteta<=3*ti+t1+t2;
 y=s1;
else;
 y=V0;
end;
```

2. Calculation of the Angular Sector of the Stator Flux in Conventional DTC

```
function y=atan(x);
phi_as=x(1);
phi_bs=x(2);
if phi_as>0
  if phi_bs>=0
     y=atan(phi_bs/phi_as);
  else
     y=atan(phi_bs/phi_as)+2*pi;
  end
elseif phi_as==0
  if phi_bs<0
     y=3*pi/2;
  elseif phi_bs>0
     y=pi/2;
  else
     y=0;
  end
else
  y=atan(phi_bs/phi_as)+pi;
end
secteur=floor((rem((y+pi/6),2*pi)/(pi/3)))+1;
```

3. Development of the Switching Table in Conventional DTC

```
function s=selection(a,b,c)
V0=[0;0;0]; V1=[1;0;0]; V2=[1;1;0]; V3=[0,1,0]; V4=[0;1;1]; V5=[0;0;1]; V6=[1;0;1]; V7=[1;1;1]; V5=[0;0;1]; V6=[1;0;1]; V7=[1;1;1]; V7=[1;1]; 
if a==1
                      if b==1
                                   switch c
                                                           case 1
                                                                                  s=v2;
                                                           case 2
                                                                                   s=v3;
                                                           case 3
                                                                                  s=v4;
                                                           case 4
                                                                                   s=v5;
                                                           case 5
                                                                                  s=v6;
                                                           case 6
                                                                                   s=v1;
                                   end
```

```
else
    switch c
      case 1
        s=v7;
      case 2
        s=v0;
      case 3
        s=v7;
     case 4
        s=v0;
      case 5
        s=v7;
      case 6
        s=v0;
   end
end
else
  if b==1
    switch c
       case 1
         s=v3;
       case 2
         s=v4;
       case 3
         s=v5;
       case 4
         s=v6;
       case 5
         s=v1;
       case 6
         s=v2;
    end
  else
    switch c
       case 1
         s=v0;
       case 2
         s=v7;
       case 3
         s=v0;
       case 4
         s=v7;
       case 5
         s=v0;
       case 6
         s=v7;
    end
  end
end
```

Appendix B

1. Parameters of the Asynchronous Motor Used During Simulation

• Nominal Voltage 230/400 V 6,4/3,7 A • Nominal Current 1,5 KW • Nominal Power 1420 tr/min • Nominal Speed • Number of Pole Pairs $4,85 \Omega$ • Stator Winding Resistance $3,805 \Omega$ • Rotor Winding Resistance 274 mH• Stator Phase Leakage Inductance • Rotor Phase Leakage Inductance 274 mH 258 mH • Mutual Inductance $0,031 \ kg.m^2$ • Moment of Inertia of Rotating Parts 0,00114 N.m.s/rad • Viscous Friction Coefficient

2.Parameters of the Two-Level Voltage Inverter Used During Simulation

• DC Voltage 500 V 10 KHz

• Switching Frequency